VSB – Technical University of Ostrava
Faculty of Electrical Engineering and Computer Science

Millimeter Wave Communications in 5G Networks and Beyond: New System Models and Performance Analysis

PHD THESIS

2023

Nhat Tien Nguyen

Millimeter Wave Communications in 5G Networks and Beyond: New System Models and Performance Analysis

Komunikace na milimetrových vlnách v 5G a dalších sítích: Nové systémové modely a analýza výkonnosti

Nhat Tien Nguyen

Study Programme: P1807 – Computer Science, Communication Technology and Applied Mathematics

Field of study: 2601V018 – Communication Technology

PhD Thesis

Supervisor: Prof. Ing. Miroslav Vozňák, Ph.D.

Ostrava, 2023

Declaration

I declare that the doctoral thesis titled "Millimeter Wave Communications in 5G Networks and Beyond: New System Models and Performance Analysis" was written independently by me, under the supervision of my doctoral thesis supervisor and using technical literature and other sources of information, which are all quoted in the thesis and listed in the references at the end of the thesis. As the author, I furthermore declare that I have not infringed any copyright in the creation of this doctoral thesis. In particular, I have not unlawfully encroached upon anyone's personal or ownership rights, and I am fully aware of the consequences of breaking Regulation S 11 and the Copyright Act No. 121/2000 Coll., as amended,and intellectual property rights in some Acts (Intellectual Property Act) and stipulated in later regulations, including the possible penalties resulting from the provisions of Criminal Act No 40/2009 Coll., Section 2, Paragraph VI, Part 4.

Ostrava, January 2023

Abstrakt

Dizertační práce zkoumala různé modely sítí a zaměřila se na tři důležité vlastnosti pro buňkové sítě příští generace s ohledem na mmW komunikace, kterými jsou: vliv útlumu a mezikanálového rušení (CCI), energetická účinnost a účinnost spektra.

Co se týče prvního cíle, dizertace obsahuje studii techniky neortogonálního vícenásobného přístupu (NOMA) v bezdrátové multiskokové relay síti využívající získávání energie, kde relay uzly sbírají energii z energetických majáků (PB). Tato část přináší přesné výrazy propustnosti pro NOMA a analýzu výkonnosti se třemi různými schématy NOMA s cílem určit optimální parametry pro propustnost navrženého systému. Dále byl navržen samoučící se shlukovací protokol (SLCP), ve kterém se uzel učí informace o sousedech, aby určil hustotu uzlů a zbytkovou energii použitou k výběru hlavy shluku CH pro zlepšení energetické účinnosti, čímž může prodloužit životnost sensorové sítě a zvýšit propustnost.

Za druhé, přístup NOMA poskytl mnoho příležitostí pro masivní připojení s nižší latencí, NOMA však může způsobovat mezikanálové rušení v důsledku opětovného využívání kmitočtů. CCI a útlum hrají klíčovou roli při rozhodování o kvalitě přijímaného signálu. V této dizertace je brána v úvahu přítomnost η a μ útlumových kanálů v síti užívající NOMA. Odvozeny jsou výrazy v uzavřené formě pro pravděpodobnost výpadku (OP) a propustnost s dokonalým postupným rušením rušení (SIC) a nedokonalým SIC. Dále se dizertace zabývá integrací přístupu NOMA do satelitní komunikační sítě a vyhodnocuje výkonnost systému při dopadech nedokonalé informace o stavu kanálu (CSI) a CCI.

Závěrem disertační práce představuje nový model pro hybridní družicově-terestriální přenosovou síť (HSTRN) založenou na NOMA vícenásobném přístupu využívající mmWave komunikaci. Satelit využívá NOMA schéma, zatímco pozemní relay uzly jsou vybaveny více anténami a aplikují protokol zesilování a předávání (AF). Je zaveden srážkový koeficient, který je uvažován jako útlumový faktor mmWave pásma při výběru nejlepšího relay uzlu. Samotné přenosové prostředí HSTRN je charakterizováno pomocí hybridních Rician a Nakagami-m kanálů. Vztahy pro vyhodnocení výkonnosti systému navrženého modelu vyjadřující ergodickou kapacitu (EC) a pravděpodobnost ztrát (OP) byly odvozeny v uzavřené formě a následně ověřeny pomocí simulační numerické metody Monte Carlo.

Klíčová slova

Abstract

The dissertation investigates different network models, focusing on three important features for next generation cellular networks with respect to millimeter waves (mmWave) communications: the impact of fading and co-channel interference (CCI), energy efficiency, and spectrum efficiency.

To address the first aim, the dissertation contains a study of a non-orthogonal multiple access (NOMA) technique in a multi-hop relay network which uses relays that harvest energy from power beacons (PB). This part derives the exact throughput expressions for NOMA and provides a performance analysis of three different NOMA schemes to determine the optimal parameters for the proposed system's throughput. A self-learning clustering protocol (SLCP) in which a node learns its neighbor's information is also proposed for determining the node density and the residual energy used to cluster head (CH) selection and improve energy efficiency, thereby prolonging sensor network lifetime and gaining higher throughput.

Second, NOMA provides many opportunities for massive connectivity at lower latencies, but it may also cause co-channel interference by reusing frequencies. CCI and fading play a major role in deciding the quality of the received signal. The dissertation takes into account the presence of η and μ fading channels in a network using NOMA. The closed-form expressions of outage probability (OP) and throughput were derived with perfect successive interference cancellation (SIC) and imperfect SIC. The dissertation also addresses the integration of NOMA into a satellite communications network and evaluates its system performance under the effects of imperfect channel state information (CSI) and CCI.

Finally, the dissertation presents a new model for a NOMA-based hybrid satellite-terrestrial relay network (HSTRN) using mmWave communications. The satellite deploys the NOMA scheme, whereas the ground relays are equipped with multiple antennas and employ the amplify and forward (AF) protocol. The rain attenuation coefficient is considered as the fading factor of the mmWave band to choose the best relay, and the widely applied hybrid shadowed-Rician and Nakagami-m channels characterize the transmission environment of HSTRN. The closed-form formulas for OP and ergodic capacity (EC) were derived to evaluate the system performance of the proposed model and then verified with Monte Carlo simulations.

Keywords

EH, NOMA, OP, WSN, clustering, millimeter waves, hybrid satellite-terrestrial networks.

Acknowledgement

I would like to mention my supervisor, Prof. Miroslav Vozňák and express my respect and deepest gratitude for his huge encouragement and immense support. I appreciate all his knowledge, contributions of ideas, time and unwavering support. Without his motivating and enthusiastic guidance, the thesis would not have been possible to complete. I would also like to thank the Faculty of Electrical Engineering and Computer Science and VSB – Technical University of Ostrava for their excellent conditions and institutional environment during my PhD studies.

I sincerely thank Dr. Dinh-Thuan Do for his professional advice and guidance. He directed me towards this challenging and exciting research and inspired me to investigate and explore it. I also thank my colleagues at the Wireless Communications and Signal Processing Lab, who together support both individuals and research groups to develop their capacities and expertise to achieve valuable results in science.

I would like to thank my colleagues at the Faculty of Electronics and Communications, Sai Gon University, for their mental support and assistance in teaching during my time at VSB – Technical University of Ostrava, Czech Republic, to complete a doctoral studies programme.

Finally, for the sacred feelings that I have for my family, I would like to dedicate special thanks and appreciation for their continuous support, sharing and being with me through life. I sincerely thank my wife, Tran Thi Phuong Thao, and our dear children, Tri Vy, Van Anh, and Tien Sy.

Contents

List of symbols and abbreviations

5G	–	Fifth Generation
6G	–	Sixth Generation
AF	–	Amplify-and-Forward
AS	–	Average Shadowing
AWGN	–	Additive White Gaussian Noise
BER	–	Bit Error Rate
BS	–	Base Station
BF	–	Beamforming
CCI	–	Co-Channel Interference
CDF	–	Cumulative Density Function
CDMA	–	Code-Division Multiple Access
CH	–	Cluster Head
CHSTN	–	Cognitive Hybrid Satellite-Terrestrial Network
CM	–	Cluster Member
CNOMA	–	Cooperative Non-Orthogonal Multiple Access
CR	–	Cognitive Radio
CRNs	–	Cognitive Relay Networks
CSI	–	Channel State Information
CSTRN	–	cognitive hybrid satellite-terrestrial relaying network
D2D	–	Device-to-Device
DF	–	Decode-and-Forward
EC	–	Ergodic Capacity
EH	–	Energy Harvesting
FD	–	Full-Duplex
FDMA	–	Frequency-Division Multiple Access
HD	–	Half-Duplex
HS	–	Heavy Shadowing
HSRN	–	Hybrid Satellite Relay Network

HSTCN	–	Hybrid Satellite-Terrestrial Cognitive Network
HSTN	–	Hybrid Satellite-Terrestrial Network
HSTRN	–	Hybrid Satellite-Terrestrial Relay Network
HSTRS	–	Hybrid Satellite-Terrestrial Relay System
HydRON	–	High Throughput Optical Network
IoT	–	Internet of Things
LEACH	–	Low Energy Adaptive Clustering Hierarchy
LoS	–	Line-of-Sight
LTE	–	Long Term Evolution
MISO	–	Multiple-Input Single-Output
MIMO	–	Multiple-Input Multiple-Output
mmWave	–	Millimeter Wave
NLoS	–	Non Line-of-Sight
NOMA	–	Non-Orthogonal Multiple Access
OMA	–	Orthogonal Multiple Access
OP	–	Outage Probability
PB	–	Power Beacon
PDF	–	Probability Density Function
PLS	–	Physical-Layer Security
PSR	–	Power Splitting-based Relaying
PU	–	Primary User
QoS	–	Quality of Service
RF	–	Radio Frequency
SC	–	Superposition Coding
SER	–	Symbol Error Rate
SU	–	Secondary User
SNR	–	Signal Noise Ratio
SIC	–	Successive Interference Cancellation
SINR	–	Signal Interference plus Noise Ratio
SOP	–	Secrecy Outage Probability
SWIPT	–	Simultaneous Wireless Information and Power Transfer
TDMA	–	Time-Division Multiple Access
TPSR	–	Time-Switching and Power Splitting
TSR	–	Time Switching-based Relaying
WPT	–	Wireless Power Transfer
WPC	–	Wireless-Powered Communication
WPCN	–	Wireless Powered Communication Network
WSN	–	Wireless Sensor Network

List of Figures

Chapter 1

Introduction

1.1 Motivation

Next generation wireless networks have been continuously developed over the past decade to meet the increasing demands for data. New techniques and resources have therefore been proposed and deployed, and with the vastly larger spectrum and magnitude increase in system capacity, mmWave is a viable candidate for next generation wireless network communications and a potential solution for the problem of limited spectrum. One of the candidate bands for deploying mmWave cellular mobile networks is the spectrum between 20 GHz and 90 GHz [1, 2]. The results in [3] demonstrated that highly directional satellite communications in mmWave frequencies (as typically mounted on satellite platforms) is able to offer high-capacity wide geographical coverage despite very long transmission distances and severe attenuation experienced at those frequencies. Although the demand for frequency access is greater, the technology allows many wireless users to transmit data simultaneously. In the old manner of multiple access techniques such as Time-Division Multiple Access (TDMA), Frequency-Division Multiple Access (FDMA) and Code-Division Multiple Access (CDMA), these technologies apply the Orthogonal Multiple Access (OMA) techniques implemented in many ad hoc wireless networks. However, conventional OMA techniques do not satisfy the high demands of future radio access networks. Fifth Generation (5G) cellular networks place high demands on throughput, delay time, user numbers and other factors. Non-orthogonal multiple access (NOMA) therefore represents a suitable candidate for radio access technology that allows many users to access frequency resources simultaneously through power levels. NOMA uses superposition coding at the transmitter and successive interference cancellation (SIC) in the uplink and downlink channels at the receiver [4]. Research towards the development of beyond-5G solutions, Sixth Generation (6G), is already gaining momentum, both in the scientific community and industry [5, 6]. The authors of [7] outlined new applications of 6G in agriculture, education, media and entertainment, tourism, transportation and logistics.

6G research is also focusing on the development of non-terrestrial communications to provide three-dimensional coverage through supplemental aerial platforms, including satellites [8, 9]. To increase the reliability and number of concurrent users accessing this resource, satellite communications combined with terrestrial networks have been proposed as hybrid satellite-terrestrial relay networks (HSTRN) [10, 11]. The novel network architecture of HSTRN has received considerable interest because it provides broadband access in a seamless, efficient and cost-effective manner, regardless of the availability of regular terrestrial infrastructures [12]. Furthermore, future integrated wireless communications will include almost all network entities such as space networks, air networks, underwater or sea networks, ground networks and wireless sensor networks (WSN) (Fig. 1.1). In the area of WSN-based Internet of Things (IoT), sensors can be distributed for many applications, such as sensing, monitoring and controlling, all which have low energy consumption and high reliability [13, 14]. These sensors are embedded with smart sensing and intelligent computing and are capable of communicating with each other. The nodes in these networks can be examined as users which transmit data to each other, either to the controller or the base station. Clustering protocols allow many users to access the resource by grouping some users together.
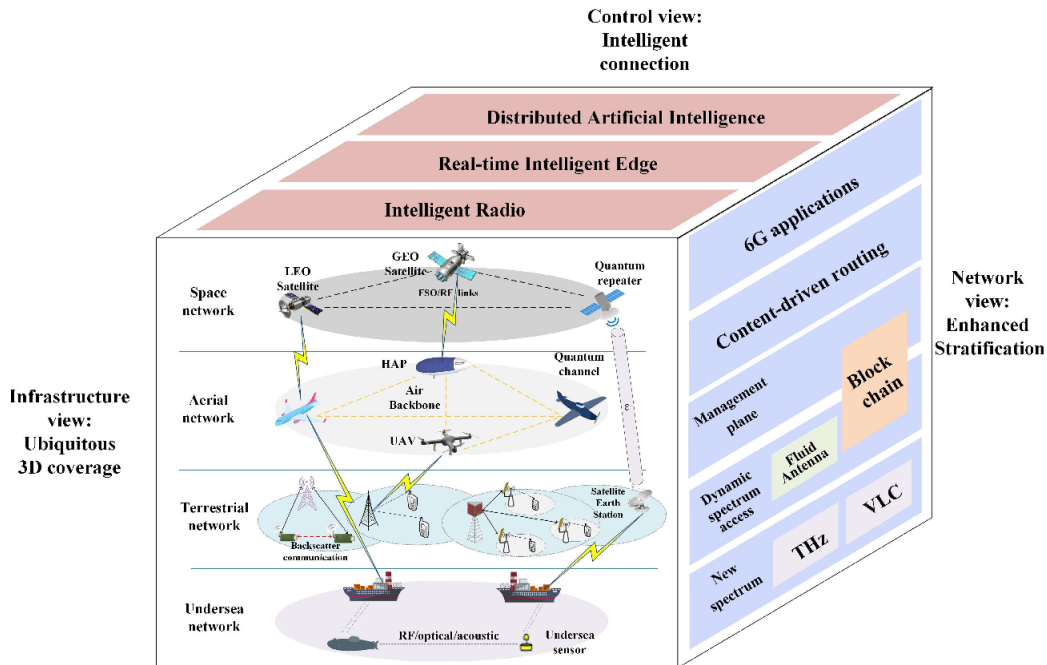
Figure 1.1: Integrated Satellite-Terrestrial architecture [9].

In the general system model, CCI and multiple relays are considered. Many techniques have been proposed for analyzing performance in terms of OP, ergodic capacity (EC) and symbol error rate (SER). The relay in HSTRN deploys the DF or AF protocol, and it can also be combined with EH, Cooperative NOMA (CNOMA) and CR techniques. The main

problems with wireless networks are energy constraints and the throughput of networks which depends on wireless applications, the number of users, QoS requirements and channel conditions in the wireless links [15, 16].Communication links are adversely affected by interference, fading and path loss, which reduce network performance to low throughput, a low packet delivery ratio and high energy consumption.

1.2   Research Aims

- Survey and study wireless network models that apply a range of advanced techniques under various channel conditions.

- Analyze the proposed network model's OP to improve spectrum efficiency.

- Propose new energy efficient techniques according to the green networking application: efficient power allocation of NOMA in HSTN and a clustering protocol in WSN.

- Apply the simulation results in an analysis to evaluate the performance of the system and proposed protocol.

1.3   Dissertation structure

The dissertation is structured as follows: Chapter 2 describes the related background knowledge to the dissertation, Chapter 3 introduces the State-of-the-Art and its specific aims, which are presented in Chapter 4. Chapters 5, 6 and 7 address the results of the research in fulfilling its aims. Finally, Chapter 8 summarizes the results of the dissertation.

Chapter 2

Background

2.1 Evolution of mobile communication network

Mobile communication networks have developed rapidly since their first appearance in the 1980s. The first generation was designed for analogue voice services, with low transmission efficiency and no security. The system, 2G based on digital modulation technologies such as Time Division Multiple Access (TDMA), Frequency Division Division (FDMA) and Code Division Multiple Access (CDMA), supported better voice services and short message service (SMS) capability. The third generation was proposed in 2000 with the goal of providing data transmission rates of at least 2 Mbps. The 3rd Generation Partnership Project (3GPP) was established to define specifications and define cellular standards and systems to achieve global roaming [17].

Introduced in the late 2000s, 4G is an all-IP network which greatly improved spectral efficiency and reduced latency. It is capable of providing high-speed data rates up to 1 Gbit-s/s downstream and 500 Mbits/s upstream. Long-Term Evolution-Advanced (LTE-A) and Wireless Interoperability for Microwave Access (WiMAX) used integrated technologies such as coordinated multi-transmit/receive (CoMP), multi-output multi-output input (MIMO) and orthogonal frequency division multiplexing (OFDM).

In recent years, the fifth generation mobile communication network has completed its initial basic testing and standardization procedures and has been deployed for commercial use. It not only uses the microwave band of the spectrum, it also uses millimeter wave (mmWave) called FR2 (24 GHz up to 54 GHz) for greater capacity and higher throughput, data rates up to 10 Gbps [18]. mmWaves have shorter ranges than lower frequency microwaves, therefore its cells are smaller in size. 5G also applies advanced access technologies, including NOMA, Beam Division Multiple Access (BDMA), Massive MIMO, EH, Software-defined networking (SDN), Filter Bank Multi-Carrier (FBMC) modulation and D2D services to increase spectrum efficiency.
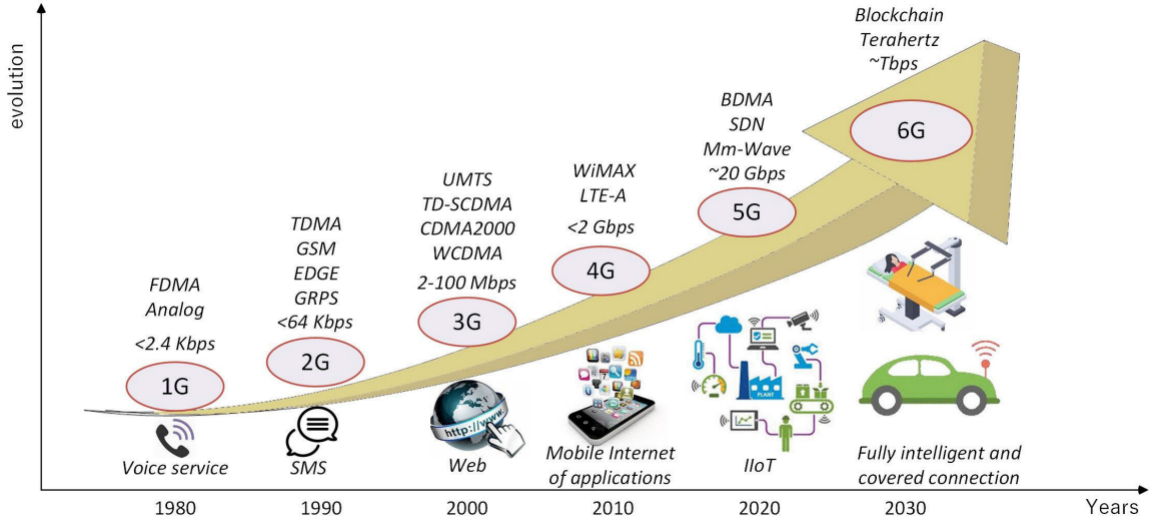
Figure 2.1: Evolution of mobile wireless systems [9].

The 6G network is targeted as a green network that enhances the performance of information transmission – high data rates up to 1 Tbps and extremely low latency of microseconds. It will feature terahertz frequency communication, space multiplexing, energy harvesting technology and the use of new materials that greatly improve energy efficiency. One 6G goal is to achieve universal connectivity by integrating satellite communication networks and underwater communications to provide global coverage [19].

2.2   Millimeter wave

2.2.1   Introduction

To solve spectrum scarcity problems and attain 5G architecture, mmWave is one of many solutions which have been explored in studies. mmWave delivers ultra-high capacity, ultra-high data rates, very large bandwidth and ultra-low latency. The frequency ranges of mmWaves are from 30 to 300 GHz, the wavelength of the electromagnetic radiation (EMR) being in the millimeter range at these frequencies, although the propagation loss in mmWave technology is higher since these frequencies cannot penetrate certain impediments such as walls, furniture or people. These wavelengths are attenuated more by rain and atmosphere. These factors should be carefully considered in calculating the RF link budget for implementing mmWaves for future application in the mobile broadband market.

The 3rd Generation Partnership Project (3GPP) defined "5G" as any system using 5G NR (5G New Radio) software, which is a new type of radio access technology (RAT) for the 5G mobile network. In 2018, 3GPP published Release 15, described as "Phase 1" standardization

11

Table 2.1: Frequency Range 2.

Band	f (GHz)	Common name	Uplink/Downlink (GHz)	Channel bandwidths (MHz)
n257	28	LMDS	$26.50 - 29.50$	50, 100, 200, 400
n258	26	K-band	$24.25 - 27.50$	50, 100, 200, 400
n259	41	V-band	$39.50 - 43.50$	50, 100, 200, 400
n260	39	Ka-band	$37.00 - 40.00$	50, 100, 200, 400
n261	28	Ka-band	$27.50 - 28.35$	50, 100, 200, 400
n262	47	V-band	$47.20 - 48.20$	50, 100, 200, 400
n263	60	V-band	$57.00 - 71.00$	100, 400, 800, 1600, 2000

for 5G NR. Named Release 16, "5G phase 2" was completed in June 2020, and Release 17 was scheduled for June 2022 [20]. 5G NR uses frequency bands in two frequency ranges, FR1 and FR2, where FR2 is in the mmWave range [21]. The study in [22] presented the new frequency bands for 5G satellites. The new Ka-band (28 GHz) and Q/V band (37 to 53 GHz) bandwidths are available for 5G satellites, and the backhaul link from the satellite to the terrestrial can also use optical bands. The U.S. Federal Communications Commission (FCC) has proposed wireless broadband for next-generation wireless services to operate in mmWaves above 24 GHz, with WRC-19.

2.2.2   mmWave Propagation

The common apprehension in wireless engineering is that rain, the atmosphere, oxygen or water vapor absorption means that the mmWave spectrum is useless in mobile communications: this is one of the challenges in implementing mmWave communication in 5G networks and beyond. The mmWave portion of the spectrum has high atmospheric attenuation and oxygen absorption, leading to decreased coverage and wave strength. Worse, mmWave travels in rainy or very humid conditions, resulting in signal loss and distortion. The proposed techniques of beamforming and taking advantage of reflection and refraction for D2D communication provide some solutions to the frequency scattering problem affecting the throughput performance of mmWaves [23]. Free-space path loss represents attenuation of the electromagnetic energy between the transmitter and receiver. In fact, propagation and attenuation vary dramatically with frequency in the mmWave spectrum due to effects from the above-mentioned environmental parameters. Figure 2.2 illustrates details of the attenuation added in Friis free space propagation at frequencies in the mmWave portion of the spectrum.

Figure 2.2 indicates that attenuation is very high at 60 GHz, 180 GHz and 320 GHz in the curve at sea level. Specifically, attenuation shows a peak at 60 GHz because of gaseous absorption by water oxygen molecules, and again at 180 GHz and 320 GHz due to water vapor molecules. However, some frequency windows have minimal attenuation compared to
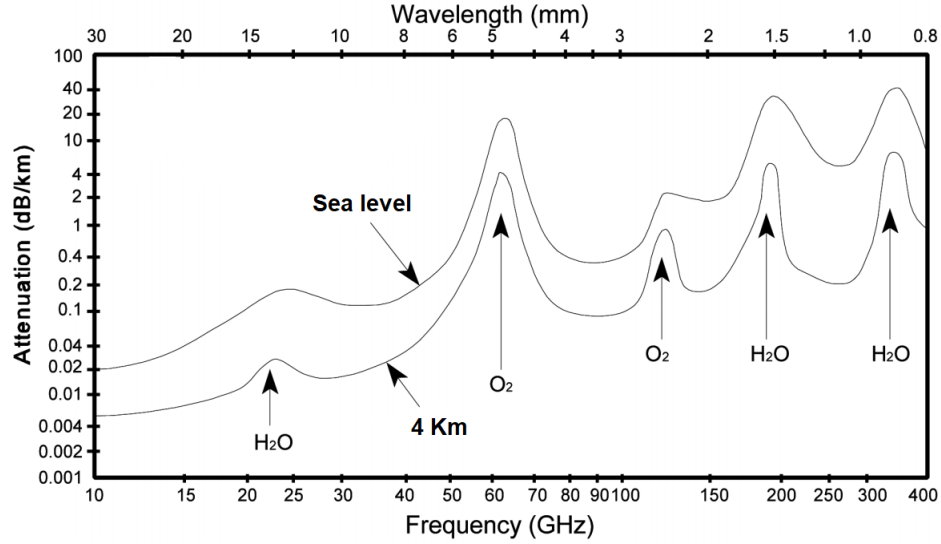
Figure 2.2: Free space propagation attenuation due to atmospheric absorption at mmWave (FCC, 1997).

peak regions, for example around 35, 94, 140 and 220 GHz, and wave propagation in these frequency ranges easily provides a perfect transmission medium for future wireless communication networks. They are viable for indoor and outdoor wireless networks, backhaul links, and macrocells, microcells and femtocells in next-generation cellular networks. The difference in altitude greatly affects the numbers of interfering molecules; Figure 2.2 clearly shows that at 4 km altitude, atmospheric attenuation is significantly lower than at sea level. It is also important to reiterate that atmospheric attenuation is not the only phenomenon affecting mmWave signals; weather conditions such as snow, rain and hail also produce high attenuation at certain frequencies. To overcome atmospheric attenuation and weather-related losses, potential solutions such as gain engineering, beam width and beam navigation should be employed in future mmWave networks.

2.3 Cognitive Radio

2.3.1 Definition

A cognitive radio network is an 'intelligent radio' which can monitor, sense and detect its surroundings and automatically reconfigure its operating parameters to best suit those conditions. It uses dynamic spectrum access (DSA) technology which is transferable to next-generation communication networks so that secondary users (SUs) can access a licensed spectrum without causing interference to primary users (PUs). Mitola introduced the term *cognitive radio* and defined it as a radio whose radio model uses rigorous inferences to achieve specific estab-

13

lished objectives in related radio domains [24]. In [25], Haykin defined an *intelligent radio communication system* as one that is aware of its environment and is able to learn and adaptively change its operating parameters (e.g., transmit power, carrier frequency and modulation method) in real time, with two main goals:

- High-reliability communication, anytime, anywhere.

- Efficient use of the radio frequency spectrum.

  Some basic concepts of a cognitive radio network:

- SDR – this was introduced by Joseph Mitola in 1991. SDR is a radio which can be reconfigured in the field to instantly change its communication protocol to another standard [26]. This allows the radio to rapidly adjust to different requirements such as new channel conditions. SDR is therefore the key to achieving cognitive radio.

- Primary user (PU) or licensed user – the user who has been licensed to use the frequency.

- Secondary User (SU) or conscious user – this user is not authorized to use the spectrum. The primary user does not need to know about the activity of other users. The secondary user must also be aware of the primary user's activity and perform special functions to not disturb the primary user.

- Spectrum hole – A frequency range which has been licensed to the primary user but may not necessarily be used by the primary user at certain times or locations.

2.3.2 Cognitive Radio Network Paradigms

The model of a cognitive radio network has been proposed with many different definitions and paradigms. Cognitive radio networks are essentially divided into three models:

- Underlay paradigm

- Overlay paradigm

- Interweave paradigm

2.3.2.1 Underlay Paradigm

The underlay paradigm is shown in Figure 2.3, and it is assumed that techniques can be used to measure the interference caused by the SU to the PU. The SU is able to transmit simultaneously alongside PU transmissions in the licensed band as long as the interference generated by SU signals to primary receivers remains below an acceptable interference threshold limit (ITL). Limiting interference can be accomplished by using multiple directional antennas to

guide the SU signal away from a PU's location or by using larger bandwidth and spectrum spreading at the SU's transmitter so that the signal power is below the noise threshold and then performing spectrum despreading at the receiver. Future technologies are anticipated to include the use of ultra-wideband (UWD) spectrum spread techniques.

SU interference to the PU can be measured by an antenna located in the cognitive user area. It is also necessary to monitor whether the transmit power meets requirements at the transmission end for cognitive users to ensure that interference is within permissible limits. The limitation of the underlay paradigm is therefore that communication between secondary users can only be done in a narrow range, but despite this, it can use multiple bands to serve multiple cognitive users.
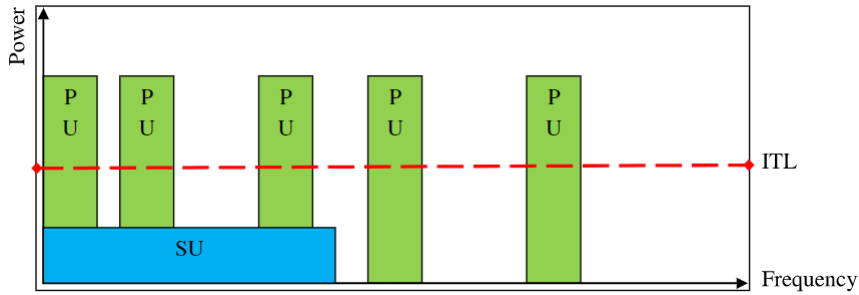
Figure 2.3: Underlay Paradigm.

2.3.2.2 Overlay Paradigm

The overlay paradigm is shown in Figure 2.4. A prerequisite for this paradigm is that the SU has complete knowledge of the PU's encoding from a *codebook* which includes all the codeword systems used by the PU. Encoding information obtained through the use of a common codeword standard by the PU or the codebook is broadcast periodically. Alternatively, the PU's codewords can be obtained by decoding by the SU's receiver. However, the overlay paradigm assumes that all the PU codewords are known as soon as the PU starts transmitting the signal. This assumption is not true under practical conditions, and decoding the codewords upon receipt of the PU's signal at the SU's receiver may be affected by fading or noise. Understanding the key user's codewords ensures that mitigation and gradual approaches are completely unaffected at the PU. Encoding can be employed in various sophisticated techniques, such as dirty paper coding (DPC) [27].

However, the SU can share some of its power to partially support the PU's data transmission by acting as a relay station to forward the signal. This implemented feature will contribute to an increase in the PU's SNR, which offsets the effects caused by cognitive radio users to the PU. This keeps the primary user's connection intact, while the SU still uses some capacity to perform data transmission. Of particular note is that the overlay paradigm can be

registered for both licensed and unlicensed bands. In the licensed band, the overlay paradigm uses the shared spectrum without affecting the PU, moreover contributing to the improvement of the PU data transmission. In unlicensed bands, the overlay paradigm improves spectral efficiency by sharing codebook knowledge to reduce interference.
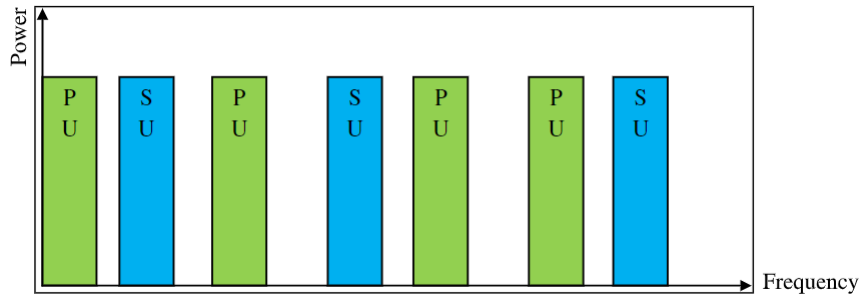
Figure 2.4: Overlay Paradigm.

2.3.2.3 Interweave Paradigm

The interweave paradigm is based on the idea of opportunistic communication, which is the original motivation for cognitive radio networks [28]. The idea arose from the results of the FCC survey, which indicated that a large portion of the licensed band is not fully used most of the time. This means that spectrum holes exist at specified times and locations and include licensed and unlicensed bands. Spectrum efficiency is improved because of frequency reuse in the empty portion of the spectrum.
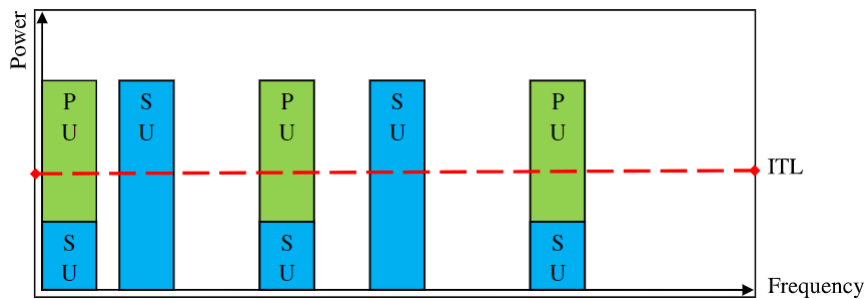
Figure 2.5: Interweave Paradigm.

The interweave paradigm requires insight into the PU's transceiver activities at each point in time. An extension of the interweave paradigm is that all active users using the given frequency band are considered primary users; each new user is considered a cognitive user which will reuse the parts of the spectrum left empty by existing users. The interweave paradigm is an intelligent wireless communication system that uses periodic monitoring techniques to

16

automatically detect spectrum holes and make use of empty parts of the spectrum to improve spectrum efficiency.

2.4   Energy Harvesting (EH)

The SWIPT technique is as an emerging solution which prolongs the lifetime of energy-constrained relay nodes in wireless networks by taking advantage of the ambient radio-frequency (RF) signal to harvest energy and process information [29, 30]. SWIPT attempts to supply power and transmit wireless signals from the source node to the destination via a relay node that harvests energy from the received RF signal and uses that energy to forward the source information, as illustrated in Figure 2.6. Information is transmitted from source node S to destination node D through an energy-constrained relay node R. The channel gains from S to R and from R to D are denoted h and g, respectively. Parameters d_1 and d_2 are the distances from S to R and from R to D, respectively. Two relaying protocols have been proposed, consisting of time-switching relaying (TSR) and power-splitting relaying (PSR).
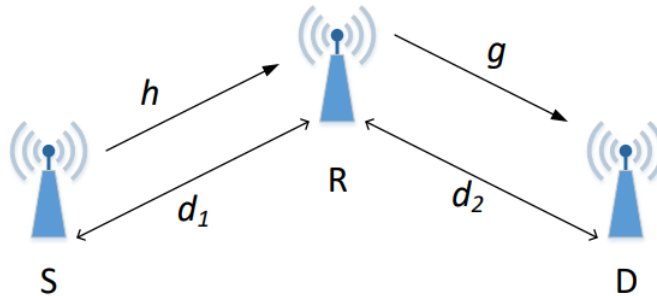
Figure 2.6: System model for EH relays.

2.4.1   Time-Switching Relaying (TSR) Protocol

The principle of TSR protocol is shown in Figure 2.7, consisting of the parameters for EH and information processing of the relay. T is the block time in which a certain information block is transmitted from the source node to the destination node. Duration αT is the block time for EH, where α is the time fraction $0 \leq \alpha \leq 1$. With the remaining block time $(1-\alpha)T$, half $(1-\alpha)T/2$, is used for information transmission from the source to the relay, and the remaining half $(1-\alpha)T/2$, is used for information transmission from the relay to the destination.

The signal received at the relay node is given by

$$y_r(t) = \frac{1}{\sqrt{d_1^m}}\sqrt{P_s}hs(t) + \sigma_{n,R}, \tag{2.1}$$

17
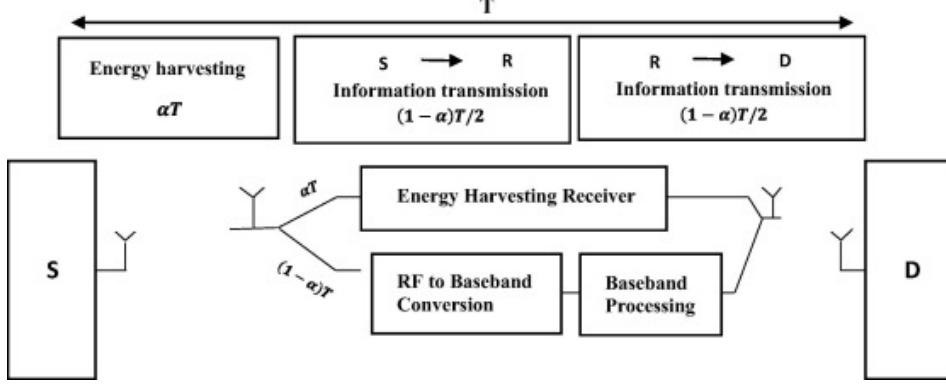
Figure 2.7: Principle of TSR protocol.

where d_1 is the distance from the source to the relay, P_S is the power of the source, h is the channel gain from the source to the relay, $\sigma_{n,R}$ denotes the Gaussian noise of the relay with zero-mean, and $s(t)$ is the information signal from the source. $\mathbb{E}\left\{|s(t)|^2\right\} = 1$, where $\mathbb{E}\{\cdot\}$ is the expectation operator and $|\cdot|$ is the absolute value operator.

The power of the relay node is

$$P_R = P_S|h|^2 d_1^{-m}. \tag{2.2}$$

The energy harvested in αT block time is obtained from

$$E_R = \alpha T \eta P_S |h|^2 d_1^{-m}, \tag{2.3}$$

where $0 < \eta < 1$ is the energy conversion efficiency. The power transmitted from the relay node to the destination is

$$P_{T_R} = \frac{E_R}{(1-\alpha)T/2} = \frac{\alpha T \eta P_S |h|^2 d_1^{-m}}{(1-\alpha)T/2}. \tag{2.4}$$

2.4.2 Power-Splitting Relaying (PSR) Protocol

The parameters of the PSR protocol for energy harvesting and information processing at the relay are illustrated in Figure 2.8, where P is the power of the received signal at the relay, and T is the total block time. During the first half of the block time $(T/2)$, ρP is used for energy harvesting, and $(1-\rho)P$ is used for information transmission from the source to the relay, where ρ is the power fraction. The remaining half $(T/2)$, $(1-\rho)P$ is used for information transmission from the relay to the destination.

18
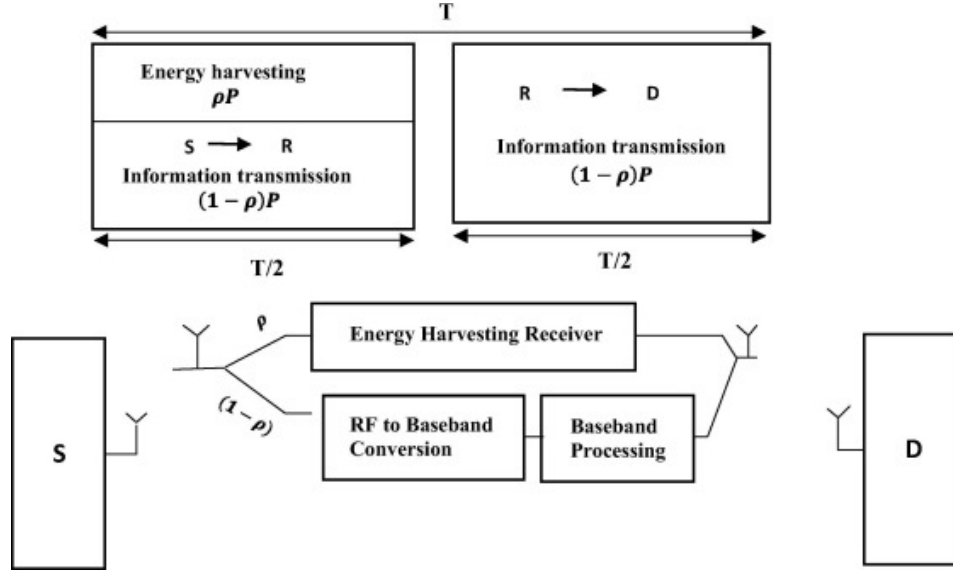
Figure 2.8: Principle of PSR protocol.

Derived from the power at the relay node (2.2), the energy harvested at the relay is

$$E_R = \eta P_S |h|^2 d_1^{-m} \rho \left(\frac{T}{2}\right), \tag{2.5}$$

where η is the harvesting efficiency and $0 < \eta < 1$. The power of transmitted signal from the relay to the destination is

$$P_{T_R} = \frac{\eta P_S |h|^2 d_1^{-m} \rho \left(\frac{T}{2}\right)}{\frac{T}{2}} = \eta P_S |h|^2 d_1^{-m} \rho. \tag{2.6}$$

Chapter 3

State-of-the-Art

Increasing demand for highly reliable and low-latency broadband communications for multimedia services has spurred research and development for next generation wireless networks. Deployments of mmWave 5G cellular mobile networks use a portion of the spectrum between 20 GHz and 90 GHz [1, 2]. HSTNs have been actively researched and proposed as potential models for the future, and mmWave will feature in the main spectrum band in future satellite networks for wireless broadband access [22]. In [3], the authors demonstrated that highly-directional satellite communications with mmWaves deliver high-capacity, broad geographic coverage. The satellite network's performance, however, is adversely affected by the masking effect, and the line of sight (LoS) link is severely degraded [31, 32]. To correct these limitations and seamlessly connect satellites to terrestrial communication systems, the authors of [33, 34] proposed an HSTRN, which uses ground nodes as relays. However, with the continuous proliferation of multimedia services, it is foreseen that the mmWave part of the spectrum may be congested and lead to a scarcity of available bands for terrestrial and satellite communications in future HSTRNs [35, 36]. Techniques to solve scarcity in the spectrum for wireless communication networks will also be studied and applied in HSTN. Recently, the European Space Agency (ESA) recommended a model that integrates satellite and terrestrial networks in optical communication systems – High Throughput Optical Network (HydRON) [37]. HydRON targets Tbps "All-Optical Network" solutions with optical connections in the Tbps region as a true "Fiber in Space" network, similar to optical fiber networks on the ground.

NOMA has numerous advantages in terms of spectral efficiency and energy efficiency to support massive connectivity, user fairness and low suspension. Some modern techniques use NOMA, which is a very suitable technology for application in 5G networks [38]. Specifically, high-power transmission can be selected for users with poor channel conditions, and lower power levels can be applied to transmissions for users with better channel conditions. At the base station, the superposition coding technique is applied to receivers. With SIC technology, stronger NOMA users with less power allocation will eliminate the greater power allocation

of all weaker communication users to decipher their own packets [39]. 5G networks provide multiple points of access to massive users, for example the IoT, sensor networks and relay communications. Satellite networks are expected to support massive connectivity services and reduce operational costs [40]. They can be deployed and integrated with geo-stationary and non-geo-stationary orbit satellites and apply cooperative transmission, EH relaying or CR networks to increase spectrum efficiency. EH technology is a promising method for supplying power to wireless communication network nodes. Energy-limited devices can harvest energy from their surroundings via radio frequencies and thereby prolong the network lifetime. RF-based EH technology can be classified into simultaneous wireless information and power transfer (SWIPT), wireless-powered backscatter communication, and wireless-powered communication (WPC) [41, 42]. The authors of [43] combined SWIPT with NOMA to transmit weaker user packets via strong users. In [44], wireless powered communication network (WPCN) technology was combined with a NOMA uplink network to increase the individual data rate. NOMA has also been examined for its effects on energy in WPC systems [45]. A downlink using NOMA was researched in combination with SWIPT [46]. In [47], NOMA security was addressed in an artificial noise-aided beamforming design which provided high security in a multiple input single output (MISO) NOMA SWIPT network. In [48, 49], EH combined with NOMA was able to prolong limited power networks. In the era of the IoT, sensors can be distributed for numerous applications in sensing, monitoring and controlling [14]. The experiment in [13, 50] integrated a WSN into the IoT and included a gateway server, middleware and a mobile client. Sensor nodes can be grouped into clusters, each cluster consisting of a cluster head (CH) and several cluster members [51, 52, 53, 54]. In [51], the authors proposed a new clustering algorithm based on Fuzzy C-Means (FCM) for WSN-based IoT applications. The algorithm applied an FCM approach to form clusters and minimize the overall energy consumption in each cluster to choose the optimal CH in each transmission round. The authors of [52] proposed a new efficient-energy data dissemination scheme that focused on data storage at the devices layer. In [53], a modified low energy adaptive clustering hierarchy (LEACH) was applied to select the number of nodes which would become a cluster relay and forward data from the cluster to the sink. The efficient cluster CH algorithm significantly extends network lifetime and produces high throughput to ensure QoS requirements. In [54], CH is selected to provide fault-resistant routing. An efficient routing path is achieved by finding the minimum number of hops given the availability of alternative routing paths.

For relaying communication systems, the evaluation of network performance should consider imperfect conditions for practical applications [55]. From the point of view of practical scenarios, the SIC procedure potentially has specific problems, such as error propagation and complexity scaling, that lead to errors during decoding. Hence, it is important to consider the undesirable influence from imperfect SIC [56]. Other works have studied network performance under imperfect conditions of CSI and SIC. In [57], the authors analyzed the outage

performance in an underlay CR-NOMA system applying a DF relay and with imperfect CSI at the receiver. In [58], the authors considered the impact of imperfect SIC on the ergodic sum capacity. The NOMA technique in satellite communications has been widely studied in relation to infrastructure network, network models, network performance and multiple access techniques [59]. In [60], the authors studied integration of the NOMA technique with multi-beam satellite networks. The performance of a NOMA-hybrid satellite relay network (HSRN) was studied in [61, 62]. The study in [63] analyzed the OP of a NOMA-based integrated cognitive HSRN. The authors of [64] examined the performance of NOMA-HSRN with the presence of hardware impairments. In [65], a cooperative NOMA-HSRN took advantage of users with better channel gain to act as relays for the remaining users in the cluster. In [66], the authors studied the effect of imperfect CSI and channel impairments in a NOMA-based terrestrial mobile communication network (TMCN) that functioned with multiple relays. In [61], the authors investigated NOMA-based integrated terrestrial satellite networks (ISTN) and the effects of relaying configurations such as AF and DF. In all the studied NOMA-HSRN models, the effects of CCI have rarely been addressed. In practice, NOMA-HSRN might experience a situation of high CCI, which is a significant concern in the deployment of NOMA and HSRN in wireless communications. The aggressive reuse of spectrum resources degrades performance as a result of CCI. A more important priority, therefore, is to consider that NOMA-HSRN performance can only be guaranteed if CCI is taken into account.

NOMA, however, gains more benefits from CR, which improves the efficiency of spectrum utilization and introduces CR-inspired NOMA scenarios. In the work [67], the authors integrated NOMA with a cognitive satellite network to increase the ergodic performance of the system. Relay network technology was also applied to expand coverage, and CR allowed the sharing of radio resources, resulting in improved use of the spectrum for the major HSTN applications. Cognitive HSTN (CHSTN) is a promising architecture under research [68] and consists of a secondary terrestrial network which is permitted to operate with the same spectrum resources as the primary satellite network. However, limited transmit power for secondary users (SU) and inefficient use of available spectrum resources are two major challenges in CHSTN which can degrade the performance of secondary networks [69, 70]. Hybrid satellite-terrestrial cooperative networks (HSTCNs) or space-air-ground integrated relay networks have received considerable interest for their advantages in improving the coverage and effectively solving the masking effect. The work in [71] investigated the integration of NOMA with CR into a holistic 5G system, which constituted a cognitive NOMA network for more intelligent spectrum sharing. Three different cognitive NOMA architectures were presented, including underlay NOMA networks, overlay NOMA networks and CR-inspired NOMA networks, allowing the SU and PU to operate simultaneously in a cognitive relay network. In [72, 73], the authors introduced NOMA as an overlay model into terrestrial communications. In [74], The authors evaluated the performance of an overlay cognitive hybrid satellite-terrestrial

relaying network (CSTRN). This type of system contains a primary satellite transmitter which is used to transmit signals to multiple terrestrial receivers, and a secondary transceiver pair on the ground. The primary satellite transmitter is employed with NOMA architecture to serve all users simultaneously. To manage spectrum access, the secondary transmitter assists primary communication by using a cooperative relaying method. The hybrid channels can be described as shadowed-Rician fading and Nakagami-m fading models. The two main performance metrics are the closed-form OP and approximate EC expressions for the PU and SU.

In the Czech Republic, significant contributions in performance analysis and recommendations for next-generation wireless network models are developed at the research laboratory led by prof. Miroslav Voznak. In 2021, Hong-Nhu Nguyen [75] delivered a Ph.D. dissertation in which he proposed models integrating satellite and terrestrial networks focused on reliable and secure transmission in HSTCNs. The author studied basic relaying models for EH and information transmission, proposed relaying models for device-to-device (D2D) communications and derived the closed-form expression, simulating OP and average throughput to analyze the effects on network performance. The research included an investigation of CR-NOMA-based integrated networks based on the mathematical analysis and simulation results of outage and throughput performance, with a fixed power distribution parameter to ensure fairness in power allocation to the end users. High throughput was obtainable at a special rate of data. The author also proposed an HSTCN relaying network based on NOMA and applied BF methods and the interference constraint to reduce the interference of the secondary network on the primary network. Ngoc-Long Nguyen's dissertation [76] on NOMA schemes for next-generation cellular networks proposed a multi-antenna model for next-generation mobile wireless networks with straight and forward NOMA techniques, where the relay performs EH supplied from a power beacon to enhance quality of service. A simile of the NOMA and traditional OMA schemes indicated that the NOMA scheme performs remarkably better than OMA. The author then studied CR-NOMA for the downlink with integrated FD, RS, FD-DF techniques and MISO architecture and calculated and analyzed the SOP parameters for optimization. Finally, he proposed a hybrid satellite-terrestrial relay system (HSTRS) that uses NOMA to improve QoS for large numbers of connections and broadband access, inferring new exact expressions for the OP and throughput of the HSTRS model to evaluate the performance of the system.

Motivated by the above research, I investigated HSTNs for this dissertation. Satellites in an HSTN deliver services to many users through a ground relay. Assuming perfect or imperfect CSI at all nodes, the benefits of enabling CR and NOMA in an HSTN system were examined. To improve the OMA protocol network performance, an energy efficient clustering protocol was deployed. Alternatively, NOMA-HSTN was also used to improve channel access, implementing CR with multiple antennas equipped at relays and users. The performance

of NOMA-HSTN under different network scenarios with high interference channels was then analyzed. It should be noted that relay nodes are required to implement both OMA and NOMA for improvements in network performance.

Chapter 4

Aims of Dissertation

This section lists the aims of the research, focusing on the different stages of the research plan. The dissertation examines the effect of different channels such as Rayleigh, Rician and Nakagami-m channels. mmWave transmission is characterized by an increase in transmission frequency which leads to greater path loss [77]. Atmospheric degradation, attenuation by rain, and path depolarization also increase with frequency [78]. However, the dissertation explores proposed models and analyzes network performance with channel parameters modeled as coefficients based on state-of-art empirical models. Various techniques are applied to the physical layer, and network performance metrics include OP, SOP, EC, average throughput, network lifetime and residual energy. The research investigates and analyzes the performance of relay models, EH, NOMA networks, CR networks, WSN and terrestrial hybrid satellite system models under the effects of fading and associated interference. The specific aims are therefore detailed below.

4.1 Aim 1: Proposal of a new system model of wireless powered transfer and applying suitable clustering protocol in mmWave WSNs to improve energy efficiency.

I propose a design for a new system model which includes a relaying model, EH, and NOMA techniques, with a subsequent analysis of the network performance. The proposed model applies NOMA in two scenarios, one with single SIC and the other with dual SIC. SWIPT technology is employed to feed energy to the relays intended to serve distant NOMA users. The difference in performance between two NOMA users therefore remains fair with careful selection of power allocation factors, which is the main contribution of this part of the research. Performance is evaluated by deriving exact OP expressions. I also propose a self-clustering protocol in mmWave WSNs for IoT applications. The IoT sensor nodes transmit collected

25

data to the sink, and several nodes form a cluster. A cluster contains one CH and M cluster members (CM). Some nodes become cluster relays which do not belong to any cluster. The cluster relay is able to transmit data directly to the sink. Network performance is analyzed according to the residual energy in nodes.

4.2 Aim 2: Study of fading channels and CCI impact on performance analysis in NOMA network models.

Recently, 5G and 6G network models have been devised to exploit relaying techniques with satellite communication, forming a new architecture designated NOMA-HSRN [61, 62]. The mmWave spectrum has also been assigned to hybrid satellite-terrestrial systems [22, 79]. Network performance has therefore seen great enhancements in device connectivity, spectrum efficiency and signal quality. Fading channels and CCI also play a major role in determining the quality of the transmitted signal, an important consideration in the deployment of NOMA and HSRN in wireless communications technology.

For the second aim, the dissertation provides an analysis of the performance of a NOMA network model under more generalized fading conditions. Specifically, a NOMA system is considered to have two users with a fading channel $\eta - \mu$. The closed-form expressions are derived for system OP and throughput under both perfect and imperfect SIC. These expressions are analyzed numerically by varying certain parameters such as fading channels, power level coefficients and the number of antennae at the receiver. The results can be used to evaluate the performance of the system associated with each parameter, thereby recommendations can be made for each user's signal quality and the system OP. The network model is then extended with a proposed NOMA-HSRN with interference channels. The dissertation analyzes the performance of this system with two shadowing effect modes, including heavy shadowing (HS) and average shadowing (AS). System OP and EC are analyzed. Closed-form expressions are derived and subjected to a numerical analysis. Performance of the NOMA and OMA systems is also compared.

4.3 Aim 3: Design of new HSTN models to improve the network performance.

The authors of [5, 80, 81, 82] suggested that future 6G networks will be required to obtain the performance to satisfy the more stringent requirements and demands of an intelligent information society in 2030. This performance requirement includes ultra-high data rates, ultra-low latency, ultra-high reliability, high energy efficiency, massive connectivity, and large frequency bands. An integrated space-air-ground-underwater network will potentially form

the core architecture of 6G networks [83, 84] and consist mainly of the following four tiers: space network, air network, ground network, and underwater network. The desire to improve the network performance of the layers in next-generation radio networks is therefore gaining momentum. For the dissertation's third aim, I investigate the performance of a NOMA cognitive hybrid satellite-terrestrial relaying network and highlight the performance gaps between multiple users. The satellite source connects to secondary destinations on the ground by activating the CR scheme, and the secondary network is a dedicated group which follows the NOMA principle. A relay operates in the secondary source and uses AF mode to serve remote NOMA users under certain interference restrictions. To characterize the transmission medium, shadowed-Rician fading and Nakagami-m fading models are widely applied to the related hybrid channels. To provide a detailed examination of the system's performance metrics, closed-form expressions are derived for the OP of the secondary destinations under power constraint interference from an adjacent primary satellite network.

Chapter 5

A Wireless Powered Relaying System Model

5.1 Throughput Analysis of NOMA and OMA Assisted Wireless Energy Harvesting K-Hop Relaying Networks

This section addresses the first aim of the dissertation and presents a wireless energy harvesting relay network assisted NOMA [NNT04], [NNT05], and [NNT12]. The work and research for this section satisfies the aim with:

- An investigation of a time-switching multi-hop relaying model.

- The deployment of a decode-and-forward relaying protocol operating in half-duplex model.

- The derivation of exact throughput analytical expressions for both NOMA and OMA-assisted wireless energy harvesting multi-hop networks.

- An analysis and comparison of throughput performance using simulation results. The closed-form throughput results are verified by independent Monte Carlo simulations.

The results of this section were previously published in the paper [NNT04].

5.1.1 Introduction

Wireless energy harvesting (EH) enables the development of new devices for Internet-of-Medical Things (IoMT), wireless sensor networks (WSNs), infrastructure and environmental monitoring and surveillance where battery-powered devices would be unsuitable [85, 86, 87]. EH also enables energy sufficiency and lifetime operation for devices placed within building materials and the human body [85]. A potential application for wireless EH is relay networks, where the source transmit power during the uplink functions as an arbitrary variable in a wireless powered communication network (WPCN) because of its intrinsic power transmission.

The dramatic increase of battery-powered communication devices means the goal of extending their life is very important; for example, the highest possible throughput in the least time and good allocation of uplink and downlink times were calculated in a study in [88], [89]. For example, in a wide-body area network (WBAN) or IoMT, the relays depend on a reliable and perpetual source of energy since replacing batteries is undesirable [88], [90]. Various types of natural source can be used for harvesting, for example thermal or chemical reactions, or vibrations, etc. However, wireless EH multi-hop relaying networks face the fundamental problem of throughput. In [91], the authors developed an optimal throughput broadcast algorithm to address the stochastic character of the source and energy collection at the relays. In [92, 93, 94], a throughput algorithm was designed to acquire solutions for the optimal time and non-convex power distribution problem in wireless energy-harvesting cognitive radio networks. The authors of [95, 96, 97] investigated WPNCs assisted by NOMA, where the signal is transmitted to a sink node, and the sink applies successive interference cancellation (SIC) to remove interference at its receivers.

This section describes the application of NOMA in a wireless EH K-hop relay network to increase throughput. The relays have no dedicated energy source and therefore depend on wireless energy harvesting from a power beacon (PB) based on the time-switching protocol [98, 99, 100]. Hence, the source node transmits its data via relays, and every node makes use of the harvested PB energy for data transmission [101, 102]. As a result, K-hop relaying networks can provide line-of-sight (LoS) in obstruction filled environments such as indoor networks, etc. [103].

5.1.2 System model

As illustrated in Figure 5.1, the source-T_0 transmits information to the destination-T_K via $K - 1$ relays denoted T_1, T_2, ..., T_{K-1}. The transmitter T_k harvests energy from the power beacon (PB) to supply energy for its decode-and-forward (DF) actions, where $k = 0, 1, ..., K - 1$. All nodes in our system have a single antenna; therefore, K orthogonal time slots are used for information transmission.

We define Q as the time for end-to-end transmission. Thus, the dedicated time slot for data transmission is $\tau = Q/K$. In addition, a portion of the time slot $\alpha\tau$ is dedicated for EH from the PB, and the remainder $(1 - \alpha)\tau$ is used for decoding and forwarding operations, where $0 < \alpha < 1$ represents the block time portion. The energy harvested by T_k is therefore expressed as [49].

$$\bar{E}_k = \eta\alpha\tau\bar{P}_P\bar{h}_{P_k} \tag{5.1}$$
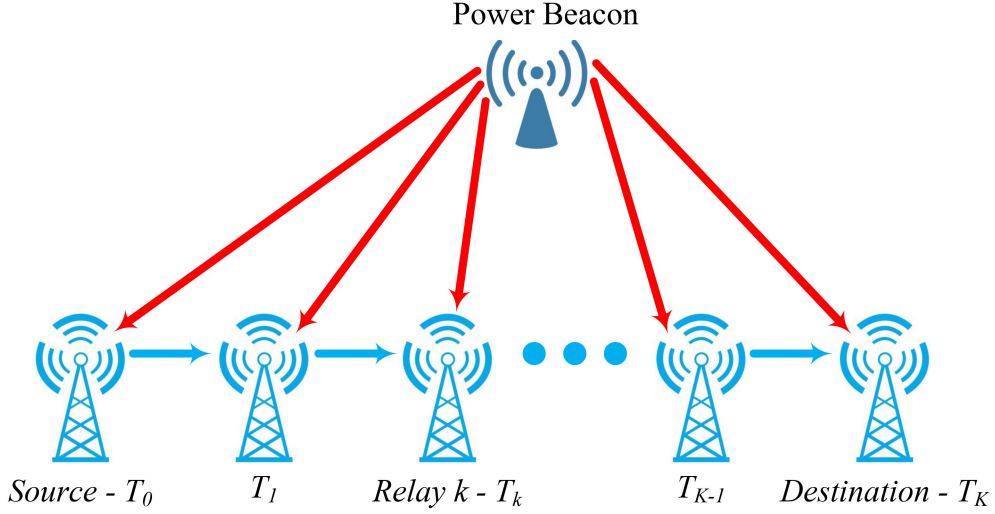
Figure 5.1: A K-hop DF relay network with EH from PB functionality.

where $(0 \leq \eta \leq 1)$ is the energy conversion efficiency, $\bar{P}_P$ is the power of PB transmitter, and $\bar{h}_{P_k}$ represents the channel between PB and T_k.

From (5.1), we obtain the T_k transmitter power as in [104]:

$$\bar{P}_k = \frac{\bar{E}_k}{(1 - \alpha) \tau} = \delta \bar{P}_{\mathrm{P}} \bar{h}_{P_k} \tag{5.2}$$

where $\delta = \frac{\eta \alpha}{1 - \alpha}$.

Remark 1: To simplify our calculations, we assume that EH operates on frequencies different from the data transmission process, and therefore interference is prevented at the relay receivers. We consider that in the $k-$th time slot, node T_{k-1} transmits data to node T_k, where $k = 1, ..., K$. To improve throughput, the relay T_{k-1} uses superposition coding to combine N signals to produce a superimposed signal expressed as

$$\bar{x} = \sum_{n=1}^{N} \sqrt{a_n \bar{P}_{k-1} \bar{x}_n} \tag{5.3}$$

where $n = 1, 2, ..., N$; a_n represents the power allocation coefficients, $\sum_{n=1}^{N} a_n = 1$ for $a_1 > a_2 > ... > a_N$; $\bar{x}_n$ is the transmitted signal.

Remark 2: Traditionally, orthogonal multiple access (OMA) has been the backbone of K-hop relaying, resulting in a data rate of $1/K$. Thus, by superposing N signals, our proposed scheme's data rate is N/K.

Assuming perfect SIC (pSIC) [105, 106, 107], and [108], the T_k the transmit signal-to-noise ratio (SNR) for decoding $\bar{x}_n$ under hardware impairments can be written as in [109]:

$$\bar{\psi}_k^n = \begin{cases} \dfrac{a_n \bar{P}_{k-1} \bar{h}_{D_k}}{\kappa^2 \bar{P}_{k-1} \bar{h}_{D_k} + \displaystyle\sum_{i=n+1}^{N} a_i \bar{P}_{k-1} \bar{h}_{D_k} + N_0} & \text{if } n<N \\[4ex] \dfrac{a_N \bar{P}_{k-1} \bar{h}_{D_k}}{\kappa^2 \bar{P}_k \bar{h}_{D_k} + N_0} & \text{if } n=N \end{cases} \tag{5.4}$$

where $\bar{h}_{D_k}$ is the channel gain between T_{k-1} and T_k, κ^2 is the combined hardware impairment [110, 111, 112], and N_0 is the additive white Gaussian noise (AWGN).

Substituting (5.2) into (5.5) yields

$$\bar{\psi}_k^n = \begin{cases} \dfrac{\rho a_n \delta \bar{h}_{P_{k-1}} \bar{h}_{D_k}}{\left(\kappa^2 + \displaystyle\sum_{i=n+1}^{N} a_i\right) \rho \delta \bar{h}_{P_{k-1}} \bar{h}_{D_k} + 1} & \text{if } n<N \\[4ex] \dfrac{\rho a_N \delta \bar{h}_{P_{k-1}} \bar{h}_{D_k}}{\kappa^2 \rho \delta \bar{h}_{P_{k-1}} \bar{h}_{D_k} + 1} & \text{if } n=N \end{cases} \tag{5.5}$$

where $\rho = \bar{P}_P / N_0$ is the transmit SNR.

Furthermore, we obtain the instantaneous channel capacity of $\bar{x}_n$ as

$$\bar{C}_k^n = (1 - \alpha) \tau \log_2 \left(1 + \bar{\psi}_k^n\right). \tag{5.6}$$

The channel capacity of $\bar{x}_n$ with DF relaying is expressed as

$$\bar{C}_{\text{e2e}}^n = \min_{k=1,2,\ldots,K} \left(\bar{C}_k^n\right). \tag{5.7}$$

Finally, we define the throughput similar to [92, 88]:

$$\mathcal{T}_{\text{NOMA}} = (1 - \alpha) \tau \bar{\gamma}_{th} \sum_{n=1}^{N} \Pr \left(\bar{C}_{\text{e2e}}^n \geq \bar{\gamma}_{th}\right), \tag{5.8}$$

where $\bar{\gamma}_{th}$ is desired target rate.

We also consider K-hop relaying with OMA. Here, T_{k-1} uses power $\bar{P}_{k-1}$ to transmit one signal to T_k. Therefore, the throughput becomes [113]:

$$\mathcal{T}_{\text{OMA}} = (1 - \alpha) \tau \gamma_{\text{th}} \Pr \left(\bar{C}_{\text{e2e}}^{\text{OMA}} \geq \bar{\gamma}_{th}\right), \tag{5.9}$$

where

$$\bar{C}_{\text{e2e}}^{\text{OMA}} = \min_{k=1,2,\ldots,K} \left((1 - \alpha) \tau \log_2 \left(1 + \frac{\rho \delta \bar{h}_{P_{k-1}} \bar{h}_{D_k}}{\kappa^2 \rho \delta \bar{h}_{P_{k-1}} \bar{h}_{D_k} + 1}\right)\right). \tag{5.10}$$

5.1.3 Throughput evaluation

5.1.3.1 Nakagami-m fading channel model

We assume the system channels follow Nakagami-m fading and also that the channel gains $\bar{h}_{P_k}$ and $\bar{h}_{D_k}$ are exponential random variables (RVs). We define Ω_{P_k} and Ω_{D_k} as the RVs channel parameters. The cumulative distribution functions (CDFs) of $\bar{h}_{P_k}$ and $\bar{h}_{D_k}$ can therefore be written as in [114], respectively:

$$F_{\bar{h}_{P_k}}(x) = 1 - e^{-\frac{x}{\beta_{P_k}}} \sum_{n=0}^{m_{P_k}-1} \frac{x^n}{n!\beta_{P_k}^n} \tag{5.11}$$

$$F_{\bar{h}_{D_k}}(x) = 1 - e^{-\frac{x}{\beta_{D_k}}} \sum_{n=0}^{m_{D_k}-1} \frac{x^n}{n!\beta_{D_k}^n} \tag{5.12}$$

The probability density functions (PDF) of $\bar{h}_{P_k}$ and $\bar{h}_{D_k}$ are obtained as in[115], respectively:

$$f_{\bar{h}_{P_k}}(x) = \frac{x^{m_{P_k}-1}}{\Gamma(m_{P_k})\beta_{P_k}^{m_{P_k}}} e^{-\frac{x}{\beta_{P_k}}} \tag{5.13}$$

$$f_{\bar{h}_{D_k}}(x) = \frac{x^{m_{D_k}-1}}{\Gamma(m_{D_k})\beta_{D_k}^{m_{D_k}}} e^{-\frac{x}{\beta_{D_k}}} \tag{5.14}$$

where $\beta_z \overset{\Delta}{=} \Omega_z/m_z, z \in (P_k; D_k)$.

Taking the path loss into account, the channel parameters Ω_{P_k} and Ω_{D_k} can be modeled as in [116]:

$$\Omega_{P_k} = d_{P_k}^{-\varepsilon}, \ \Omega_{D_k} = d_{D_k}^{-\varepsilon}, \tag{5.15}$$

where d_{P_k} and d_{D_k} are the distances of $PB \rightarrow T_k$ and $T_k \rightarrow T_{k+1}$, respectively, ε denotes the path-loss exponent, and Ω_{P_k} and m_z denote the mean and the integer fading factor.

5.1.3.2 NOMA throughput analysis

First, we calculate the probability $\Pr\left(\bar{C}_{e2e}^n \geq \gamma_{th}\right)$. Taking $n < N$ and combining (5.5)–(5.7), we obtain

$$\Pr\left(\bar{C}_{e2e}^n \geq \gamma_{th}\right) = \prod_{k=1}^{K} \Pr\left(\bar{C}_k^n \geq \gamma_{th}\right) = \prod_{k=1}^{K} \Pr\left(\frac{\rho a_n \delta \bar{h}_{P_{k-1}} \bar{h}_{D_k}}{\left(\kappa^2 + \sum_{i=n+1}^{N} a_i\right)\rho\delta \bar{h}_{P_{k-1}} \bar{h}_{D_k} + 1} \geq \theta\right) \tag{5.16}$$

where $\theta = 2^{\frac{\gamma_{th}}{(1-\alpha)\tau}} - 1$ is the SINR threshold.

It is obvious from (5.16) that if $a_n - \theta \left(\kappa^2 + \sum_{i=n+1}^{N} a_i \right) \leq 0$, then $\Pr \left(\bar{C}_{e2e}^n \geq \gamma_{th} \right) = 0$, and

if $a_n - \theta \left(\kappa^2 + \sum_{i=n+1}^{N} a_i \right) > 0$, (5.16) becomes:

$$\Pr \left(\bar{C}_{e2e}^n \geq \gamma_{th} \right) = \prod_{k=1}^{K} \Pr \left(\bar{h}_{P_{k-1}} \bar{h}_{D_k} \geq \bar{\sigma}_n \right), \tag{5.17}$$

where

$$\bar{\sigma}_n = \frac{\theta}{\left[a_n - \left(\kappa^2 + \sum_{i=n+1}^{N} a_i \right) \theta \right] \rho \delta}. \tag{5.18}$$

Remark 3: The transmit power ratio a_n must be carefully designed so that the conditions $a_n - \theta \left(\kappa^2 + \sum_{i=n+1}^{N} a_i \right) > 0$ are satisfied.

Now, the probability $\Pr \left(\bar{h}_{P_{k-1}} \bar{h}_{D_k} \geq \bar{\sigma}_n \right)$ can be formulated as

$$\Pr \left(\bar{h}_{P_{k-1}} \bar{h}_{D_k} \geq \bar{\sigma}_n \right) = \int_0^{+\infty} \left(1 - F_{\bar{h}_{P_{k-1}}} \left(\frac{\bar{\sigma}_n}{x} \right) \right) f_{\bar{h}_{D_k}} (x) \, dx. \tag{5.19}$$

Inserting (5.11), (5.12), (5.13) and (5.14) into (5.19), and then using [117, Eq. (3.471.9)], we obtain

$$
\begin{aligned}
\Pr \left(\bar{C}_{e2e}^n \geq \gamma_{th} \right) &= \prod_{k=1}^{K} \left[\int_0^{\infty} \left(1 - F_{P_{k-1}} \left(\frac{\bar{\sigma}_n}{x} \right) \right) f_{D_k} (x) \, dx \right] \\
&= \prod_{k=1}^{K} \left[\sum_{l=0}^{m_{P_{k-1}}-1} \frac{\bar{\sigma}_n^l}{l! \beta_{P_{k-1}}^l \Gamma (m_{D_k}) \beta_{D_k}^{m_{D_k}}} \times \int_0^{\infty} e^{-\frac{\bar{\sigma}_n}{\beta_{P_{k-1}} x} - \frac{x}{\beta_{D_k}}} x^{m_{D_k}-l-1} dx \right] \\
&= \prod_{k=1}^{K} \left[\sum_{l=0}^{m_{P_{k-1}}-1} \frac{2\rho_n^l}{l! \beta_{P_{k-1}}^l \Gamma (m_{D_k}) \beta_{D_k}^{m_{D_k}}} \times \left(\frac{\beta_{D_k} \bar{\sigma}_n}{\beta_{P_{k-1}}} \right)^{\frac{m_{D_k}-l}{2}} K_{m_{D_k}-l} \left(2\sqrt{\frac{\bar{\sigma}_n}{\beta_{P_{k-1}} \beta_{D_k}}} \right) \right]
\end{aligned}
\tag{5.20}
$$

where $K_u (.)$ represents the uth order of the modified Bessel function of the second kind [117, Eq. (3.471.9)].

Similarly, when $n = N$, we obtain

$$\Pr \left(\bar{C}_{e2e}^N \geq \gamma_{th} \right) = \prod_{k=1}^{K} \left[\sum_{l=0}^{m_{P_{k-1}}-1} \frac{2\bar{\sigma}_N^l}{l! \beta_{P_{k-1}}^l \Gamma (m_{D_k}) \beta_{D_k}^{m_{D_k}}} \times \left(\frac{\beta_{D_k} \bar{\sigma}_N}{\beta_{P_{k-1}}} \right)^{\frac{m_{D_k}-l}{2}} K_{m_{D_k}-l} \left(2\sqrt{\frac{\bar{\sigma}_N}{\beta_{P_{k-1}} \beta_{D_k}}} \right) \right] \tag{5.21}$$

where $\bar{\sigma}_N = \frac{\theta}{(a_N - \kappa^2\theta)\rho\delta}$.

Inserting (5.8), (5.20) and (5.21), the exact closed-form formula of $\mathcal{T}_{\mathrm{NOMA}}$ is obtained:

$$\mathcal{T}_{\mathrm{NOMA}} = (1 - \alpha)\,\tau\gamma_{th}$$
$$\times \left\{ \sum_{n=1}^{N} \prod_{k=1}^{K} \left[\sum_{l=0}^{m_{P_{k-1}}-1} \frac{2\bar{\sigma}_N^l}{l!\beta_{P_{k-1}}^l \Gamma(m_{D_k})\beta_{D_k}^{m_{D_k}}} \times \left(\frac{\beta_{D_k}\bar{\sigma}_N}{\beta_{P_{k-1}}}\right)^{\frac{m_{D_k}-l}{2}} K_{m_{D_k}-l}\left(2\sqrt{\frac{\bar{\sigma}_N}{\beta_{P_{k-1}}\beta_{D_k}}}\right) \right] \right\}.$$
$$(5.22)$$

5.1.3.3 OMA throughput analysis

For multi-hop relaying using OMA, we obtain

$$\Pr\left(\bar{C}_{\mathrm{e2e}}^{\mathrm{OMA}} \geq \gamma_{th}\right) = \prod_{k=1}^{K} \Pr\left(\bar{h}_{P_{k-1}}\bar{h}_{D_k} \geq \bar{\xi}\right)$$
$$= \prod_{k=1}^{K} \left[\sum_{l=0}^{m_{P_{k-1}}-1} \frac{2\bar{\xi}^l}{l!\beta_{P_{k-1}}^l \Gamma(m_{D_k})\beta_{D_k}^{m_{D_k}}} \times \left(\frac{\beta_{D_k}\bar{\xi}}{\beta_{P_{k-1}}}\right)^{\frac{m_{D_k}-l}{2}} K_{m_{D_k}-l}\left(2\sqrt{\frac{\bar{\xi}}{\beta_{P_{k-1}}\beta_{D_k}}}\right) \right] \quad (5.23)$$

where $\bar{\xi} = \frac{\theta}{(1-\kappa^2\theta)\rho\delta}$.

From (5.23), the throughput $\mathcal{T}_{\mathrm{OMA}}$ is expressed as

$$\mathcal{T}_{\mathrm{OMA}} = (1 - \alpha)\,\tau\gamma_{th}$$
$$\times \prod_{k=1}^{K} \left[\sum_{l=0}^{m_{P_{k-1}}-1} \frac{2\bar{\xi}^l}{l!\beta_{P_{k-1}}^l \Gamma(m_{D_k})\beta_{D_k}^{m_{D_k}}} \times \left(\frac{\beta_{D_k}\bar{\xi}}{\beta_{P_{k-1}}}\right)^{\frac{m_{D_k}-l}{2}} K_{m_{D_k}-l}\left(2\sqrt{\frac{\bar{\xi}}{\beta_{P_{k-1}}\beta_{D_k}}}\right) \right]. \quad (5.24)$$

5.1.4 Numerical results

Here, we address the main parameters of the Monte Carlo simulation. The source node is located at the origin $(0,0)$ and the destination is at $(1,0)$, and therefore the distance between the source node and destination node is 1. The coordinates of the relay T_k and the power beacon PB are then $(k/K, 0)$ and $(0.5, 0.5)$, respectively, where $k = 1, 2, ..., K-1$. We set $m_{P_{k-1}} = m_{P_k} = m_{D_{k-1}} = m_{D_k} = m = 2$. Three NOMA schemes are considered as follows. In scheme I, we consider $a_1 = 0.85$, $a_2 = 0.15$, and $N = 2$; in scheme II, we set $a_1 = 0.85$, $a_2 = 0.12$, $a_3 = 0.03$, and $N = 3$; in scheme III, the parameters are $a_n \in \{0.85, 0.12, 0.025, 0.005\}$, where $n = 1, 2, 3, 4$, and $N = 4$. The Monte-Carlo results are averaged over 10^7 independent channel executions. Table 5.1 summarizes the specific parameters.

Table 5.1: System parameters used in the throughput evaluation.

System Parameters	Values
Aggregate impairment level	$\kappa^2 = 0.01$
Targeted data rate	$\bar{\gamma}_{th} = 0.1$
Total transmission time	$Q = 1$
Pass loss exponent	$\varepsilon = 3$
Energy conversion efficiency	$\eta = 1$
Fraction of the block time	$\alpha = 0.1$
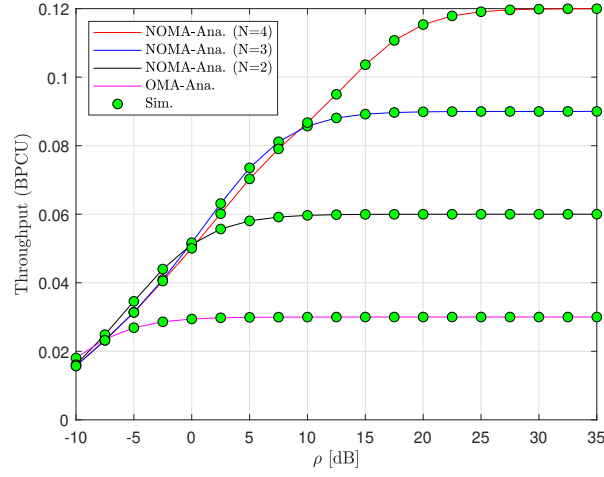
Figure 5.2: Throughput with $m = 2$, $\kappa^2 = 0.01$, $\alpha = 0.1$ and $K = 3$
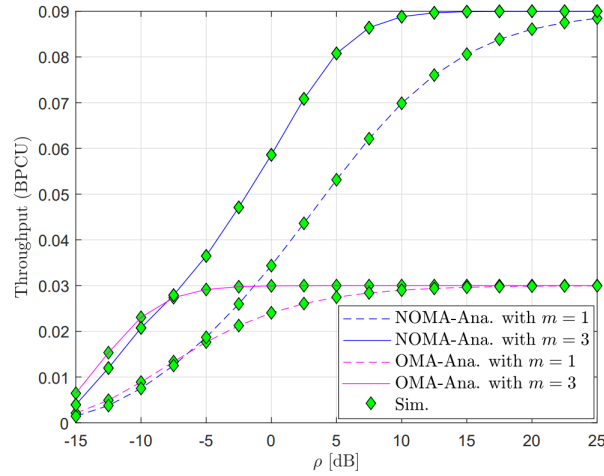
Figure 5.3: Throughput with $\kappa^2 = 0.01$, $\alpha = 0.1$ and $K = 3$

Figure 5.2 plots the relationship between throughput and transmit SNR, where parameters $m = 2, \kappa^2 = 0.01, \alpha = 0.1$ and $K = 3$, and different throughput performance curves

depending on N, the number of superposed signals. NOMA-analytical $N = 4$ indicates the best performance. Compared to OMA, NOMA outperforms OMA significantly.
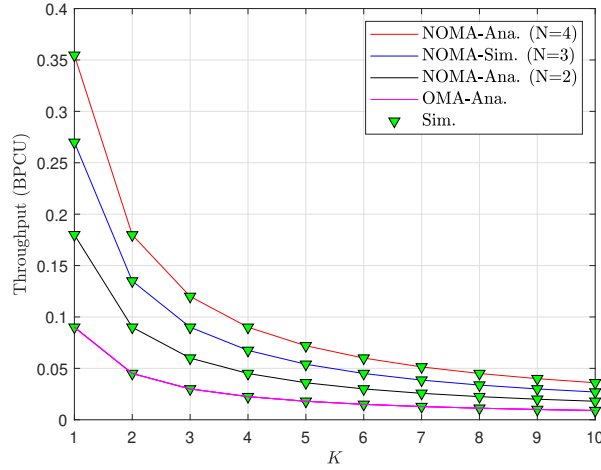
Figure 5.4: Throughput where $\kappa^2 = 0$, $m = 3$ and $\rho = 25$ (dB)
.
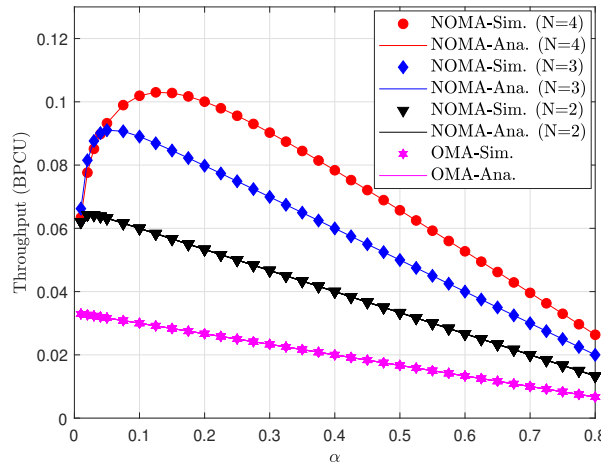
Figure 5.5: Throughput where $K = 3$, $\kappa^2 = 0$, $m = 3$ and $\rho = 10$ (dB)
.

Figure 5.3 shows the relationship between throughput and transmit SNR, where $\kappa^2 = 0.01$, $\alpha = 0.1$ and $K = 3$, and different throughput performance curves depending on the Nakagami-m fading parameter m, with NOMA-analytical $m = 3$ performing the best. Compared to OMA, NOMA outperforms OMA significantly. The throughput of OMA also reaches a ceiling at transmitting SNR $\rho = 10dB$.

Figure 5.4 and Figure 5.5 indicate the continuous trend of NOMA outperforming OMA. However, in Figure 5.4 shows a reduction in throughput with the addition of K hops. Figure. 5.5 also reveals a major decrease in throughput beyond the optimal α. This highlights the importance of designing optimal time-switching protocols. All analytical curves match the Monte Carlo simulation results well.

5.1.5   Conclusion

This section provided a throughput analysis of a NOMA-assisted wireless EH multi-hop decode-and-forward network. Exact throughput expressions were derived for NOMA and OMA assistance. The simulation results indicate that time-switching and the number of relays have a significant effect on throughput.

5.2 Self-learning Clustering Protocol in Wireless Sensor Networks for IoT applications

A WSN-based IoT is considered in this section. Wireless sensor networks have been deployed in many applications to monitor the environment or collect data from objects [NNT05], [NNT09], and [NNT10]. The network topology requires high reliability connections with low energy consumption at the sink node and long network lifetime. To address the first aim, I propose a self-learning clustering protocol to discover neighbors and the network topology. The cluster head is selected according to the information from neighbors and the residual energy of the node. The maximum number of cluster members is set according to the network's density. The proposed protocol is able to adapt to changes in the dynamic network and consume low energy, thereby ensuring network connectivity. The results show that the proposed clustering protocol performs well in terms of long network lifetime and high throughput compared to other clustering protocols and are verified with independent Monte Carlo simulations [NNT10].

5.2.1 Introduction

Wireless sensor networks have been deployed in many applications to monitor the environment or collect data from objects. Sensors are categorized into many types, for example static or mobile devices, which can be deployed to collect information about their deployment areas. In the era of the Internet of Things (IoT), these types of sensors can be distributed in many applications to perform sensing, monitoring or controlling [14]. WSN-based IoT integrates a WSN, gateway server, middle-ware, and mobile clients [118, 119]. WSN-based IoT can be deployed in smart cities to monitor the environment or urban areas, with low energy consumption [120, 121, 122]. Some WSN-based IoT networks fit the description of device-to-device (D2D) or machine-to-machine (M2M) connections and have attracted considerable attention from the research community. The quality of service (QoS) in these networks delivers good connectivity, long lifespan, high throughput and low latency. IoT objects or sensors are randomly distributed throughout the network; network lifetime is therefore affected by the link connectivity and transmission activities of sensors. In a WSN-based IoT, network topology can be divided into many clusters to save energy and extend lifespan [123, 53].

Sensor nodes can be grouped into clusters, each which consists of a cluster head and several cluster members [121, 122, 123, 53, 124]. The network contains many sensors which collect data on their environment and forward them to a sink. In LEACH, the cluster head is selected using a random value [123]. In [53], the modified LEACH selects some nodes to become cluster relays to forward data from one cluster to the sink. Effective cluster head

selection algorithms may result in high network lifespan and throughput to fulfill QoS requirements. Other studies have selected the cluster head by considering the network topology [124].

This section examines the network of a WSN-based-IoT application consisting of sensor nodes, routers and a sink. A Self-learning Clustering Protocol (SLCP) which evaluates the number of neighbors and residual energy in nodes is proposed for maintaining the network's topology. The cluster head is selected from the number and average distance to neighbors and the node's residual energy. The maximum number of cluster members is defined by the node density and ensures strong node connectivity.

5.2.2 Self-learning Clustering Protocol in WSN-IoT

5.2.2.1 Network model

The network consists of a sink and multiple nodes which are deployed in the area $L(m) \times L(m)$. The sensor nodes support IoT applications which transmit the collected data to the sink. The number of nodes in the network is N, and each node denoted n_i. Each node knows its own location and the location of the sink. Each cluster has one cluster head (CH) and M cluster members (CM). The node which does not belong to any cluster is a cluster relay (CRe). The CRe is able to transmit data directly to the sink. Some reasonable assumptions are:

- Nodes are randomly distributed in the area of $L \times L$ meters with the same initial energy of 0.5 J. The sink's location is fixed.

- Sensor nodes have certain limitations for energy, storage, radio communication capabilities, and bandwidth.

- The CM will transmit data to the CH, which then forwards the aggregated data to the sink. The CH is selected according to the residual energy, number of neighbors and average distance to neighbors.

- The CH maintains the number of CMs according to the network's density.

5.2.2.2 Energy consumption model

Let us assume that the energy consumption model follows the energy consumption model in [123]. The energy consumed to transmit the $l - bits$ message (E_{tx}) and to receive the message (E_{rx}) as in [123] is expressed as, respectively:

$$E_{tx} = l \cdot E_{\text{elec}} + \frac{l}{R} P_t \tag{5.25}$$

39

$$E_{rx} = l \cdot E_{elec} \tag{5.26}$$

where E_{elec} is the electronics energy dissipated per bit, R is the transmission rate (bit/s), and P_t is the transmitted power. Here, l/R expresses the time required to send the message.

5.2.2.3 Self-learning Clustering Protocol (SLCP)
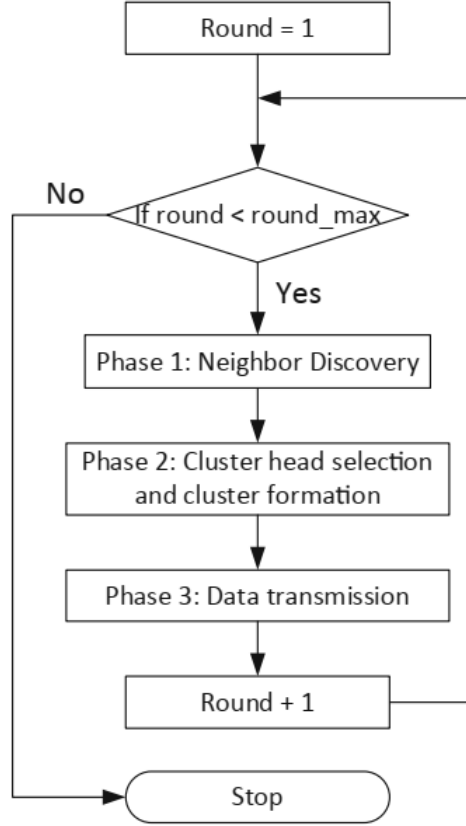
Figure 5.6: A self-learning clustering protocol in a WSN for IoT applications.

- **SLCP**

Figure 5.6 depicts the flowchart of the SLCP, which consists of three phases: Phase 1 is neighbor discovery; Phase 2 is cluster head selection and cluster formation; Phase 3 is the data transmission phase.

- **Neighbor Discovery**

In this phase, each node broadcasts a "HELLO" message which contains the node ID (n_i), node location (x_i, y_i) and residual node energy $(E_{res}(n_i))$.
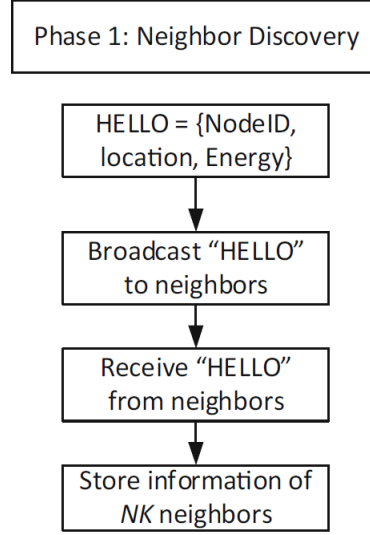
Figure 5.7: Neighbor discovery procedure.

If any nodes n_j fall within the transmission range of n_i, node n_j will successfully receive the "HELLO" message. Node n_i will then add node n_j to the list of neighbors according to the equation $\{Nei(i) = Nei(i) \cup n_j \mid d(i,j) < Tx\}$ and vice versa (Fig. 5.7).

- **Cluster Head Selection and Cluster Formation Procedure**

The cluster head is selected according to its residual energy, number of neighbors and average distance to neighbors. The number of neighbors is determined after receiving the "HELLO" message in Phase 1 . The average distance of node n_i is the average of distance to all cluster members, calculated from the equation $\{dst\,(n_i) = average\,(distance\,(n_i, n_j)) \mid n_j \in Nei\,(n_i)\}$. To control the network's topology, the average number of cluster members (M) is set according to the network's node density. Node density is denoted K and calculated from

$$K = \frac{L \times L}{\pi \times Tx^2},\tag{5.27}$$

$$M \leq K,\tag{5.28}$$

where $L \times L$ is the network area, and Tx is the transmission range of the node. Each node can is able to be a cluster head by calculating the probability of being selected as a CH. The probability of n_i being a CH is denoted $pCH(i)$ and calculated from the desired node degree, number of neighbors and residual energy:

$$p_{CH}(i) = p_{opt}\left(\alpha\frac{E_{res}}{E_{\text{init}}} + \beta\frac{dst}{Tx} + \gamma\frac{NK}{K}\right),\tag{5.29}$$

41

$$\alpha + \beta + \gamma = 1, \tag{5.30}$$

where p_{opt} is the optimal probability of being a CH, E_{res} is the residual energy, E_{init} is the initial energy, dst is the average distance to all neighbors, Tx is the transmission range, NK is the number of neighbors, and K is the maximum number of cluster members; α, β, γ represent the energy coefficient, average distance coefficient, and the number of cluster members coefficient, respectively. To balance the number of cluster heads in the network, we denote $G(r)$ as the set of nodes which are not the CH in the previous round r, as in the LEACH protocol in [123, 53]. The node will generate a random number (rdn) between 0 and 1. If the random number is less than the threshold $P_{th}(n_i)$, the node becomes a CH. The probability threshold of selecting a cluster head is defined by

$$P_{th}(n_i) = \begin{cases} \frac{p_{CH}(i)}{1 - p_{CH}(i)\left(r \bmod \left(\frac{1}{p_{CH}(i)}\right)\right)}, & \text{if } n_i \in G(r) \\ 0, & \text{otherwise} \end{cases} \tag{5.31}$$

In Phase 2, each node generates a random number rdn and then compares it to the $P_{th}(n_i)-$ the probability of being a cluster head (Fig. 5.8). If the rdn is less than the $P_{th}(n_i)$, node n_i is elected as the cluster head. Node n_i then transmits a join request "JOIN_RQT" to its neighbors.

Otherwise, node n_i can become a cluster member or cluster relay. If node n_i receives the "JOIN_RQT" from the CH, node n_i will join the cluster by transmitting the message "JOIN_ACK" to the CH. If node n_i does not receive any "JOIN_RQT" message, node will become CRe and send data directly to the sink. If node n_i receives more than one "JOIN_RQT" message, node n_i will select the CH with the minimum distance to join.

In Phase 3, the CH schedules the transmission of each CM in a TDMA frame. Each CM wakes up and transmits data during a predefined slot. The CH forwards the aggregated data to the sink node by performing a carrier sense multiple access with collision avoidance (CSMA/CA).

5.2.3   Performance evaluation

5.2.3.1   Simulation environment

In the simulations here, nodes were uniformly deployed at random in a $50 \times 50m^2$ field [119]. The sink node was fixed at the center of the network area. The percentage of cluster heads in the network varied over during the simulation time. Each node calculated the node density and probability of becoming a cluster head using (5.27) and (5.29), respectively. In WSN-based-IoT applications, we assume the network consists of N heterogeneous nodes. Any
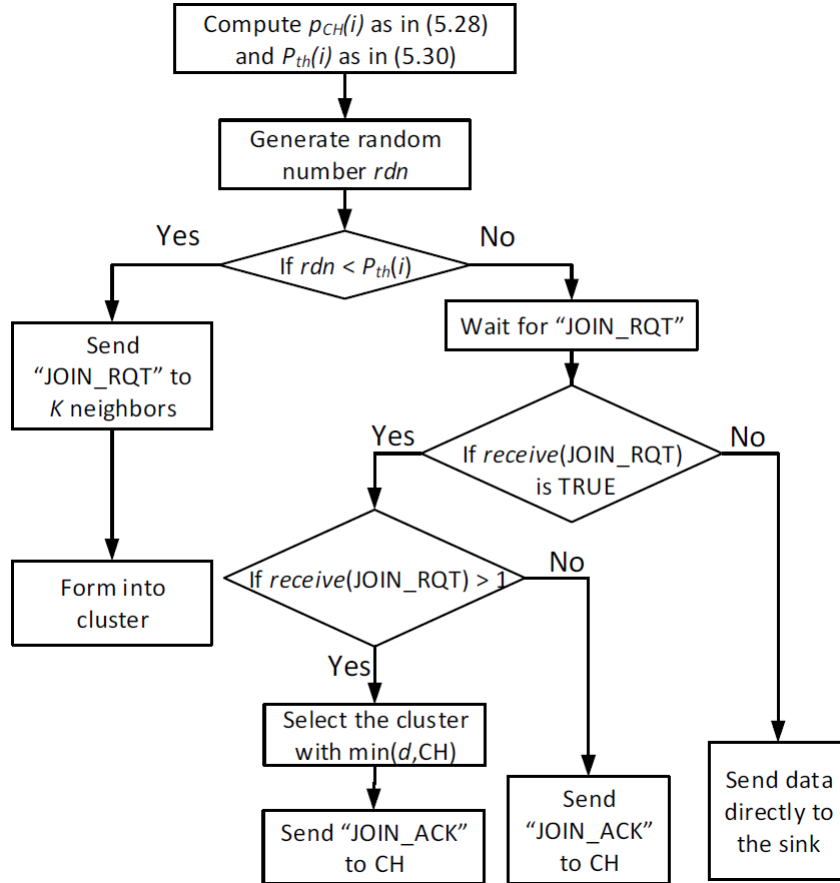
Figure 5.8: The cluster formation procedure.

node may elect to be the cluster head or a cluster relay. The energy consumption model for transmitting and receiving data was calculated according to the model in [123, 53]. SLCP was compared to the LEACH and Modified LEACH in [123, 53]. The detailed simulation parameters are listed in Table 5.2. To focus on energy efficiency, the energy coefficient was set to 0.5 and the other coefficients to 0.25.

5.2.3.2   Simulation results

- **Network Lifetime**

To evaluate the network performance, network lifetime is measured by the number of alive nodes in the network. Network lifetime is calculated as the duration until a half of its nodes shut down because of depleted batteries. The simulation results in Figure 5.9 reveal that the number of alive nodes in SLCP is greater than in LEACH or Modified LEACH. With SLCP, the cluster head is selected according to the number of neighbors, which may change as a

Table 5.2: Simulation parameters

Parameter	Value
Network size	$50m \times 50m$
Number of nodes	100
Packet size	4000 bits
Probability p_{opt}	0.5
α (energy coefficient)	0.5
β (distance coefficient)	0.25
γ (cluster member coefficient)	0.25
Initial energy E_0	0.5 J
Energy for data aggregation	5/nbit/signal
Transmitting and receiving energy E_{elect}	5 nJ/bit

result of mobility. SLCP is therefore able to select the effective CH, which reduces energy consumption during transmission.
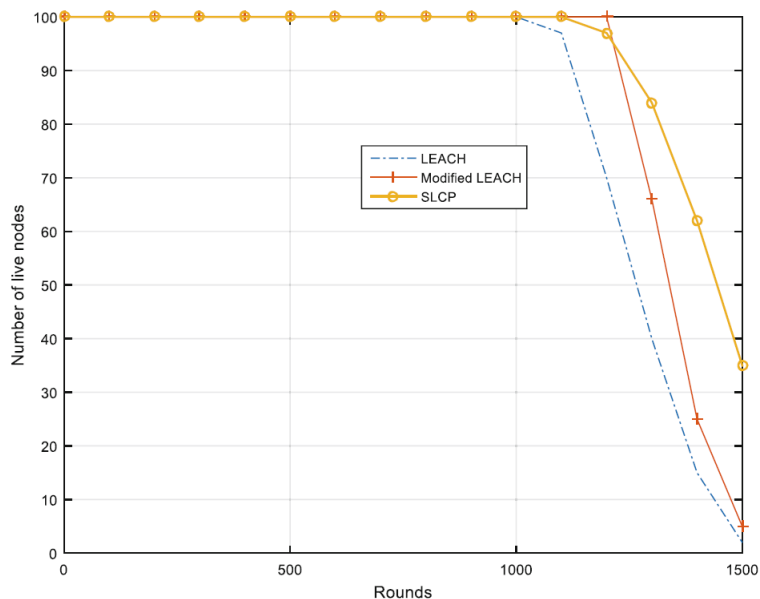
Figure 5.9: Number of live nodes.

- **Residual Energy.**

Figure 5.10 shows that the average residual energy with SLCP is greater than LEACH or Modified LEACH. The number of CMs is limited to a predefined number, resulting in fewer transmissions in the network. The CH is selected according to residual energy; any node with low residual energy will therefore not become a CH. The CM will also select the CH with the minimum distance to join, which results in lower energy consumption during transmission.
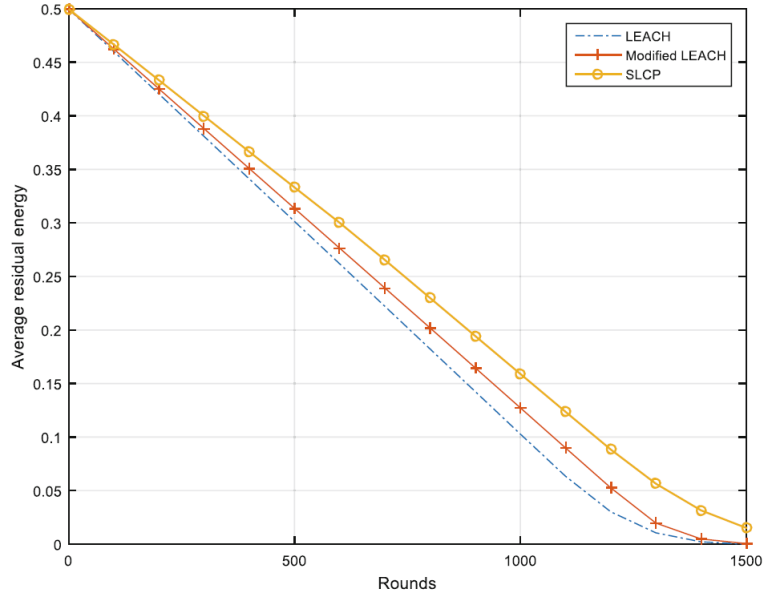
Figure 5.10: Average residual energy at one node.
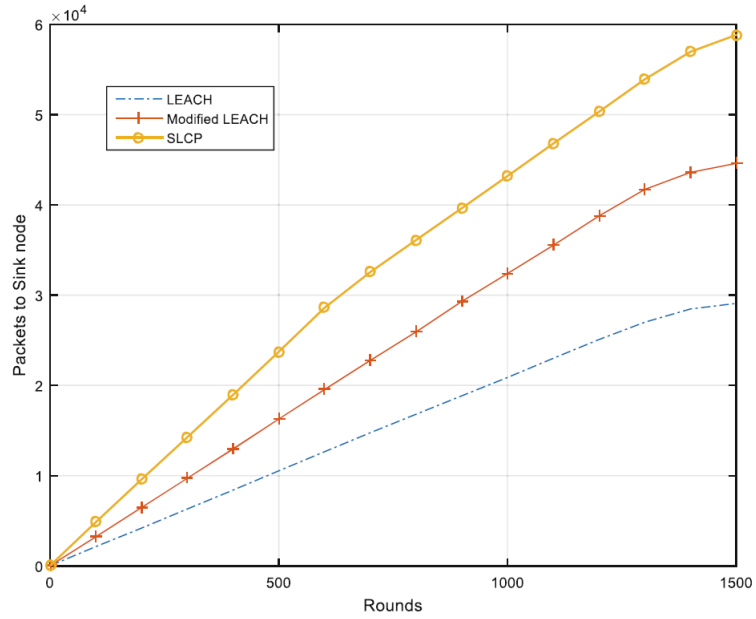
Figure 5.11: Total successfully received packets at the sink.

Furthermore, CHs are selected according to the network density and number of neighbors in the network topology. If any node has shut down, the CH will learn about this by receiving the message "JOIN_ACK". Consequently, the CH in the previous round may become a CH in the next round, thereby reducing the number of broadcast messages. The node also calculates the network's node density, and the CH will therefore select suitable cluster members for

prolonging network connectivity and receiving high numbers of packets.

- **Successfully Received Packets at the Sink.**

The successfully received packets at the sink are the sum of the packets transmitted from the nodes to the sink node (Fig. 5.11). SLCP achieves better performance than LEACH and Modified LEACH in terms of greater numbers of successfully received packets. SLCP achieves a longer network lifetime and higher residual energy for transmitting and receiving greater numbers of packets.

5.2.4   Conclusion

This section described a proposed SLCP algorithm to maintain the number of cluster members while considering changes in the network topology. Sensors for IoT applications require long network lifespan and high residual energy. Analysis of the simulation results reveal that SLCP is effective in a dynamic network by learning the network's topology. SLCP therefore outperforms other clustering protocols by sustaining a longer network lifetime and successfully receiving a greater number of packets at the sink node.

Chapter 6

Impact of Generalized Fading Channels and CCI on System Performance

6.1 Outage performance analysis of NOMA under η - μ fading channels with conditions of imperfect SIC

For the second aim, the effect of generalized fading in a NOMA system with $\eta - \mu$ fading channels was investigated. Closed-form expressions for outage probability (OP) and system throughput under conditions of perfect SIC (pSIC) and imperfect SIC (ipSIC) were derived. The expressions were numerically analyzed by varying system parameters such as fading channels, power level coefficients, and the number of antennae at receivers. The results indicated that each parameter is significant in enhancing the user's signal quality and improving the system's OP. The results were verified with Monte Carlo simulations [NNT03].

6.1.1 Introduction

The NOMA technique has proven its immense advantages in the trending technologies for wireless networks. During data transmission in NOMA, signals are superimposed and sent to the user. At the user's end, the successive interference cancellation (SIC) technique is applied to separate these superimposed signals [125]. During this procedure, the system is fully aware of the channel state information (CSI). In ideal research cases, the CSI and SIC are considered perfect, although these conditions can be fully imperfect in real-time scenarios. Any study of minimal imperfections would therefore be a valid direction in practical research.

Although NOMA has immense advantages in wireless networking, it also has major challenges such as multipath fading and shadowing effects. Few statistical models can differentiate multipath fading based on line-of-sight (LoS) and non-LoS (NLoS) such as Rayleigh, Rice, Rician, Nakagami-m, etc. [126, 127, 128]. Research on various performance measurements

47

such as OP, channel capacity and bit error rate has been performed to understand the effects. $\alpha - \eta - \mu$ is considered a more generalized fading model for understanding mathematical evaluations and performance comparisons in any system. A number of authentic studies have also evaluated the performance of fading models such as $\alpha - \mu$, $\alpha - \eta$, $\eta - \mu$, $\lambda - \mu$, and $\kappa - \mu$ [129, 130] in terms of OP, bit error rate and average capacity. In [131], the author studied the generalized fading effect of combined $\alpha - \eta - \mu$ channels. In $\eta - \mu$ channels, η is the correlation between in-phase and quadrature multipath clusters, and μ defines the number of multipath clusters. Similarly, in $\kappa - \mu$ channels, κ represents the ratio of power dominants, and μ defines the number of multipath clusters. The special cases of $\eta - \mu$ are Rayleigh, Nakagami-m and Hoyt distributions, and the special cases of $\kappa - \mu$ are Rayleigh, Nakagami-m, and Rician distributions. Generalized fading channels are evaluated according to the performance of channels.

As mentioned above, the effect of fading has a significant role in analyzing the efficacy of a system. Studying the effect of various fading models in the NOMA system is therefore still a major task. Although a few research articles have studied $\alpha - \eta - \mu$, only the ideal cases such as perfect CSI and pSIC were examined. Motivated by this analysis, this chapter provides a detailed analysis of the OP of a NOMA system with two users under $\eta - \mu$ fading distribution in different scenarios. The ipSIC scenario and its effect on the fading channel is also discussed. The major contributions of this section are derived expressions of exact OP and throughput for a NOMA system with two users under $\eta - \mu$ fading distribution in pSIC and ipSIC conditions, and a validation of the system performance based on these derived expressions and Monte Carlo simulations.

6.1.2 System model and channel characteristics

6.1.2.1 System model

The system model shown in Figure 6.1 consists of a base station (BS) which transmits the signals between two users D_1 and D_2, using the NOMA technique over $\eta - \mu$ fading channels. D_1 and D_2 have M and N antennae, respectively. The channels from the BS to D_1 and D_2 are $g_{1,m}$ and $g_{2,n}$, respectively. The signals received at two NOMA users D_1 and D_2 are given by [132].

$$\tilde{y}_1^m = g_{1,m} \left(\sqrt{P\nu_1}\tilde{x}_1 + \sqrt{P\nu_2}\tilde{x}_2 \right) + \tilde{\omega}_1^m, \tag{6.1}$$

$$\tilde{y}_2^n = g_{2,n} \left(\sqrt{P\nu_1}\tilde{x}_1 + \sqrt{P\nu_2}\tilde{x}_2 \right) + \tilde{\omega}_2^n, \tag{6.2}$$

where P denotes the normalized transmission power at the BS, $\tilde{\omega}_1^m \sim \mathcal{CN}(0, N_0)$ and $\tilde{\omega}_2^n \sim \mathcal{CN}(0, N_0)$ denote the additive white Gaussian noise (AWGN) at the user nodes D_1
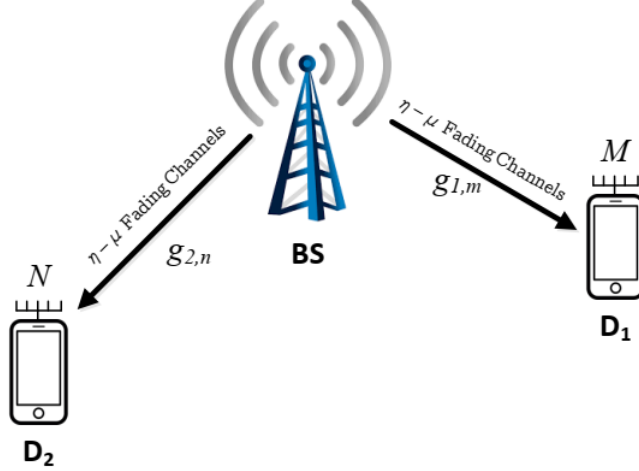
Figure 6.1: Downlink NOMA with $\eta - \mu$ fading channels.

and D_2, respectively, and $\tilde{x}_1$ and $\tilde{x}_2$ are assumed to be normalized unity power signals for the two users, i.e., $E\left\{|\tilde{x}_1|^2\right\} = E\left\{|\tilde{x}_2|^2\right\} = 1$, where E is the Expectation operator. The power allocation factor ν_j satisfies the relationship $\nu_2 > \nu_1$ for $\sum_{j=1}^{2} \nu_j = 1$, which is for the purpose of fairness between users.

In the first phase, the signal to interference-plus-noise ratio (SINR) after treating $\tilde{x}_1$ as interference is given by

$$\tilde{\Gamma}_{D_1,x_2}^{m} = \frac{\nu_2 P|g_{1,m}|^2}{1 + \nu_1 P|g_{1,m}|^2} = \frac{\nu_2 \rho \gamma_1}{1 + \nu_1 \rho \gamma_1}, \tag{6.3}$$

where $\gamma_1 \triangleq |g_{1,m}|^2$, and the transmit signal-to-noise ratio (SNR) calculated at the BS is $\rho = P/N_0$. Note that γ_1 and γ_2 are independent random variables (RVs).

Under ipSIC conditions, the SINR of detect $\tilde{x}_2$ is given as in [133]

$$\tilde{\Gamma}_{D_1,x_1}^{m,ipSIC} = \frac{\nu_1 \rho \gamma_1}{1 + \rho|h_I|^2}, \tag{6.4}$$

where $|h_I|^2 \sim \mathcal{CN}\left(0, \lambda_I\right)$ such that $\lambda_I \left(0 \leq \lambda_I < 1\right)$ indicates the level of residual interference caused by ipSIC as in [134] and $\mathcal{CN} \sim (x, y)$ is the complex normal distribution with average x and variance y.

Similarly, the instantaneous SINR at D_2 to detect $\tilde{x}_2$ is expressed as

$$\tilde{\Gamma}_{D_2,x_2}^{n} = \frac{\nu_1 P|g_{2,n}|^2}{1 + |g_{2,n}|^2 P \gamma_2} = \frac{\nu_1 \rho \gamma_2}{1 + \nu_2 \rho \gamma_2}, \tag{6.5}$$

where $\gamma_2 \triangleq |g_{2,n}|^2$.

6.1.2.2 Channel Characteristics

First, let us suppose that the antenna numbers of two users are equivalent, i.e., $N = M$. The probability density function (PDF) of $\gamma = \gamma_1 = \gamma_2$ as given by [135, Eq. (1)] is

$$f_\gamma(x) = \frac{2\sqrt{\pi}\mu^{\mu-0.5}h^\mu x^{\mu-0.5}}{\Gamma(\mu) H^{\mu-0.5}\bar{\gamma}^{\mu-0.5}} e^{-\frac{2\mu h}{\bar{\gamma}}x} I_{\mu-0.5}\left(\frac{2\mu H}{\bar{\gamma}}x\right), \tag{6.6}$$

where $\Gamma(x)$ is the Gamma function, $I_z(.)$ is the modified Bessel function of the first kind, $\bar{\gamma} = \mathbb{E}\{\gamma\}$, μ represents the fading severity, $h = (2 + \eta^{-1} + \eta)/4$ and $H = (\eta^{-1} - \eta)/4$ such that $0 < \eta < \infty$ for arbitrary values of μ. According to [130, Eq. (2)], the cumulative distribution functions (CDF) of γ are expressed as

$$F_\gamma(x) = \frac{(\Lambda_1\Lambda_2)^\mu}{\Gamma(1+2\mu)}x^{2\mu}\Phi_2(\mu, \mu; 1+2\mu; -\Lambda_1 x, -\Lambda_2 x), \tag{6.7}$$

where $\Phi_2 \equiv \Phi_2^{(2)}$ is the confluent Lauricella function [136], $\Lambda_1 = \frac{2\mu(h-H)}{\bar{\gamma}}$ and $\Lambda_2 = \frac{2\mu(h+H)}{\bar{\gamma}}$. For integer values of μ and with the help of [137, Eq. (15)] and [117, Eq. (8.352.6)], $F_\gamma(x)$ can be greatly simplified to

$$F_\gamma(x) = \frac{\sqrt{\pi}}{\Gamma(\mu)} \sum_{k=0}^{\infty} \frac{H^{2k}\Gamma(2(\mu+k))}{k!\Gamma(\mu+k+0.5)2^{2(\mu+k)-1}h^{\mu+2k}} \left[1 - e^{-2\mu hx} \sum_{l=0}^{2(\mu+k)-1} \frac{(2\mu h)^l x^l}{m!}\right]. \tag{6.8}$$

Finally, we obtain PDF and CDF of $|h_I|^2$ as in [138]

$$f_{|h_I|^2}(x) = \frac{1}{\lambda_I}e^{-\frac{x}{\lambda_I}}, \tag{6.9}$$

$$F_{|h_I|^2}(x) = 1 - e^{-\frac{x}{\lambda_I}}. \tag{6.10}$$

6.1.3 Analysis of outage probability

The OP of D_1 under ipSIC is calculated as

$$\begin{aligned}
\tilde{P}_{D_1}^{ipSIC} &= \Pr\left(\underbrace{\max}_{m\in M}\left\{\tilde{\Gamma}_{D_1,x_2}^m\right\} < \tilde{\gamma}_{th2}| \underbrace{\max}_{m\in M}\left\{\tilde{\Gamma}_{D_1,x_1}^{m,ipSIC}\right\} < \tilde{\gamma}_{th1}\right) \\
&= \prod_{n=1}^{N}\left[1 - \Pr\left(\tilde{\Gamma}_{D_1,x_2}^m > \tilde{\gamma}_{th2}, \tilde{\Gamma}_{D_1,x_1}^{m,ipSIC} > \tilde{\gamma}_{th1}\right)\right] \\
&= \left[1 - \Pr\left(\gamma_1 > \delta_2, \gamma_1 > \delta_1\left(\rho|h_I|^2 + 1\right)\right)\right]^M,
\end{aligned} \tag{6.11}$$

where $\tilde{\gamma}_{thi} = 2^{2R_i} - 1$, for $i = 1, 2$ is called the target rate at D_i, $\delta_2 = \tilde{\gamma}_{th2}[\rho(\nu_2 - \nu_1\tilde{\gamma}_{th2})]^{-1}$ and $\delta_1 = \tilde{\gamma}_{th1}(\nu_1\rho)^{-1}$. We assume that $\delta_1\left(\rho|h_I|^2 + 1\right) \gg \delta_2$, $\tilde{P}_{D_1}^{ipSIC}$ can be calculated by

$$
\begin{aligned}
\tilde{P}_{D_1}^{ipSIC} &= \left[1 - \Pr\left(\gamma_1 > \delta_1\left(\rho|h_I|^2 + 1\right)\right)\right]^M \\
&= \left\{1 - \int_0^\infty f_{|h_I|^2}(x)\left[1 - F_{\gamma_1}\left(\delta_1\left(\rho x + 1\right)\right)\right]dx\right\}^M.
\end{aligned}
\tag{6.12}
$$

<u>Case 1</u>: When $\mu \in \mathbb{N}, \forall \mu \geq 0$, then we use PDF of (6.9) and CDF of (6.8), (6.12):

$$
\begin{aligned}
\tilde{P}_{D_1}^{ipSIC} &= \left\{1 - \int_0^\infty f_{|h_I|^2}(x)\left[1 - F_{\gamma_1}\left(\delta_1\left(\rho x + 1\right)\right)\right]dx\right\}^M \\
&= \left\{\frac{\sqrt{\pi}}{\Gamma(\mu)}\sum_{k=0}^\infty \frac{H^{2k}\Gamma(2(\mu+k))}{k!\Gamma(\mu+k+0.5)2^{2(\mu+k)-1}h^{\mu+2k}}\right. \\
&\quad \left.\times\left[1 - \frac{e^{-2\mu h\delta_1}}{\lambda_I}\sum_{m=0}^{2(\mu+k)-1}\frac{(2\mu h\delta_1)^m}{m!}\int_0^\infty e^{-\left(\frac{1}{\lambda_I}+2\mu h\delta_1\rho_S\right)x}(\rho_S x+1)^m\,dx\right]\right\}^M
\end{aligned}
\tag{6.13}
$$

Using [117, Eq. (1.111) and Eq. (3.351.3)], $\tilde{P}_{D_1}^{ipSIC}$ is given by

$$
\begin{aligned}
\tilde{P}_{D_1}^{ipSIC} &= \left\{\frac{\sqrt{\pi}}{\Gamma(\mu)}\sum_{k=0}^\infty \frac{H^{2k}\Gamma(2(\mu+k))}{k!\Gamma(\mu+k+0.5)2^{2(\mu+k)-1}h^{\mu+2k}}\right. \\
&\quad \left.\times\left[1 - e^{-2\mu h\delta_1}\sum_{m=0}^{2(\mu+k)-1}\sum_{r=0}^m \binom{m}{r}\frac{r!(2\mu h\delta_1)^m\lambda_I^r\rho_S^r}{m!(1+2\lambda_I\mu h\delta_1\rho_S)^{r+1}}\right]dx\right\}^M.
\end{aligned}
\tag{6.14}
$$

<u>Case 2</u>: When $\mu \in \mathbb{I}, \forall \mu \geq 0$, then we use the PDF of (6.9) and CDF of (6.7), (6.12):

$$
\begin{aligned}
\tilde{P}_{D_1}^{ipSIC} &= \left\{1 - \frac{1}{\lambda_I}\int_0^\infty e^{-\frac{x}{\lambda_I}}\left[1 - \frac{(\Lambda_1\Lambda_2)^\mu}{\Gamma(1+2\mu)}\left(\delta_1\left(\rho_S x+1\right)\right)^{2\mu}\right.\right. \\
&\quad \left.\left.\times\Phi_2\left(\mu,\mu;1+2\mu;-\Lambda_1\delta_1\left(\rho_S x+1\right),-\Lambda_2\delta_1\left(\rho_S x+1\right)\right)\right]dx\right\}^M.
\end{aligned}
\tag{6.15}
$$

Specifically, let $q = \frac{x}{\lambda_I}$, and use Gauss-Laguerre integration as in [139, Eq. (25.4.45)]. The closed-form approximation of the $\tilde{P}_{D_1}^{ipSIC}$ is expressed as

$$
\tilde{P}_{D_1}^{ipSIC} \approx \left[\frac{(\Lambda_1\Lambda_2)^\mu\delta_1^{2\mu}}{\Gamma(1+2\mu)}\sum_{w=1}^W \mathcal{X}_w\Theta(q_w)^{2\mu}\Phi_2\left(\mu,\mu;1+2\mu;-\Lambda_1\delta_1\Theta\left(q_w\right),-\Lambda_2\delta_1\Theta\left(q_w\right)\right)\right]^M
\tag{6.16}
$$

51

where $\Theta(q_w) = (\rho_S \lambda_I q_w + 1)$, $\mathcal{X}_w$ and q_w are the weight and abscissas for Gauss-Laguerre integration, respectively. More specifically, q_w is the w-th zero of the Laguerre polynomial $\mathcal{L}_W(q_w)$, and the corresponding the w-th weight is given by $\mathcal{X}_w = \frac{(W!)^2 q_w}{[\mathcal{L}_{W+1}(q_w)]^2}$. The parameter W is used to ensure a complexity-accuracy trade off.

From (6.11), we have pSIC. Let us set $\rho|h_I|^2 \approx 0$ and obtain the OP $\tilde{P}_{D_1}^{pSIC}$ as follows:

$$\tilde{P}_{D_1}^{pSIC} = [1 - \Pr(\gamma_1 > \delta_2, \gamma_1 > \delta_1)]^M = [1 - \Pr(\gamma_1 > \delta_{\max})]^M = [F_{\gamma_2}(\delta_{\max})]^M$$

$$\overset{\mu \in \mathbb{N}}{=} \left\{ \frac{\sqrt{\pi}}{\Gamma(\mu)} \sum_{k=0}^{\infty} \frac{H^{2k}\Gamma(2(\mu+k))}{k!\Gamma(\mu+k+0.5)2^{2(\mu+k)-1}h^{\mu+2k}} \left[1 - e^{-2\mu h \delta_{\max}} \sum_{l=0}^{2(\mu+k)-1} \frac{(2\mu h \delta_{\max})^l}{l!}\right] \right\}^M$$

$$\overset{\mu \in \mathbb{I}}{=} \left[\frac{(\Lambda_1 \Lambda_2)^\mu \delta_{\max}^{2\mu}}{\Gamma(1+2\mu)} \Phi_2(\mu, \mu; 1+2\mu; -\Lambda_1 \delta_{\max}, -\Lambda_2 \delta_{\max}) \right]^M$$

(6.17)

where $\delta_{\max} = \max(\delta_1, \delta_2)$.

Finally, The OP of D_2 is calculated as

$$\tilde{P}_2 = \Pr\left(\underbrace{\max_{n \in N}}\left\{\tilde{\Gamma}_{D_2,x_2}^n\right\} < \tilde{\gamma}_{th2}\right)$$

$$= \prod_{n=1}^{N} [1 - \Pr(\tilde{\gamma}_{th2} > \tilde{\gamma}_{th2})] = [1 - \Pr(\gamma_2 > \delta_2)]^N = [F_{\gamma_2}(\delta_2)]^N.$$

(6.18)

<u>Case 1</u>: When $\mu \in \mathbb{N}, \forall \mu \geq 0$, then we use CDF of (6.8), (6.18):

$$\tilde{P}_2 = \left\{ \frac{\sqrt{\pi}}{\Gamma(\mu)} \sum_{k=0}^{\infty} \frac{H^{2k}\Gamma(2(\mu+k))}{k!\Gamma(\mu+k+0.5)2^{2(\mu+k)-1}h^{\mu+2k}} \left[1 - e^{-2\mu h \delta_2} \sum_{l=0}^{2(\mu+k)-1} \frac{(2\mu h \delta_2)^l}{l!}\right] \right\}^N.$$

(6.19)

<u>Case 2</u>: When $\mu \in \mathbb{I}, \forall \mu \geq 0$, then we use CDF of (6.7), (6.18):

$$\tilde{P}_2 = \left[\frac{(\Lambda_1 \Lambda_2)^\mu \delta_2^{2\mu}}{\Gamma(1+2\mu)} \Phi_2(\mu, \mu; 1+2\mu; -\Lambda_1 \delta_2, -\Lambda_2 \delta_2) \right]^N.$$

(6.20)

6.1.4 Throughput analysis

Further analysis can be performed using additional metrics such as the total system throughput, which can be calculated from the OP. Throughput can be determined in delay-limited mode at set target rates R_1 and R_2 and is consequently expressed as in [140]:

$$\tau_1^\star = \left(1 - \tilde{P}_{D_1}^\star\right) R_1, \star \in \{ipSIC, pSIC\},$$

(6.21)

$$\tau_2 = \left(1 - \tilde{P}_2\right) R_2. \tag{6.22}$$

6.1.5   Numerical results

The parameters of μ and η were set as in [130], and the number of antennae M and N of U_1 and U_2 were the same value and equal to 2. The Monte Carlo results averaged more than 10^7 independent channel realizations. The target data-rates for the fixed-rate transmission were $R_1 = R_2 = 1$. The mean value of the channel power gains of the interference signal was $\lambda_I = 0.01$. The power allocation coefficients were $\nu_1 = 0.2$ and $\nu_2 = 0.8$. The number of points for the Gauss-Laguerre quadrature was $W = 40$.

Figure 6.2 plots the simulation of OP versus transmit SNR for various values of (μ, η) fading distribution, with the same number of antennae $N = M = 2$. By varying the value of μ, the outage performance changes significantly under pSIC and ipSIC conditions for both users. As μ increases, the performance at the users increases comparatively, thereby enhancing overall system performance. The simulation indicates that ipSIC has less performance than pSIC. It can be called the worst scenario since in all cases, it demonstrates a very low level of performance.
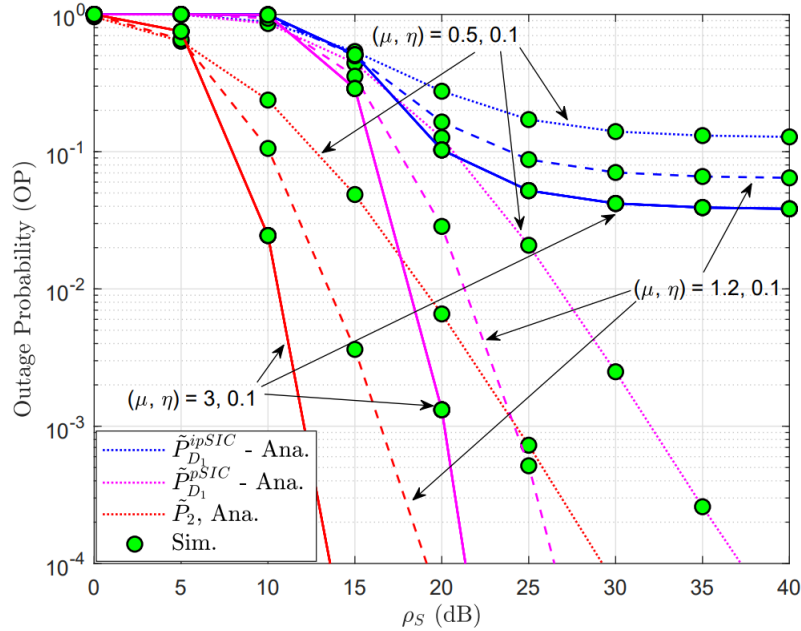
Figure 6.2: OP versus transmit SNR for different values of (μ, η) fading distribution, where $N = M = 2$.

Figure 6.3 plots the simulation for OP versus transmit SNR for different numbers of antennae at D_1 and D_2, where $R_1 = R_2 = 1$, $\eta = 0.1$ and $\mu = 1.2$. As the numbers of
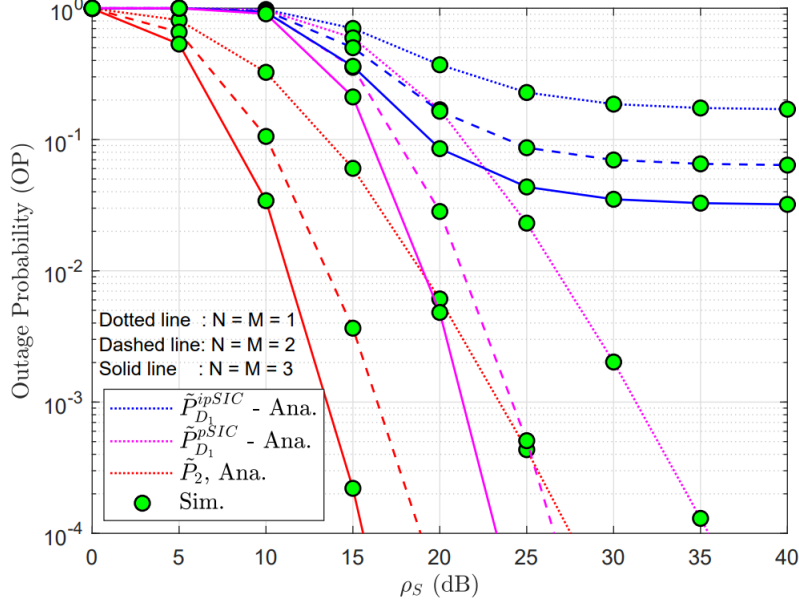
Figure 6.3: OP versus transmit SNR for different numbers of antennae at D_1 and D_2, where $R_1 = R_2 = 1$, $\eta = 0.1$ and $\mu = 1.2$.

antennae increase, the difference between the performance of each user in both ipSIC and pSIC becomes large. The graphs indicate that D_2 has better performance than D_1 in both scenarios because it has the highest power allocation. This demonstrates the effect of power allocation in improving the performance at the users.

Figure 6.4 plots the simulation for OP versus power allocation coefficients at D_2 for different values of transmit SNR, where $\lambda_I = 0.1$ (dB), $R_1 = R_2 = 0.5$, $\eta = 0.5$ and $\mu = 1$, clearly indicating the performance of both users under ipSIC and pSIC conditions. As the power allocation increases for a certain user, the performance at that user also increases, whereas the performance at the other user decreases. The primary finding is that with an increase in the transmit SNR, the system performance increases respectively in all scenarios.

Figure 6.5 plots the simulation for throughput versus transmit SNR under different levels of ipSIC at D_1, where $\nu_1 = 0.05$, $\nu_2 = 0.95$, $\eta = 0.5$ and $\mu = 1$. The results indicate that with a reduction in the level of ipSIC, the throughput performance at the user increases. The simulation also charts the throughput performance at the user under pSIC and indicates that D_2 has the better throughput.

6.1.6   Conclusion

This section investigated a NOMA system serving two users D_1 and D_2, with $\eta - \mu$ fading channels. Both pSIC and ipSIC were evaluated, and the closed-form OP expressions and system throughput expressions for each condition were derived. The simulations indicated
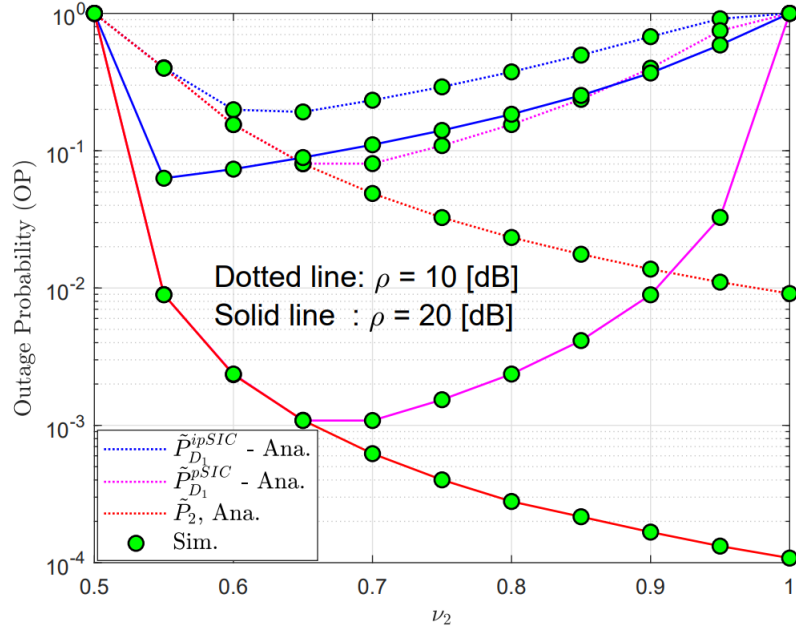
Figure 6.4: OP versus power allocation coefficients at D_2 for different values of transmit SNR, where $\lambda_I = 0.1$ (dB), $R_1 = R_2 = 0.5$, $\eta = 0.5$ and $\mu = 1$.
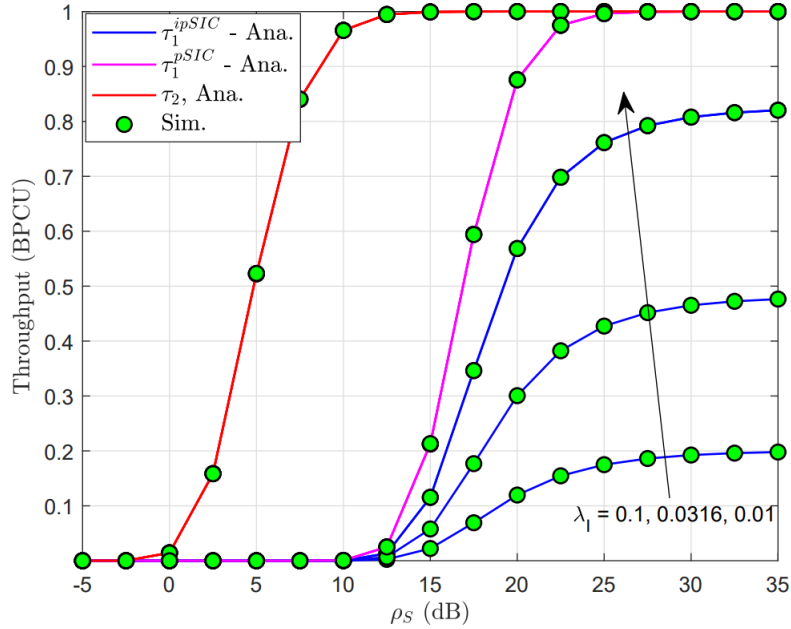
Figure 6.5: Throughput versus transmit SNR for different levels of ipSIC at D_1, with $\nu_1 = 0.05$, $\nu_2 = 0.95$, $\eta = 0.5$ and $\mu = 1$.

that varying the values of η while keeping μ constant has a significant role in enhancing system performance, even comparatively in ipSIC mode. The results also illustrated the system

performance for examples which varied the number of antennas, power level coefficients, and transmit SNR. The main finding is that the outage performance of the system increases rapidly as the transmit SNR increases, regardless of the scenario.

6.2 Analysis of the impact of CCI on performance in downlink satellite terrestrial systems: outage probability and ergodic capacity perspective

This section addresses the second aim of the dissertation by investigating the integration of NOMA with a satellite communications network [NNT01], [NNT02], [NNT06], [NNT07], [NNT08], [NNT11] and evaluating system performance under conditions of imperfect channel state information and co-channel interference from nearby systems. The results of this section were published in [NNT02]. The main contributions in this section are:

- An analysis of a NOMA-based terrestrial satellite relay network which encounters interference from nearby sources. The network uses a shadowed-Rician channel between the satellite and the relay and a Nakagami-m channel between the relay and the destination.

- An analysis and comparison of the system's performance under heavy shadowing (HS) and average shadowing (AS) effects resulting from the shadowing channel links. Multiple antennae relays are also investigated for their effect on performance.

- Derived closed-form expressions for outage probability (OP) and ergodic capacity (EC) at both users in a dedicated NOMA user group.

- A numerical analysis and Monte Carlo simulations for the derived expressions to verify their authenticity and analyze system performance. The system's performance in HS mode is demonstrated by varying the interference links and mean square error of the channels.

6.2.1 Introduction

Satellite communications are especially able to provide radio access in difficult areas [22]. Because satellite networks can provide higher quality of services (QoS) for comparatively less cost, they can also attain significant improvements in the efficiency of fixed and mobile satellite services. In the evolution of fifth generation (5G) networks, satellite communications have been viewed as a potential addition to many technologies such as the Internet of Things (IoT), sensor networks and relaying communications [141]. The future of satellite networks is expected to support services of massive connectivity and reduce operational costs. Therefore, they can be deployed by integrating them with various geostationary and non-geostationary orbital satellites and applying cooperative transmission or cognitive radio networks to increase spectrum efficiency. To date, most satellite networks have adopted the orthogonal multiple access (OMA) technique for the transmission and reception of data [142].

The major disadvantage of OMA is that it cannot satisfy the growing requirements of communications networks. Under OMA, efficient spectrum use and limitations on the number of users have become major challenges which diminish system performance. In this section, NOMA is considered as a method for tackling the challenges raised by OMA. Of the two NOMA categories, Power-Domain NOMA was applied, since much of the research has proved that this system has the most promising features. In NOMA, signals are transmitted superimposed in the same resource block by varying the power level of each user according to the channel gain. To identify the required user signal at the receiver, the system applies SIC and thereby extracts the required signal. As mentioned, NOMA uses the same resource block for multiple users and thus increases the efficiency of spectrum use at a reasonable level of implemented complexity [143], [144]. The NOMA technique has achieved significant attention from researchers and is a promising technology with advantages that can be exploited in 5G communications. Numerous studies have been performed to compare the performance of the NOMA system to OMA. The main finding is that NOMA is efficient [145], [146]. With increased spectrum efficiency, NOMA performance may be more widespread through the use of NOMA in conjunction with other techniques.

Various studies have introduced the NOMA technique in satellite communications [59, 60, 67, 61, 62, 63, 64, 147, 148]. In [60], the authors studied integration of the NOMA technique with multi-beam satellite networks, while in [67], the authors investigated integration of NOMA with cognitive satellite networks to increase the ergodic performance of the system. The performance of NOMA-hybrid satellite relay networks (HSRN) was studied in [61, 62]. NOMA integrated cognitive HSRN has been studied to analyze outage performance [63]. The performance of a similar system was studied in [61] and [64] with the effect of hardware impairments. The research in [149, 150, 151] studied NOMA-based satellite-terrestrial networks and increasing spectrum efficiency by beamforming. The study in [65]evaluated a cooperative NOMA-HSRN where the user with better channel gain acted as a relay to the remaining users in the cluster. In [66], the authors studied the effect of imperfect CSI and channel impairments (CI) in a NOMA-based terrestrial mobile communications network (TMCN) functioning with multiple relays. In [61], the authors considered NOMA-based integrated terrestrial satellite networks (ISTN) to study the effect of relaying configurations such as amplify and forward (AF) and decode and forward (DF). The authors of [152] investigated a system similar to system studied in [61] and explored the effect of CI under a DF relay configuration.

In the context of NOMA-HSRN, the effect of co-channel interference (CCI) in all system models has rarely been addressed. In practice, NOMA-HSRN might experience a situation of high CCI, which is an important consideration in the deployment of NOMA and HSRN in wireless communications. It can be demonstrated that aggressive reuse of spectrum resources leads to degraded performance under the effect of CCI. Consequently, this is more than simply an important priority consideration, as the performance of NOMA-HSRN is guaranteed only

if CCI is taken into account. To the best of my knowledge, the performance degradation in NOMA-HSRN due to CCI has not yet been solved. Aiming to overcome the effect of CCI, which is unavoidable in practical scenarios, the authors of [153] reported degraded performance in a single-user hybrid satellite-terrestrial amplify-and-forward relay network (HSTAFRN) with multiple Rayleigh-faded interference sources. The performance metrics of a downlink multi-user HSTAFRN were examined using a fixed-gain relaying protocol under the effect of CCI [154]. The authors of [155] employed dual-hop relay networks which assumed interference-limited relays and noisy destinations. These may arise from cell-edge or frequency-division relaying [156], although NOMA-HSRN still experiences worse performance under the effect of CCI. In [157], the authors analyzed the performance of mmWaves in a multi-user HSRN system with a shadowed-Rician channel for the link from satellite to the relay. The authors of [158] deployed a single-antenna satellite for a multi-user HSTAFRN system and evaluated its outage performance under the effect of both CCI and outdated CSI.

Satellite networks have been designed to replace terrestrial communications systems, but challenges still exist in some aspects of signal processing. The studies referred to above suggest that integrating NOMA with satellite systems extends the efficiency of communication between users. Although satellite systems have numerous advantages, challenges such as fading effect and interference require solutions. The majority of research has studied the effect of multiple scenarios, including imperfect SIC, imperfect CSI and channel impairments, but none has addressed the effect on system performance from CCI. Therefore, this section discusses the effect of interference by considering shadowing and interference links in dual-user communications occurring under a NOMA-assisted satellite network. The effects of both heavy shadowing (HS) and average shadowing (AS) and the effect of interference links on communications channels in HS mode were investigated. In contrast to similar studies summarized in Table 6.1 and to highlight the superiority of NOMA-aided satellite systems, performance was analyzed fully in terms of OP and EC.

6.2.2 System model

This section describes the configuration consisting of a satellite (S), relay (R) and two users $D_i, i \in (1,2)$ (Fig. 6.6). All nodes are equipped with a single antenna, and the relay operates with the DF protocol. The relay node is also affected by N co-channel interference sources $\{I_n\}_{n=1}^N$. The link from S to D_i is not available because of heavy shadowing [159]. h_R denotes the channel coefficient from S to R on a shadowed-Rician channel, h_i denotes the channel coefficients from R to D_i on a Nakagami-m channel, h_{nR} denotes the channel coefficient of the link between the n-th interference source and relay, using independent and non-identically distributed (i.ni.d.) Nakagami-m random variables (RVs). Under these conditions, the CSI procedure exhibits error.

Table 6.1: Summary of related works.

References	Context built on NOMA	Performance Analysis	Contributions
[60]	Multi-beam satellite systems	Data rate fairness	Performance comparison of SIC to simultaneous non-unique detection (SND)
[67]	Cognitive hybrid satellite terrestrial networks	EC	Investigated improvement of the radio spectrum efficiency
[61, 63]	Hybrid satellite terrestrial networks	Outage performance	Investigated power allocation and user fairness problems
[64]	Integrated satellite terrestrial networks	Outage performance and energy efficiency	Investigated system performance under the effect of hardware impairments
[150]	Integrated satellite terrestrial networks	System capacity	Investigated beamforming for maximization of the minimum channel correlation and achieved efficient user pairing with the proposed scheme
[61]	Hybrid satellite terrestrial relay networks	Outage performance	Investigated the system under the effect of imperfect CSI and analyzed the system with channel estimation errors and fading parameters. Proposed a low complexity algorithm to yield efficient results.
Our research	Terrestrial satellite relay networks with CCI and imperfect CSI	Outage Performance and EC	Investigated and compared performance with CCI and imperfect CSI.

The estimation channel is expressed as in [61]:

$$h_j = \hat{h}_j + e_j, \tag{6.23}$$

where $j \in \{R, 1, 2\}$, e_j is the error term for $CN(0, \sigma_{e_j}^2)$ [160].

The power-domain-assisted NOMA signal from the source transmits user signals superimposed in the same resource block by varying the power coefficient of each user according to their CSI. At the receiver's end, perfect SIC is assumed to extract the desired signal from the superimposed signal. Imperfect CSI should therefore be studied in practical scenarios. Satellite-terrestrial networks need relays to power signals before forwarding them to mobile users. The main aim in designing a relay is to address signal transmission at long distances. The satellite must allocate suitable power levels to expected users. The first user D_1 is assumed to be distant, and a weak signal such as this requires a higher power allocation. The
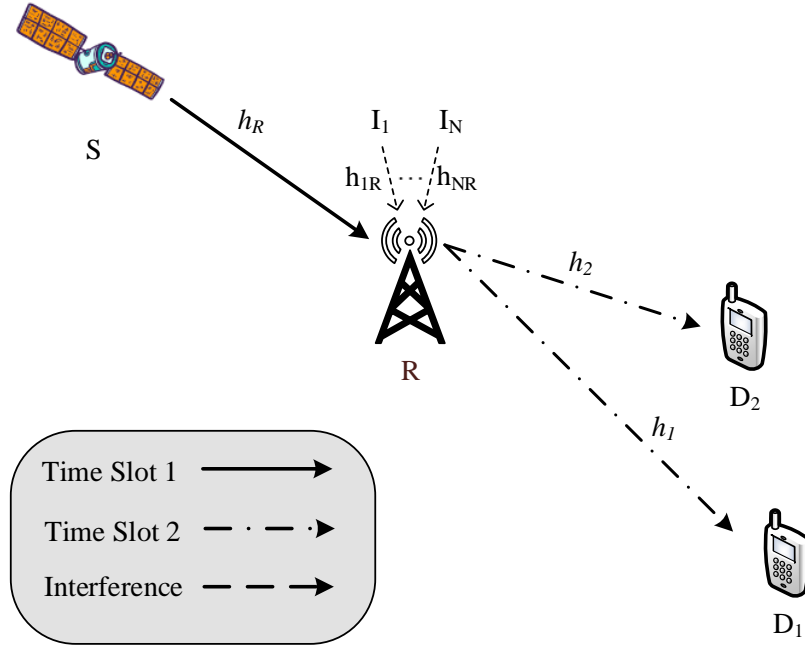
Figure 6.6: System model

near user D_2 simply acquires the lower transmit power level. In the first phase, S transmits the signal $\sqrt{P_S A_1} x_1 + \sqrt{P_S A_2} x_2$ to R, where P_S is the transmit power, A_1 and A_2 are power allocations such that $A_1 + A_2 = 1$ and $A_1 > A_2$, assumed under the NOMA scheme. Then, the signal received at R is expressed as

$$y_R = \left(\sqrt{A_1} x_1 + \sqrt{A_2} x_2 \right) \sqrt{P_S} \left(\hat{h}_j + e_j \right) + \sum_{n=1}^{N} \sqrt{P_{cn}} h_{nR} x_n + n_R, \qquad (6.24)$$

where P_{Cn} is the transmit power of the n-th interference source, and n_R is the additive white Gaussian noise (AWGN) at R for $CN(0, N_0)$. The signal to interference plus noise ratio (SINR) is then used to decode x_1, expressed as

$$\Gamma_{R \to x_1} = \frac{\rho_S A_1 \left| \hat{h}_R \right|^2}{\rho_S A_2 \left| \hat{h}_R \right|^2 + \gamma_C + \rho_S \sigma_{e_R}^2 + 1}, \qquad (6.25)$$

where $\rho_S = \frac{P_S}{N_0}$ is the transmit SNR, $\rho_{Cn} = \frac{P_{Cn}}{N_0}$, and $\gamma_C = \sum_{n=1}^{N} \rho_{Cn} |h_{nR}|^2$. The SINR decoded x_2 is expressed as

Table 6.2: Table of parameters.

Notation	Definition
N	The number of CCI sources affecting the relay.
x_i	Messages for destination D_i
x_n	Unit energy signal of the n-th interference source
A_i	Power allocation coefficients, where $A_1 + A_2 = 1$ and $A_1 > A_2$.
P_S	Transmit power at S
P_R	Transmit power at R
P_{Cn}	Transmit power of the n-th interference source
P_{Cn}	Transmit power of the n-th interference source
n_j	Additive white Gaussian noise (AWGN) for $CN(0, N_0)$
h_R	Channel coefficient from S to R
h_i	Channel coefficient from R to D_i
h_{nR}	Channel coefficient from n-th interference source to the relay
$\hat{h}_j$	Estimated channel coefficients
e_j	Channel estimation error
$\Gamma(.)$	Complete Gamma function
$\Gamma(.,.)$	Upper incomplete Gamma function
$_1F_1(.,.,.)$	Confluent hypergeometric function of the first kind
$G^{1,1}_{1,1}[.]$	Meijer's G-function
$G^{1,1,1,1,1}_{1,[1,1],0,[1,1]}[.,.]$	Meijer's G-function with two variables

$$\Gamma_{R \to x_2} = \frac{\rho_S A_2 \left| \hat{h}_R \right|^2}{\gamma_C + \rho_S \sigma_{e_R}^2 + 1}. \tag{6.26}$$

In the second phase, relay R forwards the signals to ground users. The signal received at D_i is expressed as

$$y_{D_i} = \left(\sqrt{A_1} x_1 + \sqrt{A_2} x_2 \right) \sqrt{P_R} \left(\hat{h}_i + e_i \right) + n_i, \tag{6.27}$$

where P_R is the transmit power at R, and n_{D_i} AWGN for $CN(0, N_0)$. The other main parameters are listed in Table 6.2. The SINR which decodes x_1 at D_1 is expressed as

$$\Gamma_{D_1 \to x_1} = \frac{\rho_R A_1 \left| \hat{h}_1 \right|^2}{\rho_R A_2 \left| \hat{h}_1 \right|^2 + \rho_R \sigma_{e_1}^2 + 1}, \tag{6.28}$$

where $\rho_R = \frac{P_R}{N_0}$. The SINR which decodes signal x_1 at D_2 is expressed as in [160]:

$$\Gamma_{D_2 \to x_1} = \frac{\rho_R A_1 \left|\hat{h}_2\right|^2}{\rho_R A_2 \left|\hat{h}_2\right|^2 + \rho_R \sigma_{e_2}^2 + 1}, \tag{6.29}$$

Applying SIC, the SINR which decodes its own signal x_2 at D_2 is expressed as

$$\Gamma_{D_2 \to x_2} = \frac{\rho_R A_2 \left|\hat{h}_2\right|^2}{\sigma_{e_2}^2 + 1}. \tag{6.30}$$

For performance analysis, these SINRs provide important information for calculating probabilities.

6.2.3 Performance analysis

This section provides an analysis of the two main system metrics with the assumed channel models described below.

6.2.3.1 Channel model

Following the results obtained in [161], the probability density function (PDF) of $|\hat{h}_R|^2$ is expressed as

$$f_{|\hat{h}_R|^2}(x) = \alpha_R e^{-\beta_R x} {}_1F_1(m_R, 1, \delta_R x), \tag{6.31}$$

where $\alpha_R = \frac{\left(\frac{2b_R m_R}{2b_R m_R + \Omega_R}\right)^{m_R}}{2b_R}$, $\beta_R = (2b_R)^{-1}$, $\delta_R = \frac{\Omega_R}{2b_R(2b_R m_R + \Omega_R)}$, m_R is the fading severity parameter, $2b_R$ and Ω_R denote multipath components and the average power of LoS, respectively, and ${}_1F_1(.,.,.)$ is the confluent hypergeometric function of the first kind [117, Eq. 9.210.1]. Using [162], we can rewrite the PDF of $|h_R|^2$ as

$$f_{|\hat{h}_R|^2}(x) = \alpha_R \sum_{k=0}^{m_R-1} \xi(k) x^k e^{-\Xi_R x}, \tag{6.32}$$

where $\xi(k) = \frac{(-1)^k (1-m_R)_k \delta_R^k}{(k!)^2}$, $\Xi_R = \beta_R - \delta_R$, and $(.)_x$ denotes the Pochhammer symbol [117, p. xliii]. Based on [117, Eq.3.351.2], the the cumulative distribution function (CDF) of $\left|\hat{h}_R\right|^2$ is expressed as

$$F_{|\hat{h}_R|^2}(x) = 1 - \alpha_R \sum_{k=0}^{m_R-1} \xi(k) \sum_{l=0}^{k} \frac{k! x^l e^{-\Xi_R x}}{l! (\Xi_R)^{k-l+1}}. \tag{6.33}$$

The PDF and CDF of $|h_i|^2$ are then expressed as in [138]:

$$f_{|\hat{h}_i|^2}(x) = \left(\frac{m_i}{\Omega_i}\right)^{m_i} \frac{x^{m_i-1}e^{-\left(\frac{m_i}{\Omega_i}\right)x}}{\Gamma(m_i)}, \tag{6.34}$$

and

$$\begin{aligned}
F_{|\hat{h}_i|^2}(x) &= 1 - \frac{1}{\Gamma(m_i)}\Gamma\left(m_i, \frac{m_i x}{\Omega_i}\right) \\
&= 1 - \sum_{b_i=0}^{m_i-1} \frac{1}{b_i!}\left(\frac{m_i x}{\Omega_i}\right)^{+b_i} e^{-\left(\frac{m_i}{\Omega_i}\right)x},
\end{aligned} \tag{6.35}$$

where m_i and Ω_i are the fading severity parameter and average power, respectively, and $\Gamma(.,.)$ is the upper incomplete gamma function [117].

The PDF of γ_C is also calculated with corresponding severity parameters $\{m_{Cn}\}_n^N$ and average powers $\{\Omega_{Cn}\}_n^N$. The PDF of γ_C is expressed as in [163], [164] and [154]:

$$f_{\gamma_C}(x) = \left(\frac{m_I}{\Omega_I}\right)^{m_I} \frac{x^{m_I-1}}{\Gamma(m_I)}e^{-\left(\frac{m_I}{\Omega_I}\right)x}, \tag{6.36}$$

where the parameters m_I and Ω_I are obtained from moment based estimators. For this, we define $\Theta = \sum_{n=1}^{I}|h_{nR}|^2$, and without loss of generality, we assume no power control is used, i.e., $P_{Cn} = P_C$ or $\rho_{Cn} = \rho_C$. Then, we have $\Omega_I = \rho_C\Omega_C$, where $\Omega_C = E[\Theta] = \sum_{n=1}^{N}\Omega_{Cn}$ and $m_I = \frac{\Omega_C^2}{E[\Theta^2]-\Omega_C^2}$. From this, the exact moments of Θ are expressed as

$$\begin{aligned}
E[\Theta^n] &\approx \sum_{n_1=0}^{n}\sum_{n_2=0}^{n_1}\cdots\sum_{n_{N-1}=0}^{n_{N-2}}\binom{n}{n_1}\binom{n_1}{n_2}\binom{n_{N-2}}{n_{N-1}} \\
&\times E\left[|h_{1R}|^{2(n-n_1)}\right]E\left[|h_{1R}|^{2(n_1-n_2)}\right]\cdots E\left[|h_{1R}|^{2(n_{N-1})}\right]
\end{aligned} \tag{6.37}$$

where $E[|h_{iR}|^n] = \frac{\Gamma\left(m_{Cn}+\frac{n}{2}\right)}{\Gamma(m_{Cn})}\left(\frac{m_{Cn}}{\Omega_{Cn}}\right)^{-\frac{n}{2}}$.

6.2.3.2 Outage probability of D_1

An outage event of D_1 occurs when R and D_1 cannot detect x_1 correctly. The OP of D_1 is therefore expressed as

$$\begin{aligned}
P_{D_1} &= \Pr\left(\min\left(\Gamma_{R\to x_1}, \Gamma_{D_1\to x_1}\right) < \gamma_1\right) \\
&= 1 - \underbrace{\Pr\left(\Gamma_{R\to x_1} > \gamma_1\right)}_{B_1}\underbrace{\Pr\left(\Gamma_{D_1\to x_1} > \gamma_1\right)}_{B_2},
\end{aligned} \tag{6.38}$$

where $\gamma_i = 2^{2R_i} - 1$, and R_i is the target rate.

Proposition 1: Here, the closed-form of B_1 is

$$B_1 = \alpha_R \sum_{k=0}^{m_R-1} \sum_{l=0}^{k} \sum_{p=0}^{l} \binom{l}{p} \frac{\xi(k)\, k!\, \Gamma(m_I + p)}{l!\, \Gamma(m_I)\, (\Xi_R)^{k-l+1}} e^{-\Xi_R \phi_1 \left(\rho_S \sigma_{e_R}^2 + 1\right)}$$
$$\times \left(\phi_1 \left(\rho_S \sigma_{e_R}^2 + 1\right)\right)^l \left(1 + \frac{\Omega_I \Xi_R \phi_1}{m_I}\right)^{-m_I - p} \left(\frac{\Omega_I}{m_I \left(\rho_S \sigma_{e_R}^2 + 1\right)}\right)^p \tag{6.39}$$

Proof: See Appendix A (pp. 75).

Next, using (6.28), B_2 is rewritten as

$$B_2 = \Pr\left(\frac{\rho_R A_1 \left|\hat{h}_1\right|^2}{\rho_R A_2 \left|\hat{h}_1\right|^2 + \rho_R \sigma_{e_1}^2 + 1} > \gamma_1\right)$$
$$= \Pr\left(\left|\hat{h}_1\right|^2 > \phi_2\right) \tag{6.40}$$
$$= 1 - F_{\left|\hat{h}_1\right|^2}(\phi_2)$$

where $\phi_2 = \frac{\left(\rho_R \sigma_{e_1}^2 + 1\right)\gamma_1}{(A_1 - A_2 \gamma_1)\rho_R}$. Based on the CDF of $\hat{h}_i$ in (6.35), B_2 is expressed as

$$B_2 = \sum_{b_1=0}^{m_1-1} \frac{e^{-\frac{m_1 \phi_2}{\Omega_1}}}{b_1!} \left(\frac{m_1 \phi_2}{\Omega_1}\right)^{b_1}. \tag{6.41}$$

Finally, substituting (6.39) and (6.41) into (6.38), P_{D_1} is obtained from

$$P_{D_1} = 1 - \alpha_R \sum_{k=0}^{m_R-1} \sum_{l=0}^{k} \sum_{p=0}^{l} \sum_{b_1=0}^{m_1-1} \binom{l}{p} \frac{\xi(k)\, k!\, \Gamma(m_I + p)\, e^{-\Xi_R \phi_1 \left(\rho_S \sigma_{e_R}^2 + 1\right) - \frac{m_1 \phi_2}{\Omega_1}}}{b_1!\, l!\, \Gamma(m_I)(\Xi_R)^{k-l+1} \left(\phi_1 \left(\rho_S \sigma_{e_R}^2 + 1\right)\right)^{-l}}$$
$$\times \left(\frac{m_1 \phi_2}{\Omega_1}\right)^{b_1} \left(1 + \frac{\Omega_I \Xi_R \phi_1}{m_I}\right)^{-m_I - p} \left(\frac{\Omega_I}{m_I \left(\rho_S \sigma_{e_R}^2 + 1\right)}\right)^p \tag{6.42}$$

6.2.3.3 Outage probability of D_2

The outage events of D_2 occurs when R and D_2 cannot detect x_2 correctly. The OP of D_2 is therefore expressed as

$$P_{D_2} = \Pr\left(\min\left(\Gamma_{R \to x_2}, \Gamma_{D_2 \to x_2}\right) < \gamma_2\right)$$
$$= 1 - \Pr\left(\Gamma_{R \to x_2} > \gamma_2\right) \Pr\left(\Gamma_{D_2 \to x_2} > \gamma_2\right) \tag{6.43}$$

Proposition 2: The closed-form OP of P_{D_2} is obtained from

$$P_{D_2} = 1 - \alpha_R \sum_{k=0}^{m_R-1} \sum_{l=0}^{k} \sum_{p=0}^{l} \sum_{b_2=0}^{m_2-1} \binom{l}{p} \frac{k!\xi(k)\Gamma(m_I+p) e^{-\Xi_R\psi_1\left(\rho_S\sigma_{e_R}^2+1\right)-\frac{m_2\psi_2}{\Omega_2}}}{b_2!l!\Gamma(m_I)(\Xi_R)^{k-l+1}\left(\psi_1\left(\rho_S\sigma_{e_R}^2+1\right)\right)^{-l}}$$

$$\times \left(\frac{m_2\psi_2}{\Omega_2}\right)^{b_2} \left(1 + \frac{\Omega_I\Xi_R\psi_1}{m_I}\right)^{-m_I-p} \left(\frac{\Omega_I}{m_I\left(\rho_S\sigma_{e_R}^2+1\right)}\right)^p$$

(6.44)

Proof: See [Appendix B](#) (pp. 76)

6.2.3.4 Diversity order

To gain some insight, we derive the asymptotic OP of D_i under a high SNR ($\rho = \rho_S = \rho_R \to \infty$). The diversity order is defined as in [165]:

$$d = -\lim_{\rho\to\infty} \frac{\log\left(P_{D_i}^\infty\right)}{\log(\rho)}, \tag{6.45}$$

where $P_{D_i}^\infty$ is the asymptotic OP of D_i.

Proposition 3: The asymptotic OP of D_1 is expressed as

$$P_{D_1}^\infty = 1 - \left(1 - \frac{1}{\Gamma(m_1+1)}\left(\frac{m_1\phi_2}{\Omega_1}\right)^{m_1}\right)$$
$$\times \left(1 - \alpha_R\phi_1\left(\frac{(m_I)!}{\Gamma(m_I)}\left(\frac{\Omega_I}{m_I}\right) + \left(\rho_S\sigma_{e_R}^2+1\right)\right)\right) \tag{6.46}$$

Proof: See [Appendix C](#) (pp. 76)

Similarly, the asymptotic of D_2 is expressed as

$$P_{D_2}^\infty = 1 - \left(1 - \frac{1}{\Gamma(m_2-1)}\left(\frac{m_2\psi_2}{\Omega_2}\right)^{m_2}\right)$$
$$\left(1 - \alpha_R\psi_1\left(\frac{(m_I)!}{\Gamma(m_I)}\left(\frac{\Omega_I}{m_I}\right) + \left(\rho_S\sigma_{e_R}^2+1\right)\right)\right) \tag{6.47}$$

The results in (6.46) and (6.47) refer to limits of outage performance in the region of high SNR. It can be predicted that the outage performance of two ground users will encounter the lower bound, even though other system parameters have improved. As discussed, the diversity is therefore zero.

6.2.3.5 Ergodic capacity of D_1

The EC of x_i is expressed as in [166]:

$$R_{x_1} = \frac{1}{2 \log (2)} \int_0^{\frac{A_1}{A_2}} \frac{1 - F_{Q_1} (x)}{1 + x} dx, \tag{6.48}$$

where $Q_1 = \min \left(\Gamma_{R \to x_1}, \Gamma_{D_1 \to x_1} \right)$.

Proposition 4: The closed-form EC of x_1 is expressed as (6.49), where $\Psi_1 = \frac{\left(\rho_S \sigma_{e_R}^2 + 1 \right) \Xi_R (1 + \theta_p)}{A_2 \rho_S (1 - \theta_p)} + \frac{m_1 \left(\rho_R \sigma_{e_1}^2 + 1 \right) (1 + \theta_p)}{A_2 \Omega_1 \rho_R (1 - \theta_p)}$.

$$
\begin{aligned}
R_{x_1} \approx{} & \frac{\alpha_R}{2 \ln (2)} \sum_{k=0}^{m_R - 1} \sum_{l=0}^{k} \sum_{p=0}^{l} \sum_{b_1=0}^{m_1 - 1} \binom{l}{p} \frac{\xi (k) k!}{b_1! l! \Gamma (m_I)} \frac{\Gamma (m_I + p)}{(\Xi_R)^{k-l+1}} \\
& \times \left(\frac{\left(\rho_R \sigma_{e_1}^2 + 1 \right) m_1}{\Omega_1 \rho_R} \right)^{b_1} \left(\frac{\Omega_I}{m_I \left(\rho_S \sigma_{e_R}^2 + 1 \right)} \right)^p \left(\frac{\left(\rho_S \sigma_{e_R}^2 + 1 \right)}{\rho_S} \right)^l \\
& \times \frac{\pi}{P} \sum_{p=0}^{P} \frac{A_1 \sqrt{1 - \theta_p^2} e^{-\Psi_1}}{2 A_2 + A_1 (1 + \theta_p)} \left(1 + \frac{\Omega_I \Xi_R (1 + \theta_p)}{A_2 m_I \rho_S (1 - \theta_p)} \right)^{-m_I - p} \left(\frac{(1 + \theta_p)}{A_2 (1 - \theta_p)} \right)^{b_1 + l}
\end{aligned}
\tag{6.49}
$$

Proof: See Appendix D (pp. 77)

6.2.3.6 Ergodic capacity D_2

Similarly, the EC of x_2 is expressed as

$$R_{x_2} = \frac{1}{2 \ln (2)} \int_0^{\infty} \frac{1 - F_{Q_2} (y)}{1 + y} dy, \tag{6.50}$$

where $Q_2 = \min \left(\Gamma_{R \to x_2}, \Gamma_{D_1 \to x_2} \right)$.

Proposition 5: The closed-form EC of x_1 is expressed as (6.51), where $\Psi_2 = \frac{\Xi_R \left(\rho_S \sigma_{e_R}^2 + 1 \right)}{\rho_R A_2} + \frac{m_2 \left(\rho_R \sigma_{e_2}^2 + 1 \right)}{\Omega_2 \rho_R A_2}$, and $G_{1,[1:1],0,[1:1]}^{1,1,1,1,1} [., .]$ denotes the Meijer-G function with two variables [167].

$$R_{x_2} = \frac{\alpha_R}{2\ln(2)} \sum_{k=0}^{m_R-1} \sum_{l=0}^{k} \sum_{p=0}^{l} \sum_{b_2=0}^{m_2-1} \binom{l}{p} \frac{k!\xi(k)(\Xi_R)^{-k+l-1}}{b_2!l!\Gamma(m_I)}$$

$$\times \left(\frac{m_2(\rho_R\sigma_{e_2}^2+1)}{\Omega_2\rho_R A_2}\right)^{b_2} \left(\frac{(\rho_S\sigma_{e_R}^2+1)}{\rho_R A_2}\right)^{l} \left(\frac{\Omega_I}{m_I(\rho_S\sigma_{e_R}^2+1)}\right)^{p} \tag{6.51}$$

$$\times G_{1,[1:1],0,[1:1]}^{1,1,1,1,1} \left[\begin{array}{c} \frac{\Omega_I\Xi_R}{m_I\rho_R A_2\Psi_2} \\ \frac{1}{\Psi_2} \end{array} \middle| \begin{array}{c} 1+l+b_2 \\ 1-m_I-p \\ - \\ 0,0 \end{array}\right]$$

Proof: See Appendix E (pp. 78)

6.2.4   Consideration on case of Multiple Antenna Relay

This section examines how a multiple-antenna relay affects the performance of two users D_i. In particular, a DF relay can be equipped with K_R receiver antennas and K_T transmit antennas. To represent mathematical expressions from this point onward, $\mathbf{h_R} = [\mathbf{h_R^1}, \mathbf{h_R^2}, ..., \mathbf{h_R^{K_R}}]^{\mathbf{T}}$ denotes the $K_R \times 1$ channel vector between S and R, $\mathbf{h_i} = [\mathbf{h_i^1}, \mathbf{h_i^2}, ..., \mathbf{h_i^{K_T}}]^{\mathbf{T}}$ denotes the $K_T \times 1$ channel vector between R and D_i. In this first phase, the signal received at R assisted by (6.23) is expressed as

$$\begin{aligned} y_R^{II} &= \left(\sqrt{A_1}x_1 + \sqrt{A_2}x_2\right)\sqrt{P_S}\mathbf{w_R^H}\hat{\mathbf{h_R}} \\ &+ \left(\sqrt{A_1}x_1 + \sqrt{A_2}x_2\right)\sqrt{P_S}\mathbf{w_R^H}\mathbf{e_R} \\ &+ \sum_{n=1}^{N}\sqrt{P_{cn}}h_{nR}x_n + \mathbf{w_R^H}\mathbf{n_R} \end{aligned} \tag{6.52}$$

where $\mathbf{n_R}$ denotes the vector of zero mean AWGN with variance N_0 and $\mathbf{w_R} = \frac{\hat{\mathbf{h_R}}}{\|\hat{\mathbf{h_R}}\|_{\mathbf{F}}}$. The SINR is used to decode x_1 is therefore expressed as

$$\Gamma_{R\to x_1}^{II} = \frac{A_1\eta_R}{A_2\eta_R + \rho_S\sigma_{e_R}^2 + \gamma_C + 1}, \tag{6.53}$$

where $\eta_R = \rho_S\left\|\hat{\mathbf{h_R}}\right\|_F^2$. The SINR used to decode x_2 is expressed as

$$\Gamma_{R\to x_2}^{II} = \frac{A_2\eta_R}{\rho_S\sigma_{e_R}^2 + \gamma_C + 1} \tag{6.54}$$

In the second phase, the received signal at D_i is expressed as

$$y_{D_i}^{II} = \left(\sqrt{A_1}x_1 + \sqrt{A_2}x_2\right)\sqrt{P_R}\hat{\mathbf{h}}_i^{\;H}\mathbf{w_i}$$
$$+ \left(\sqrt{A_1}x_1 + \sqrt{A_2}x_2\right)\sqrt{P_R}\mathbf{e_i} + \mathbf{n_{D_i}} \tag{6.55}$$

where $\mathbf{w_i} = \frac{\hat{\mathbf{h}}_i}{\|\hat{\mathbf{h}}_i\|_{\mathbf{F}}}$. The SINR which decodes x_1 at D_1 is expressed as

$$\Gamma_{D_1 \to x_1}^{II} = \frac{\eta_1 A_1}{\eta_1 A_2 + \rho_R \sigma_{e_1}^2 + 1}, \tag{6.56}$$

where $\eta_i = \rho_R \left\|\hat{\mathbf{h}}_i\right\|_F^2$, the SINR which decodes signal x_1 at D_2 is expressed as

$$\Gamma_{D_2 \to x_1}^{II} = \frac{\eta_2 A_1}{\eta_2 A_2 + \rho_R \sigma_{e_2}^2 + 1} \tag{6.57}$$

Similarly, the SINR which decodes its own signal x_2 at D_2 is calculated from

$$\Gamma_{D_2 \to x_2}^{II} = \frac{\eta_2 A_2}{\rho_R \sigma_{e_2}^2 + 1} \tag{6.58}$$

6.2.4.1   Statistical characterization

This section considers $\hat{\mathbf{h}}_{\mathbf{R}}$ and $\hat{\mathbf{h}}_i$ with independent and identically distributed (i.i.d.) entries as in [168]. The PDF of η_R is then expressed as in[169]:

$$f_{\eta_R}(x) = \frac{\alpha_R^{K_R}}{\Gamma(K_R)} e^{-\frac{\beta_R}{\rho_S}x} \sum_{a=0}^{\infty} \frac{(m_R K_R)_a \, \delta_R^a}{a! \, (K_R)_a \, (\rho_S)^{K_R+a}} x^{K_R+a-1}. \tag{6.59}$$

Assisted by [117, Eq. 3.351.2], the CDF of η_R is expressed as

$$F_{\eta_R}(x) = 1 - \frac{\alpha_R^{K_R}}{\Gamma(K_R)} \sum_{a=0}^{\infty} \sum_{b=0}^{K_R+a-1} \frac{\Gamma(K_R+a)(m_R K_R)_a \delta_R^a}{a! b! \, (K_R)_a \, (\rho_S)^b \, (\beta_R)^{K_R+a-b}} x^b e^{-\frac{\beta_R}{\rho_S}x}. \tag{6.60}$$

The CDF of η_I is also expressed as in [169]:

$$F_{\eta_i}(x) = \frac{\gamma\left(m_i K_T, \frac{m_i}{\rho_R \Omega_i}x\right)}{\Gamma(m_i K_T)} \tag{6.61}$$

6.2.4.2   Outage probability

Proposition 6:

The OP of D_1 is expressed as

Table 6.3: SYSTEM PARAMETERS.

System Parameters	Values
Monte Carlo simulation	10^6 iterations
Power allocation	$A_1 = 0.7$ and $A_2 = 0.3$
Target rate	$R_1 = 0.3$ and $R_2 = 0.5$ bits per channel use
Mean square error of channel	$\sigma^2 = \sigma_{e_R}^2 = \sigma_{e_1}^2 = \sigma_{e_2}^2 = 0.001$
Fading severity	$m_1 = m_2 = 2$
Average power	$\Omega_1 = \Omega_2 = 1$

$$
P_{D_1}^{II} = 1 - \frac{\alpha_R^{K_R}}{\Gamma\left(K_R\right)\Gamma\left(m_I\right)} \sum_{a=0}^{\infty} \sum_{b=0}^{K_R+a-1} \sum_{c=0}^{b} \binom{b}{c} \frac{\Gamma\left(K_R+a\right)\left(m_R K_R\right)_a}{a!b!\left(K_R\right)_a}
$$
$$
\times \left(\frac{m_I}{\Omega_I}\right)^{m_I} \frac{\Gamma\left(m_I+c\right)\delta_R^a\left(\bar{\phi}_1\right)^b e^{-\frac{\beta_R\bar{\phi}_1\left(\rho_S\sigma_{e_R}^2+1\right)}{\rho_S}}}{\left(\rho_S\right)^b\left(\beta_R\right)^{K_R+a-b}\left(\rho_S\sigma_{e_R}^2+1\right)^{c-b}\Gamma\left(m_1 K_T\right)}
$$
$$
\times \left(\frac{m_I}{\Omega_I}+\frac{\beta_R\phi_1}{\rho_S}\right)^{-m_I-c}\Gamma\left(m_1 K_T,\frac{m_1\bar{\phi}_1\left(\rho_R\sigma_{e_1}^2+1\right)}{\rho_R\Omega_1}\right). \tag{6.62}
$$

Proof: See Appendix F (pp. 79)

Similarly, the OP of D_2 can be expressed as

$$
P_{D_2}^{II} = 1 - \frac{\alpha_R^{K_R}}{\Gamma\left(K_R\right)\Gamma\left(m_I\right)} \sum_{a=0}^{\infty} \sum_{b=0}^{K_R+a-1} \sum_{c=0}^{b} \binom{b}{c} \frac{\Gamma\left(K_R+a\right)\left(m_R K_R\right)_a}{a!b!\left(K_R\right)_a}
$$
$$
\times \left(\frac{m_I}{\Omega_I}\right)^{m_I} \frac{\Gamma\left(m_I+c\right)\delta_R^a\left(\bar{\phi}_2\right)^b e^{-\frac{\beta_R\bar{\phi}_2\left(\rho_S\sigma_{e_R}^2+1\right)}{\rho_S}}}{\left(\rho_S\right)^b\left(\beta_R\right)^{K_R+a-b}\left(\rho_S\sigma_{e_R}^2+1\right)^{c-b}\Gamma\left(m_2 K_T\right)}
$$
$$
\times \left(\frac{m_I}{\Omega_I}+\frac{\beta_R\bar{\phi}_2}{\rho_S}\right)^{-m_I-c}\Gamma\left(m_2 K_T,\frac{m_2\bar{\phi}_2\left(\rho_R\sigma_{e_2}^2+1\right)}{\rho_R\Omega_2}\right) \tag{6.63}
$$

where $\bar{\phi}_2 = \frac{\gamma_2}{A_2}$.

6.2.5 Simulation results and discussion

In this section, we set $\rho_C = 1$ dB, $\rho = \rho_S = \rho_R$ and the main parameters according to Table 6.3. The shadowed-Rician fading parameters for the satellite link are taken from [170] and summarized in Table 6.4. Additionally, the interference channels parameters were set and calculated according to the respective analytical curves in [154] and are listed in Table 6.5. Monte Carlo simulations were produced in MATLAB.

Table 6.4: SATELLITE LINK PARAMETERS.

Shadowing	m_R	b_R	Ω_R
Heavy shadowing (HS)	1	0.063	0.0007
Average shadowing (AS)	5	0.251	0.279

Table 6.5: INTERFERENCE LINK PARAMETERS.

N	1	2	3	4	5
Ω_{Cn}	1	2.5	2.5	3.2	3.5
m_{Cn}	1	2	2.5	3	3.5
Ω_I	1	3.5	6	9.2	12.7
m_I	1	2.9697	5.4340	8.4317	11.9136

Figure 6.7 plots the outage performance versus the ρ (dB) for different shadowing satellite links. The results indicate that the performance of the system under AS exceeds the system under HS, suggesting that the satellite channel conditions contribute significantly to system performance at the ground user. The results also show a difference in performance between the NOMA and OMA systems. In the OMA system, the gap between the two curves indicates that as the SNR increases, system performance increases as in the NOMA system. The strict match of the Monte-Carlo simulations with the analytical simulations also indicates the authenticity of the derived expressions.
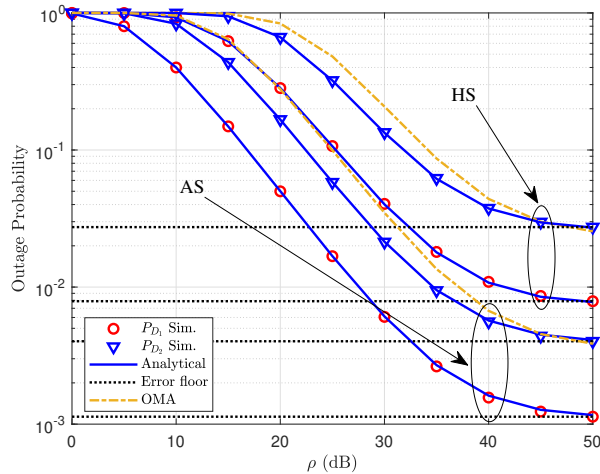
Figure 6.7: OP vs ρ(dB) in different satellite links.

Figure 6.8 represents the contribution of multiple antennae at the relay contribute in improving the system performance at the ground user. A relay with $K_T = K_R = 3$ exhibits a
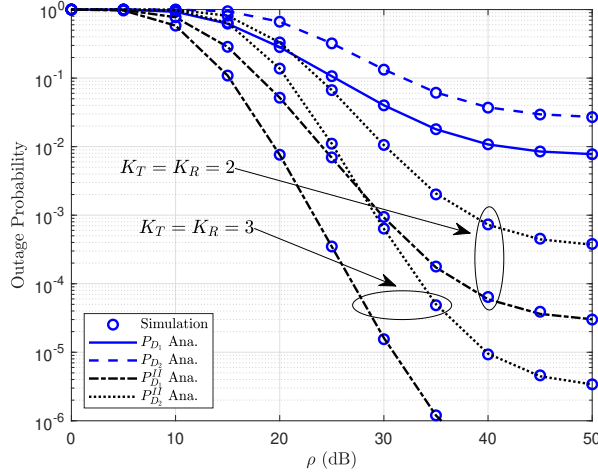
Figure 6.8: OP vs ρ(dB), varying $K_T = K_R$ with the satellite link under HS.

major difference in outage behavior can be observed compared to a relay with $K_T = K_R = 2$, a possible reason being that higher diversity from a multi-antenna design strengthens the signal received at the ground user, hence improving outage performance.
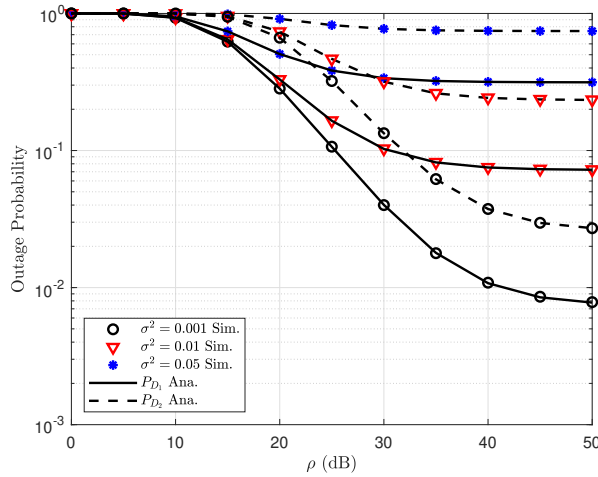
Figure 6.9: OP vs ρ(dB), varying σ^2 with the satellite link under HS.

Figure 6.9 indicates the impact of imperfect CSI on OP when the value of ρ is changed for case of HS. It is clear that performance could be affected by CSI error and varying σ^2. An increase in the value of σ^2 shows a reduction in performance at the user, whereas a reduction in the value of σ^2 produces better performance at both users. As the SNR increases, the performance at both users continues to increase, whereas in similar conditions (Fig.6.10), the number of interfering links at both users was varied while keeping σ^2 constant. Considering

72

the impact of CCI, the simulation shows that with a greater number of interference links, the performance at both users decreases. However, in all the links, the curves for each user meet at a saturated point at high SNR, indicating that in the high SNR region, interference links do not have a great effect on performance at the user.
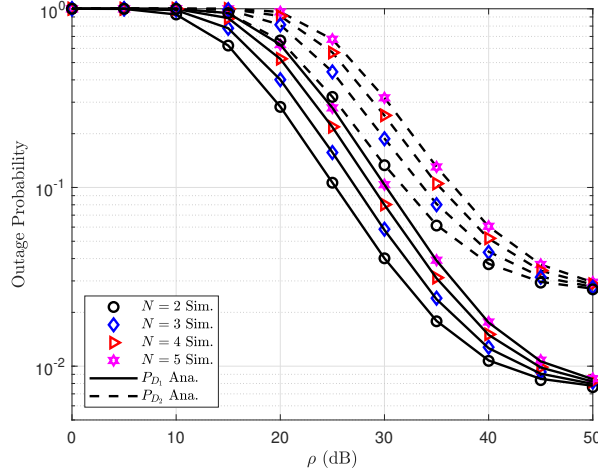
Figure 6.10: OP vs ρ(dB), varying N with the satellite link under HS.

Figure 6.11 plots the simulation for outage performance versus ρ (dB) with the different satellite links, as in Figure 6.7. The EC rates of the message at D_1 are almost the same in both HS and AS modes, but for messaging at D_2, the gap between the curves of EC in both modes is comparatively very high. With a simultaneous increase in the SNR, the gap increase is unlike D_1.
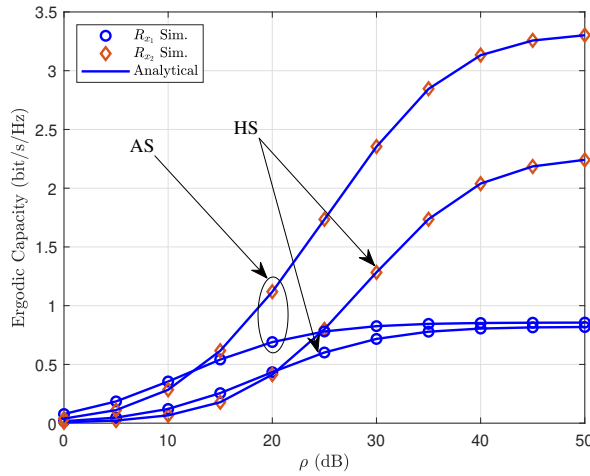
Figure 6.11: EC vs ρ(dB) with different satellite links.

Figure 6.12 and Figure 6.13 indicate the several curves of EC versus ρ (dB) under HS. The impact of CSI error levels of σ^2 are shown in Figure 6.12. Figure 6.13 confirms that the number of CCI sources affects the level of degradation in EC performance. Figure 6.12 indicates that as the value of σ^2 increases, the gap between the curves increases simultaneously at high SNR values. Figure 6.13 plots EC versus ρ (dB), varying N with a satellite link under HS. Although the differences between the curves are evident at medium SNR values, the curves for both users converge at a single point at higher SNRs, suggesting that a greater number of interference links does not have much differential effect on EC at higher SNRs.
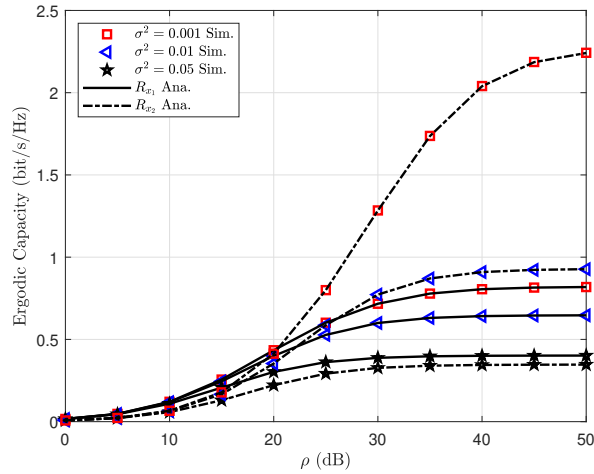
Figure 6.12: EC vs ρ(dB), varying σ^2 with the satellite link under HS.
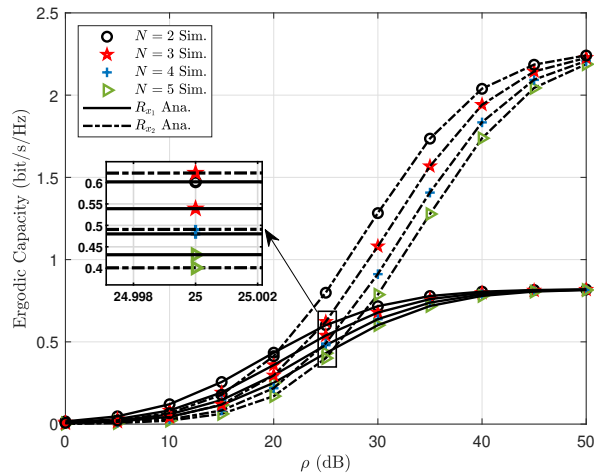
Figure 6.13: EC vs ρ(dB), varying N with the satellite link under HS.

6.2.6 Conclusion

This section described the use of NOMA for communication between a satellite to a relay and the relay to users. The performance of the system was investigated in terms of OP and EC under the effect of CCI at the relay. The performance gap between two destinations is a result of the differences in power level allocated at the destinations. The closed-form expressions for OP and EC at both users were also derived. As the channel error increased, both the OP and EC of the users were affected significantly. The effect of CCI on both OP and EC was more prominent when the SNR was in range of 20–30 dB, whereas a greater number of interference links indicated little effect in the region of high SNR. For example, if the number of interference sources is 5, the OP of the system experiences a decrease of approximately 40% at an SNR of 30 dB at the satellite. The OP and EC saturate at SNRs of 50 dB and 45 dB, respectively. System performance in terms of both OP and EC was also simulated and compared between AS and HS modes.

Appendix A

Using (6.25), B_1 is expressed as

$$
B_1 = \Pr \left(\frac{\rho_S A_1 \left| \hat{h}_R \right|^2}{\rho_S A_2 \left| \hat{h}_R \right|^2 + \gamma_C + \rho_S \sigma_{e_R}^2 + 1} > \gamma_1 \right)
$$

$$
= \Pr \left(\left| \hat{h}_R \right|^2 > \left(\gamma_C + \rho_S \sigma_R^2 + 1 \right) \phi_1 \right),
\tag{6.64}
$$

where $\phi_1 = \frac{\gamma_1}{(A_1 - A_2 \gamma_1)\rho}$. B_1 is therefore expressed as

$$
B_1 = \int_0^\infty f_{\gamma_C}(x) \left(1 - F_{\left| \hat{h}_R \right|^2} \left(\left(x + \rho_S \sigma_R^2 + 1 \right) \phi_1 \right) \right) dx.
\tag{6.65}
$$

Substituting (6.33) and (6.34) into (6.65), B_1 is rewritten as

$$
B_1 = \alpha_R \sum_{k=0}^{m_R-1} \sum_{l=0}^{k} \frac{\xi(k) k! (\phi_1)^l e^{-\Xi_R \phi_1 \left(\rho_S \sigma_R^2 + 1 \right)}}{l! \Gamma(m_I) (\Xi_R)^{k-l+1}} \left(\frac{m_I}{\Omega_I} \right)^{m_I}
$$

$$
\times \int_0^\infty x^{m_I - 1} \left(x + \rho_S \sigma_R^2 + 1 \right)^l e^{-\left(\frac{m_I + \Omega_I \Xi_R \phi_1}{\Omega_I} \right) x} dx.
\tag{6.66}
$$

Based on [117, Eq. 1.111] and [117, Eq. 3.381.4], the closed-form of B_1 is expressed as

$$
B_1 = \alpha_R \sum_{k=0}^{m_R-1} \sum_{l=0}^{k} \sum_{p=0}^{l} \binom{l}{p} \frac{\xi(k) k! \Gamma(m_I + p)}{l! \Gamma(m_I) (\Xi_R)^{k-l+1}} e^{-\Xi_R \phi_1 \left(\rho_S \sigma_R^2 + 1 \right)}
$$

$$
\times \left(\phi_1 \left(\rho_S \sigma_R^2 + 1 \right) \right)^l \left(1 + \frac{\Omega_I \Xi_R \phi_1}{m_I} \right)^{-m_I - p} \left(\frac{\Omega_I}{m_I \left(\rho_S \sigma_R^2 + 1 \right)} \right)^p.
\tag{6.67}
$$

This completes the proof.

Appendix B

Let us denote the first and second terms of (6.43) as C_1 and C_2, respectively. Using (6.26), C_1 can then be expressed as

$$
\begin{aligned}
C_1 &= \Pr\left(\frac{\rho_S A_2 \left|\hat{h}_R\right|^2}{\gamma_C + \rho_S \sigma_{e_R}^2 + 1} > \gamma_2\right) \\
&= \Pr\left(\left|\hat{h}_R\right|^2 > \psi_1\left(\gamma_C + \rho_S \sigma_{e_R}^2 + 1\right)\right) \\
&= \int_0^\infty f_{\gamma_C}(x)\, F_{\left|\hat{h}_R\right|^2}\left(\left(x + \rho_S \sigma_{e_R}^2 + 1\right)\psi_1\right)\, dx,
\end{aligned}
\tag{6.68}
$$

where $\psi_1 = \frac{\gamma_2}{\rho_S A_2}$. As in Proposition 1, we obtain C_1 as

$$
\begin{aligned}
C_1 &= \alpha_R \sum_{k=0}^{m_R-1} \sum_{l=0}^{k} \sum_{p=0}^{l} \binom{l}{p} \frac{k!\, \xi(k)\, \Gamma(m_I + p)}{l!\, \Gamma(m_I)\, (\Xi_R)^{k-l+1}} e^{-\Xi_R \psi_1 \left(\rho_S \sigma_{e_R}^2 + 1\right)} \\
&\times \left(\psi_1\left(\rho_S \sigma_{e_R}^2 + 1\right)\right)^l \left(1 + \frac{\Omega_I \Xi_R \psi_1}{m_I}\right)^{-m_I - p} \left(\frac{\Omega_I}{m_I\left(\rho_S \sigma_{e_R}^2 + 1\right)}\right)^p.
\end{aligned}
\tag{6.69}
$$

Next, C_2 is calculated as

$$
\begin{aligned}
B_2 &= \Pr\left(\frac{\rho_R A_2 \left|\hat{h}_2\right|^2}{\rho_R \sigma e_2^2 + 1} > \gamma_2\right) \\
&= \Pr\left(\left|\hat{h}_2\right|^2 > \psi_2\right) \\
&= \sum_{b_2=0}^{m_2-1} \frac{e^{-\frac{m_2 \psi_2}{\Omega_2}}}{b_2!} \left(\frac{m_2 \psi_2}{\Omega_2}\right)^{b_2},
\end{aligned}
\tag{6.70}
$$

where $\psi_2 = \frac{\left(\rho_R \sigma_{e_2}^2 + 1\right)\gamma_2}{\rho_R A_2}$.

Using (6.69) and (6.70), the closed-form OP of D_2 is obtained as (6.44).

This completes the proof.

Appendix C

In the high SNR region, the CDF of $|\hat{h}_R|^2$ and $|\hat{h}_i|^2$ are respectively expressed as

$$
F_{|\hat{h}_R|^2}^\infty(x) = \alpha_R x
\tag{6.71}
$$

and

$$F_{|h_i|^2}(x) = \frac{1}{\Gamma(m_i + 1)} \left(\frac{m_i}{\Omega_i} x \right)^{m_i}. \tag{6.72}$$

Next, the asymptotic OP of D_1 is calculated as

$$P_{D_1}^\infty = 1 - B_1^\infty \times B_2^\infty \tag{6.73}$$

Then, B_1^∞ is expressed as

$$\begin{aligned}
B_1^\infty &= 1 - \Pr\left(\left| \hat{h}_R \right|^2 < \left(\gamma_C + \rho_S \sigma_{e_R}^2 + 1 \right) \phi_1 \right) \\
&= 1 - \int_0^\infty f_{\gamma_C}(x) F_{|\hat{h}_R|^2}^\infty \left(\left(x + \rho_S \sigma_{e_R}^2 + 1 \right) \phi_1 \right).
\end{aligned} \tag{6.74}$$

Using (6.71) and (6.36), B_1^∞ can be rewritten as

$$\begin{aligned}
B_1^\infty &= 1 - \left(\frac{m_I}{\Omega_I} \right)^{m_I} \frac{\alpha_R \phi_1}{\Gamma(m_I)} \int_0^\infty \frac{x^{m_I - 1} e^{-\left(\frac{m_I}{\Omega_I} \right) x}}{\left(x + \rho_S \sigma_{e_R}^2 + 1 \right)^{-1}} \\
&= 1 - \left(\frac{m_I}{\Omega_I} \right)^{m_I} \frac{\alpha_R \varphi_1}{\Gamma(m_I)} \left(\int_0^\infty x^{m_I} e^{-\left(\frac{m_I}{\Omega_I} \right) x} dx \right. \\
&\quad + \left. \left(\rho_S \sigma_{e_R}^2 + 1 \right) \int_0^\infty x^{m_I - 1} e^{-\left(\frac{m_I}{\Omega_I} \right) x} dx \right).
\end{aligned} \tag{6.75}$$

B_1^∞ is thus expressed as

$$B_1^\infty = 1 - \alpha_R \phi_1 \left(\frac{(m_I)!}{\Gamma(m_I)} \left(\frac{\Omega_I}{m_I} \right) + \left(\rho_S \sigma_{e_R}^2 + 1 \right) \right). \tag{6.76}$$

The term B_2^∞ can therefore be expressed as

$$\begin{aligned}
B_2^\infty &= \Pr\left(\left| \hat{h}_1 \right|^2 > \phi_2 \right) \\
&= 1 - F_{|\hat{h}_1|^2}^\infty (\phi_2) \\
&= 1 - \frac{1}{\Gamma(m_1 + 1)} \left(\frac{m_1 \phi_2}{\Omega_1} \right)^{m_1}.
\end{aligned} \tag{6.77}$$

Substituting (6.76) and (6.77) into (6.73), we obtain (6.46).

This completes the proof.

Appendix D

First, the CDF of Q_1 is expressed as

$$F_{Q_1}(x) = \alpha_R \sum_{k=0}^{m_R-1} \sum_{l=0}^{k} \sum_{p=0}^{l} \sum_{b_1=0}^{m_1-1} \binom{l}{p} \frac{\xi(k)\,k!\,\Gamma(m_I + p)}{b_1!\,l!\,\Gamma(m_I)(\Xi_R)^{k-l+1}}$$

$$\times \left(\frac{(\rho_R \sigma_{e_1}^2 + 1)\,m_1 x}{(A_1 - A_2 x)\,\Omega_1 \rho_R} \right)^{b_1} \left(1 + \frac{\Omega_I \Xi_R x}{(A_1 - A_2 x)\,m_I \rho_S} \right)^{-m_I - p} \left(\frac{\Omega_I}{m_I (\rho_S \sigma_{e_R}^2 + 1)} \right)^{p} \qquad (6.78)$$

$$\times e^{-\frac{x(\rho_S \sigma_{e_R}^2 + 1)\Xi_R}{(A_1 - A_2 x)\rho_S} - \frac{(\rho_R \sigma_{e_1}^2 + 1)m_1 x}{(A_1 - A_2 x)\Omega_1 \rho_R}} \left(\frac{x(\rho_S \sigma_{e_R}^2 + 1)}{(A_1 - A_2 x)\,\rho_S} \right)^{l}.$$

Substituting (6.78) into (6.48), we obtain R_{x_1} as

$$R_{x_1} = \frac{\alpha_R}{2\ln(2)} \sum_{k=0}^{m_R-1} \sum_{l=0}^{k} \sum_{p=0}^{l} \sum_{b_1=0}^{m_1-1} \binom{l}{p} \frac{\xi(k)\,k!\,\Gamma(m_I + p)}{b_1!\,l!\,\Gamma(m_I)(\Xi_R)^{k-l+1}}$$

$$\times \left(\frac{(\rho_R \sigma_{e_1}^2 + 1)\,m_1}{\Omega_1 \rho_R} \right)^{b_1} \left(\frac{\Omega_I}{m_I (\rho_S \sigma_{e_R}^2 + 1)} \right)^{p} \left(\frac{(\rho_S \sigma_{e_R}^2 + 1)}{\rho_S} \right)^{l}$$

$$\times \int_{0}^{A_1/A_2} \frac{1}{1 + x} \left(1 + \frac{\Omega_I \Xi_R x}{(A_1 - A_2 x)\,m_I \rho_S} \right)^{-m_I - p} \left(\frac{x}{(A_1 - A_2 x)} \right)^{b_1 + l} \qquad (6.79)$$

$$\times e^{-\frac{(\rho_S \sigma_{e_R}^2 + 1)\Xi_R x}{(A_1 - A_2 x)\rho_S} - \frac{(\rho_R \sigma_{e_1}^2 + 1)m_1 x}{(A_1 - A_2 x)\Omega_1 \rho_R}}.$$

Using the Gaussian-Chebyshev property and denoting $\theta_p = \cos\left(\frac{2p-1}{2P}\pi \right)$, the closed-form EC of x_1 (6.49) can be obtained.

This completes the proof.

Appendix E

Similarly, the CDF of Q_2 is expressed as

$$F_{Q_2}(y) = 1 - \alpha_R \sum_{k=0}^{m_R-1} \sum_{l=0}^{k} \sum_{p=0}^{l} \sum_{b_2=0}^{m_2-1} \binom{l}{p} \frac{k!\,\xi(k)\Gamma(m_I + p)}{b_2!\,l!\,\Gamma(m_I)(\Xi_R)^{k-l+1}}$$

$$\times \left(\frac{m_2 (\rho_R \sigma_{e_2}^2 + 1)}{\Omega_2 \rho_R A_2} \right)^{b_2} \left(\frac{(\rho_S \sigma_{e_R}^2 + 1)}{\rho_R A_2} \right)^{l} \left(\frac{\Omega_I}{m_I (\rho_S \sigma_{e_R}^2 + 1)} \right)^{p} \qquad (6.80)$$

$$\times \frac{y^{l+b_2}}{\left(1 + \frac{\Omega_I \Xi_R}{m_I \rho_R A_2} y \right)^{m_I + p}} e^{-\Psi_2 y},$$

where $\Psi_2 = \frac{\Xi_R (\rho_S \sigma_{e_R}^2 + 1)}{\rho_R A_2} + \frac{m_2 (\rho_R \sigma_{e_2}^2 + 1)}{\Omega_2 \rho_R A_2}$. Next, we can calculate R_{x_2} as

$$R_{x_2} = \frac{\alpha_R}{2\ln(2)} \sum_{k=0}^{m_R-1} \sum_{l=0}^{k} \sum_{p=0}^{l} \sum_{b_2=0}^{m_2-1} \binom{l}{p} \frac{k!\xi(k)\Gamma(m_I+p)}{b_2!l!\Gamma(m_I)(\Xi_R)^{k-l+1}}$$

$$\times \left(\frac{m_2(\rho_R\sigma_{e_2}^2+1)}{\Omega_2\rho_R A_2}\right)^{b_2} \left(\frac{(\rho_S\sigma_{e_R}^2+1)}{\rho_R A_2}\right)^{l} \left(\frac{\Omega_I}{m_I(\rho_S\sigma_{e_R}^2+1)}\right)^{p} \tag{6.81}$$

$$\times \int_0^\infty \frac{y^{l+b_2}e^{-\Psi_2 y}}{(1+y)\left(1+\frac{\Omega_I\Xi_R}{m_I\rho_R A_2}y\right)^{m_I+p}}.$$

Using [171], we have

$$(1+ax)^{-b} = \frac{1}{\Gamma(b)}G_{1,1}^{1,1}\left[ax\,\middle|\,\begin{matrix}1-b\\0\end{matrix}\right] \tag{6.82}$$

where $G_{1,1}^{1,1}[.,.]$ is the Meijer G-function [117]. Substituting (6.82) into (6.81), R_{x_2} is rewritten as

$$R_{x_2} = \frac{\alpha_R}{2\ln(2)} \sum_{k=0}^{m_R-1} \sum_{l=0}^{k} \sum_{p=0}^{l} \sum_{b_2=0}^{m_2-1} \binom{l}{p} \frac{k!\xi(k)(\Xi_R)^{l-k-1}}{b_2!l!\Gamma(m_I)}$$

$$\times \left(\frac{m_2(\rho_R\sigma_{e_2}^2+1)}{\Omega_2\rho_R A_2}\right)^{b_2} \left(\frac{(\rho_S\sigma_{e_R}^2+1)}{\rho_R A_2}\right)^{l} \left(\frac{\Omega_I}{m_I(\rho_S\sigma_{e_R}^2+1)}\right)^{p} \tag{6.83}$$

$$\times \int_0^\infty y^{l+b_2}e^{-\Psi_2 y}G_{1,1}^{1,1}\left[x\,\middle|\,\begin{matrix}0\\0\end{matrix}\right]G_{1,1}^{1,1}\left[\frac{\Omega_I\Xi_R}{m_I\rho_R A_2}y\,\middle|\,\begin{matrix}1-m_I-p\\0\end{matrix}\right]$$

Based on [172, p. 2.6.2], (6.32) is obtained.

This completes the proof.

Appendix F

The OP of D_1 can be expressed as

$$P_{D_1}^{II} = 1 - \underbrace{\Pr\left(\Gamma_{R\to x_1}^{II} > \gamma_i\right)}_{F_1}\underbrace{\Pr\left(\Gamma_{D_1\to x_1}^{II} > \gamma_i\right)}_{F_2} \tag{6.84}$$

Assisted by (6.53), the first term F_1 is obtained from

$$F_1 = \Pr\left(\frac{A_1\eta_R}{A_2\eta_R+\rho_S\sigma_{e_R}^2+\gamma_C+1} > \gamma_1\right)$$

$$= \Pr\left(\eta_R > \bar{\phi}_1\left(\rho_S\sigma_{e_R}^2+\gamma_C+1\right)\right) \tag{6.85}$$

$$= \int_0^\infty f_{\gamma_C}(x)\left(1-F_{\eta_R}\left(\bar{\phi}_1\left(\rho\sigma_{e_R}^2+x+1\right)\right)\right)dx,$$

where $\bar{\phi}_1 = \frac{\gamma_1}{(A_1 - A_2\gamma_1)}$. Based on (6.36) and (6.59), F_1 can be calculated as

$$
\begin{aligned}
F_1 = {} & \frac{\alpha_R^{K_R}}{\Gamma(K_R)\Gamma(m_I)} \left(\frac{m_I}{\Omega_I}\right)^{m_I} \sum_{a=0}^{\infty} \sum_{b=0}^{K_R+a-1} \frac{\Gamma(K_R+a)(m_R K_R)_a}{a!b!(K_R)_a} \\
& \times \frac{\delta_R^a (\phi_1)^b \, e^{-\frac{\beta_R \bar{\phi}_1 \left(\rho_S \sigma_{e_R}^2 + 1\right)}{\rho_S}}}{(\rho_S)^b (\beta_R)^{K_R+a-b}} \int_0^{\infty} x^{m_I-1} \left(\rho_S \sigma_{e_R}^2 + x + 1\right)^b e^{-\left(\frac{m_I}{\Omega_I} + \frac{\beta_R \bar{\phi}_1}{\rho_S}\right)x}
\end{aligned}
$$

(6.86)

The second term of (6.85) is therefore calculated by

$$
\begin{aligned}
F_2 &= \Pr\left(\eta_1 > \left(\bar{\phi}_1\left(\rho_R \sigma_{e_1}^2 + 1\right)\right)\right) \\
&= 1 - F_{\eta_1}\left(\bar{\phi}_1\left(\rho_R \sigma_{e_1}^2 + 1\right)\right) \\
&= \frac{1}{\Gamma(m_1 K_T)}\Gamma\left(m_1 K_T, \frac{m_1 \bar{\phi}_1\left(\rho_R \sigma_{e_1}^2 + 1\right)}{\rho_R \Omega_1}\right)
\end{aligned}
$$

(6.87)

Substituting (6.86) and (6.36) into (6.84), we obtain the expected result. This completes the proof.

Chapter 7

Performance Analysis of NOMA-based Hybrid Satellite-Terrestrial Relay System Using mmWave Technology

This chapter discusses the dissertation's third aim. A new NOMA-based HSTRN system model [NNT01], [NNT02], [NNT08], [NNT11] is proposed, and the system performance is analyzed. The results of this section were previously published in [NNT01]. The key contributions to the dissertation's third aim are summarized as follows:

- A proposed NOMA-based HSTRN using mmWave communications, where a geostationary Earth orbit (GEO) satellite and amplify and forward (AF) protocol relaying are considered to serve multiple devices in NOMA to improve the spectrum.

- Analyze system performance based on Nakagami-m and shadowed-Rician channels. Furthermore, investigate the rain attenuation values to select the best relay.

- The benchmarks for comparing the NOMA-based scheme to the OMA-based scheme are supplied, demonstrating the benefits of the NOMA scheme.

- The closed-form of outage probability (OP) and ergodic capacity (EC) are expressed, and Monte Carlo simulations are presented to further confirm the accuracy of the findings.

7.1   Introduction

Recently, satellite communication (SatCom) has been one of the potential technologies for the 5G network and beyond, which brings many advantages such as high throughput, outstanding reliability, extensive coverage, inexpensive operations, and energy-efficient [173, 174, 175].

Therefore, the integration of SatCom into current terrestrial communication systems has received considerable attention in researching and proposing models of the integrated satellite-terrestrial network (ISTN) [176, 177]. In SatCom, geostationary Earth orbit (GEO), middle Earth orbit (MEO), and low Earth orbit (LEO) satellites can operate efficiently in the high frequency bands of mmWave (e.g. Ka/Q/V-band) [157]. They effectively provide system throughput and extensive coverage of the terrestrial wireless network [178, 179]. However, using traditional OMA techniques in SatCom would result in a waste of block resources, such as the time / frequency / code block due to the limitation in the number of simultaneously connected users, the ability to meet for services requires low latency and high throughput [31, 180]. Contributing to solving the limitations of OMA, a promising technology for 5G has been proposed, NOMA [181]. NOMA helps improve resource efficiency and increase the number of users served in the same resource block with higher data speed, higher reliability, and lower latency than the conventional OMA scheme [182]. With these advantages, the combination of SatCom with NOMA will significantly improve network performance; therefore, this is a promising job for the future.

Under the influence of rain, fog, and obstacles, the performance of ground users will be severely affected. Therefore, the hybrid satellite-terrestrial relay network (HSTRN) is proposed to solve the above problems. The authors in [183] presented the relay selection as well as round-robin scheduling schemes for the physical-layer security (PLS) in HSTRN, where secrecy performance has been analyzed with the decode and forward (DF) relaying protocol. To evaluate the security and reliability of a satellite-terrestrial network with multiple ground relays in the presence of an eavesdropper, the authors in [184] deployed a friendly jammer and an amplify and forward-based relaying scheme to subtract the consequence of the eavesdropper on system performance. In [154], the authors investigated the EC in HSTRN with an adopted AF relaying protocol. Furthermore, the authors combined opportunistic scheduling for terrestrial destinations. To achieve optimal power performance, rate adaptation and truncated channel inversion with fixed rate in HSTRN have been proposed in [185]. In [186], the authors employed a cache-enabled for HSTRN, which is regarded as the common and most widely used content-based caching strategy. The average symbol error rate (ASER) has been examined in both the cases of a degraded LoS link and without a degraded LoS link, which is presented in [16] and [15], respectively. The authors in [187] analyzed the OP performance of decode-and-forward HSTRN with the best relay selection technique while taking into account a multiple-relay scenario. Also, the performance of downlink HSTRN with relay selection was presented in [188]. Furthermore, hardware impairments (HIs) and interference are considered for the relay and terrestrial destination. The effect of co-channel interference (CCI) in HSTRN has been evaluated in terms of bit error rate at the relay and destination nodes in [189]. To increase the total throughput and reduce system complexity, full-duplex (FD) and relay selection techniques are applied at the relay proposed in [190].

Table 7.1: Features, methodology and challenges of previous works on NOMA-based Satellite Networks.

Papers (years)	Features	Methodology	Challenges
[188] (2020)	MIMO-DF relay protocol, relay selection and GEO satellite	OP, throughput of system and asymptotic outage are analyzed	Without NOMA, low frequency
[191] (2020)	Satellite network cooperative with NOMA	OP and asymptotic outage are analyzed	Without relay, two destinations, low frequency
[192] (2021)	DF MIMO relay protocol, cooperative with NOMA	OP and asymptotic outage are analyzed	Two destinations, low frequency
[193] (2021)	DF relay protocol, relay selection, GEO satellite, satellite network cooperative with NOMA	OP, asymptotic outage and EC are analysis	Two destinations, single antenna at relay, low frequency
[194] (2022)	DF relay protocol, relay selection, LEO satellite, cooperative with NOMA	OP and asymptotic outage are analyzed	Two destinations, low frequency, single antenna at relay
[195] (2022)	AF relay protocol, Multiple destinations, GEO satellite, cooperative with NOMA	OP and asymptotic outage are analyzed	Single relay, low frequency, single antenna at relay

The NOMA scheme is considered to improve spectrum efficiency and serve multiple users in a time/frequency/code block in conjunction with HSTRN. Recently, the investigations on the impact of NOMA on satellite-terrestrial network (STN) in order to use spectrum efficiently and serve multiple users at the block resources [196, 197, 198, 149]. The exact outage behaviors of NOMA-based STN and the asymptotic analysis were studied in [196]. Identical OP analysis was achieved in [197], where the authors discussed the effectiveness of NOMA-based uplink of land mobile satellite (LMS) communications. The authors in [198] considered the OP and asymptotic OP obtained after evaluating the system performance of NOMA-based HSTRN with the AF protocol. To maximize the sum rate of the suggested NOMA-based HSTRN, the authors provided an iterative penalty function-based beamforming (BF) method. This algorithm could quickly get the BF weight vector and power coefficient [149]. To collaborate with the primary satellite network for dynamic spectrum access, the secondary terrestrial network and the overlay cognitive integrated satellite-terrestrial relay network (CISTRN) based on NOMA were examined in [NNT08],[199]. Moreover, the authors in [200] analyzed the performance of the secondary network when the near user employed the full-duplex mode

and used the DF protocol to enhance the performance of the far user in the NOMA network. In [201], the authors investigated the OP and average transit time for an underlay cognitive NOMA-based HSTRN with an HD secondary receiver. Table 7.1 summarizes the related work on the NOMA-based satellite network, in which its features, methodology, and challenges are highlighted in the previous works. To the best of our knowledge, the NOMA-based HSTRN with mmWave communications has not yet been disclosed.
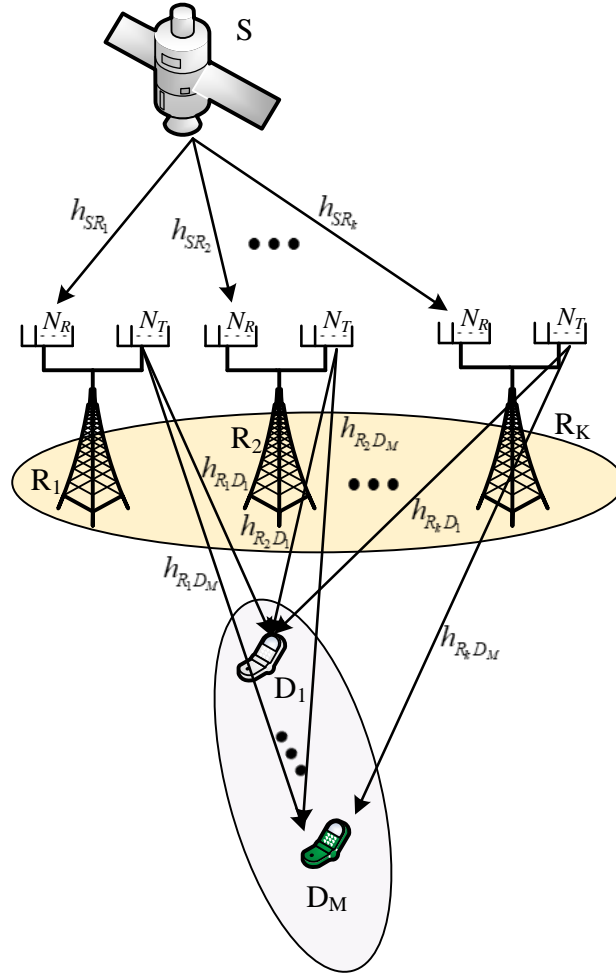
7.2 System model

Figure 7.1: The system model of the satellite using mmWave communications

The system model consists of an AF-multirelay satellite cooperative NOMA network as shown in Figure 7.1, which consists of the source node S, the K terrestrial relay nodes

Table 7.2: The table of main notations.

Notation	Definition
K	Number of relays
M	Number of Devices
N_R	Number received antenna of relays
N_T	Number transmit antenna of relays
P_S	Transmit power of satellite
P_R	Transmit power of relays
x_i	The signal of D_i
ϖ_i	The power allocation
$\vartheta_{r,k*}$	The expected rain attenuation of link from S to R_{k*}
$\vartheta_{d,m*}$	The expected rain attenuation of link from R_{k*} to devices D_m
G_S	The antenna gain at the satellite
$G_R^{\max}$	The antenna gain at relays
$(\bullet)^H$	Hermitian transpose
$\|\bullet\|_F$	Frobenius norm
$J_\nu(\bullet)$	The first-kind Bessel function with order ν
$\mathcal{B}(\bullet, \bullet)$	Beta function
$\gamma(\bullet, \bullet)$	The lower incomplete gamma function
$K_\nu(\bullet)$	The second-kind Bessel function with order ν

$R_k(k = 1, 2, ..., K)$ equipped with N_R receiving antennas and N_T transmitting antennas, and M devices $D_m(m = 1, 2, ..., M)$. Furthermore, assuming that the direct communication links between S and D_m are not available due to the heavy shadowing [161]. Therefore, satellite S communicates with terrestrial devices with the help of the best terrestrial relay R_{k*} based on opportunistic scheduling [157].

In the first phase, the satellite transmits the signal $x_S = \sum_{i=1}^{M} \sqrt{\varpi_i} x_i$ to the relay node R_{k*}, and the relay node performs the maximum ratio combining (MRC) to combine the received signals [202]. Hence, the received signal at the best relay node is given by

$$
\begin{aligned}
y_{SR_{k*}} &= \sqrt{L_S G_S(\phi) G_R P_S} \vartheta_{r,k*} \mathbf{h}_{SR_{k*}} \mathbf{w}_{SR_{k*}}^H x_S + n_{R_{k*}} \\
&= \sqrt{L_S G_S(\phi) G_R P_S} \vartheta_{r,k*} \mathbf{h}_{SR_{k*}} \mathbf{w}_{SR_{k*}}^H \sum_{i=1}^{M} \varpi_i x_i + n_{R_{k*}}
\end{aligned}
\tag{7.1}
$$

where $\mathbf{h}_{\mathbf{SR_{k*}}} = [\mathbf{h}_{\mathbf{SR_{k*}}}^{\mathbf{1}}, \mathbf{h}_{\mathbf{SR_{k*}}}^{\mathbf{2}}, ..., \mathbf{h}_{\mathbf{SR_{k*}}}^{\mathbf{N_R}}]^{\mathbf{T}}$ is the $N_R \times 1$ channel coefficient vector between S and R_{k*}, $\vartheta_{r,k*}$ denote the expected rain attenuation between S and R_{k*}, $\mathbf{w}_{\mathbf{SR_{k*}}} = \frac{\mathbf{h}_{\mathbf{SR_{k*}}}}{\|\mathbf{h}_{\mathbf{SR_{k*}}}\|_{\mathbf{F}}}$ is the receive beamforming weight vector and $n_{R_{k*}}$ is the vector of zero mean additive white

Gaussian noise (AWGN) with variance N_0. Then the desired relay node amplifies the received signal $y_{SR_{k*}}$ by a gain factor $G = \sqrt{\frac{1}{P_S \|\mathbf{h_{SR_{k*}}}\|_F^2 \vartheta_{r,k}^2 + N_0}}$, and performs maximum ratio transmission (MRT) to forward it to the desired destination node according to the feedback of the pilot signal from each destination node during second phase[202]. Additionally, the free space pathloss coefficient L_S can be expressed as [201, 193, 203]

$$L_S = \frac{\lambda^2}{(4\pi d_R)^2 N_p} \tag{7.2}$$

where $\lambda = \frac{c}{f_c}$ is the wavelength, c is the light speed, f_c is the carrier frequency, d_R is the distance between the satellite and R_{k*}, $N_p = K_B T B_\omega$ is noise power, K_B denote the Boltzmann constant, T is the noise temperature of the terrestrial receiver and B_ω represents the bandwidth. For the R_{k*} location, ϕ represents the angle between R_{k*} and beam center compared to the satellite. In addition, G_R denotes the antenna gain at R_{k*}, $G_S(\phi)$ denotes the satellite beam gain, and the beam gain $G_S(\phi)$ is given as [193]

$$G_S(\phi) = G_S^{\mathrm{max}} \left(\frac{J_1(u)}{2u} + 36 \frac{J_3(u)}{u^3} \right)^2 \tag{7.3}$$

where G_S^{max} denotes the maximal beam gain and u can be expressed as

$$u = 2.07123 \frac{\sin(\phi)}{\sin(\phi_{3dB})} \tag{7.4}$$

where ϕ_{3dB} is the constant 3-dB angle for the beam.

Next, the received signal at the desired destination node is given by

$$
\begin{aligned}
y_{R_{k*}D_m} &= G\vartheta_{d,m*}\sqrt{L_{D_m}P_R}\mathbf{h}_{R_{k*}D_m}^H \mathbf{w}_{R_{k*}D_m} y_{SR_{k*}} + n_{D_m} \\
&= G\mathbf{h}_{R_{k*}D_m}^H \mathbf{w}_{R_{k*}D_m} \sqrt{L_S L_{D_m} G_S(\phi) G_R P_S P_R} \\
&\quad \times \vartheta_{d,m*}\vartheta_{r,k*}\mathbf{h}_{SR_{k*}}\mathbf{w}_{SR_{k*}}^H \sum_{i=1}^{M} \varpi_i x_i \\
&\quad + G\vartheta_{d,m*}\sqrt{L_{D_m}P_R}\mathbf{h}_{R_{k*}D_m}^H \mathbf{w}_{R_{k*}D_m} \mathbf{n}_{R_{k*}} + n_{D_m}
\end{aligned}
\tag{7.5}
$$

where $\mathbf{h}_{R_{k*}D_m} = [h_{R_{k*}D_m,1}, h_{R_{k*}D_m,2}, ..., h_{R_k D_m, N_T}]^T$ is the $N_T \times 1$ channel coefficient vector from R_{k*} to D_m, $\vartheta_{d,m*}$ denote the expected rain attenuation between R_{k*} and D_m, $\mathbf{w}_{R_k D_m} = \frac{\mathbf{h}_{R_k D_m}}{\|\mathbf{h}_{R_k D_m}\|_F}$ is the transmitting beamforming weight vector. Without loss of generality, the channel gains from R_k to D_m are ordered $h_{R_k D_1} \leqslant h_{R_k D_2} \leqslant \ldots h_{R_k D_M}$

and n_{D_m} is the zero mean additive white Gaussian noise (AWGN) with variance N_0. In

the mmWave network, the path loss L_{D_m} in the terrestrial link can be modeled as [204]

$$L_{D_m} = \kappa + 10\nu \log(d_m) + \theta \tag{7.6}$$

where κ and ν denote the linear model parameters, θ is accounting for variances in shadowing fading and d_m denotes the distance between R_{k*} and D_m.

Following NOMA procedures [105], the received signal to interference and noise ratio (SINR) at m-th device to detect the information of q-th device $(m > q)$ is given below.

$$\gamma_{m \to q} = \frac{\bar{\eta}_m P_S P_R G^2 \|\mathbf{h}_{SR_{k*}}\|_F^2 \|\mathbf{h}_{R_{k*}D_m}\|_F^2 \varpi_q}{\bar{\eta}_m P_S P_R G^2 \|\mathbf{h}_{SR_{k*}}\|_F^2 \|\mathbf{h}_{R_{k*}D_m}\|_F^2 \sum\limits_{i=q+1}^{M} \varpi_i + (G\vartheta_{d,m*})^2 P_R L_{D_m} \|\mathbf{h}_{R_{k*}D_m}\|_F^2 N_0 + N_0}$$

$$= \frac{\rho_S \rho_{D_m} \bar{\eta}_m \varpi_q}{\bar{\eta}_m \rho_S \rho_{D_m} \sum\limits_{i=q+1}^{M} \varpi_i + \rho_{D_m} L_{D_m} \vartheta_{d,m*}^2 + \rho_S \vartheta_{r,k*}^2 + 1}$$

$$\tag{7.7}$$

In which, $\bar{\eta}_m = L_S L_{D_m} G_S(\phi) G_R (\vartheta_{d,m*} \vartheta_{r,k*})^2$, $\eta = \frac{P_S}{N_0}$, $\eta_R = \frac{P_R}{N_0}$, $\rho_S = \eta_S \|\mathbf{h}_{SR_{k*}}\|_F^2$ and $\rho_{D_m} = \eta_R \|\mathbf{h}_{R_{k*}D_m}\|_F^2$.

Then the received SINR of m-th device to detect the information by treating $M - p$ devices's signals as interference is given by

$$\gamma_m = \frac{\rho_S \rho_{D_m} \bar{\eta}_m \varpi_m}{\bar{\eta}_m \rho_S \rho_{D_m} \sum\limits_{i=m+1}^{M} \varpi_i + \rho_{D_m} L_{D_m} \vartheta_{d,m*}^2 + \rho_S \vartheta_{r,k}^2 + 1} \tag{7.8}$$

After the information of $M-1$ devices can be detected, the received SINR for M-th device is given by

$$\gamma_M = \frac{\rho_S \rho_{D_M} \bar{\eta}_M \varpi_M}{\rho_{D_M} L_{D_M} \vartheta_{d,m*}^2 + \rho_S \vartheta_{r,k}^2 + 1} \tag{7.9}$$

7.3 Statistical Analysis

The rain attenuation is the important attenuation factor in mmWave band channels. The expected value of the rain attenuation from S to R_{k*} link can be treated as a constant during a transmission phase. Therefore, to reduce computational complexity, satellite can select the desired relay node according to the feedback of expected rain attenuation rather than the channel gain vector, namely

$$k* = \arg\min_{k=1,\ldots,K} (\vartheta_{r,k}) \tag{7.10}$$

Therefore, the rain attenuation value of R_k can be expressed as $A* = \min(\vartheta_{r,1}, \ldots, \vartheta_{r,K})$. Assuming that the rain attenuation values are independently and identically distributed (IID). The cumulative density function (CDF) of $A*$ can be given by $F_{A*}(x) = 1 - [1 - F_A(x)]^K$, where $F_A(x)$ is the CDF of the lognormal rain attenuation distribution [205]. In order to investigate the effect of the different number of relays, we need to derive the expected value of $A*$, which can validate the means of our proposed relay selection scheme and shown in [157].

Next, assuming that the channel conditions of all hops are IID. Furthermore, mmWave satellite-terrestrial communications are mainly impaired by the masking effect and weather conditions, especially rain attenuation [206]. Under the Shadowed-Rician fading model for the satellite links, the probability density function (PDF) of ρ_S is given by [168]

$$f_{\rho_S}(x) = \sum_{i_1=0}^{m_{SR}-1} \cdots \sum_{i_{N_R}=0}^{m_{SR}-1} \frac{\Xi(N_R)}{\eta_S^\Lambda} x^{\Lambda-1} e^{-\frac{\Delta}{\eta_S}x} \tag{7.11}$$

where

$$\Xi(N_R) = \prod_{\tau=1}^{N_R} \zeta(\xi_\tau) \alpha^{N_R} \prod_{\upsilon=1}^{N_R-1} \mathcal{B}\left(\sum_{\updownarrow=\infty}^{\upsilon} \xi_\updownarrow + \upsilon, \zeta_{\upsilon+\infty} + \infty\right) \tag{7.12}$$

$\zeta(a) = \frac{(-1)^a(1-m_{SR})_a \delta^a}{(a!)^2}$, $\Lambda = \sum_{\tau=1}^{N} \xi_\tau + N_R$, $\Delta = \beta_{SR} - \delta_{SR}$, $\alpha = \frac{\left(\frac{2b_{SR}m_{SR}}{2b_{SR}m_{SR}+\Omega_{SR}}\right)^{m_U}}{2b_{SR}}$, $\beta = \frac{1}{2b_{SR}}$ and $\delta = \frac{\Omega_{SR}}{2b_{SR}(2b_{SR}m_{SR}+\Omega_{SR})}$, Ω_{SR}, $2b_{SR}$ and $m_S R$ are the average power of the LOS and multipath components and the fading severity parameter, respectively. Based on [207, Eq. 3.351.2], the CDF of ρ_S is given as

$$F_{\rho_S}(x) = 1 - \sum_{i_1=0}^{m_{SR}-1} \cdots \sum_{i_{N_R}=0}^{m_{SR}-1} \Xi(N_R)$$
$$\times \sum_{n=0}^{\Lambda-1} \frac{\Gamma(\Lambda)}{n!\Delta^{\Lambda-n}\eta_S^n} x^n e^{-\frac{\Delta}{\eta_S}x} \tag{7.13}$$

Considering the characterization of Nakagami-m fading, the PDF and CDF of unordered estimated channel gains $\tilde{\rho}_{D_m}$ are given respectively as[153]

$$f_{\tilde{\rho}_{D_m}}(x) = \left(\frac{\lambda_{RD_m}}{\eta_R}\right)^{m_{RD}N_T} \frac{x^{m_{RD}N_T-1} e^{-\frac{\lambda_{RD_m}x}{\eta_R}}}{\Gamma(m_{RD}N_T)} \tag{7.14}$$

$$F_{\tilde{\rho}_{D_m}}(x) = \frac{\gamma\left(m_{RD}N_T, \frac{\lambda_{RD_m}x}{\eta_R}\right)}{\Gamma(m_{RD}N_T)}, \tag{7.15}$$

where Ω_{RD_m} is the average power, $m_{RD} = m_{RD_1} = \ldots = m_{RD_M}$ is the fading severity and $\lambda_{RD_m} = \frac{m_{RD}}{\Omega_{RD_m}}$. Using order statistics [208], the PDF and CDF of the ordered channel gains

ρ_{D_m} are respectively given by

$$
f_{\rho_{D_m}}(x) = \Theta \sum_{a=0}^{M-m} (-1)^a \binom{M-m}{a}
$$
$$
\times f_{\tilde{\rho}_{D_m}}(x) \left[F_{\tilde{\rho}_{D_m}}(x) \right]^{m+a-1}
\tag{7.16}
$$

$$
F_{\rho_{D_m}}(x) = \Theta \sum_{a=0}^{M-m} \frac{(-1)^a}{m+a} \binom{M-m}{a} \left[F_{\tilde{\rho}_{D_m}}(x) \right]^{m+a}
\tag{7.17}
$$

where $\Theta = \frac{M!}{(m-1)!(M-m)!}$. Then, using the series form of $\gamma(\bullet, \bullet)$ in [207, Eq. 8.352.1] and applying binomial and multinomial expansions [207, p. 0.314], we can rewrite (7.16) as

$$
f_{\rho_{D_m}}(x) = \Theta \sum_{a=0}^{M-m} \sum_{b=0}^{m+a-1} \sum_{c=0}^{b(m_{RD}N_T-1)} \binom{M-m}{a}
$$
$$
\times \binom{m+a-1}{b} \frac{(-1)^{a+b} \omega_c^b}{\Gamma(m_{RD}N_T)} \left(\frac{\lambda_{RD_m}}{\eta_R} \right)^{m_{RD}N_T+c}
\tag{7.18}
$$
$$
\times x^{m_{RD}N_T+c-1} e^{-\frac{\lambda_{RD}(b+1)}{\eta_R} x}
$$

where $\varepsilon_l = \frac{1}{l!}$, ω_c^b can be calculated as $\omega_0^b = \varepsilon_0^b$, $\omega_1^b = \varepsilon_1^b$, $\omega_{b(m_{RD}N_T-1)}^b = \varepsilon_{m_{RD}N_T-1}^b$, when $2 \leqslant c \leqslant m_{RD}N_T - 1$ we have $\omega_c^b = \frac{1}{c\varepsilon_0} \sum_{g=1}^{c} [gb - c + g]\varepsilon_g \omega_{c-g}^b$, and when $m_{RD}N_T \leqslant c \leqslant m_{RD}N_T - 1$, we have $\omega_c^b = \frac{1}{c\varepsilon_0} \sum_{g=1}^{m_{RD}N_T} [gb - c + g]\varepsilon_g \omega_{c-g}^b$.

7.4 Performance Analysis

In this section, the OP of the satellite network cooperative with NOMA will be analyzed in terms of OP and system diversity order. To this end, both exact and asymptotic expressions for the OP will be studied.

7.4.1 Outage probability

The outage event will occur at D_m if D_m fails to decode its own signal or the signal of D_q. The OP at D_m is expressed as

$$
P_m = 1 - \Pr\{E_{m,1}, E_{m,2}, \ldots, E_{m,m}\}
\tag{7.19}
$$

where $E_{m,q}$ denotes the event that D_m can successfully detect the D_q's signal and can be given by

$$
E_{m,q} = \left\{ \gamma_{m \to q} > \gamma_{th_q} \right\}
\tag{7.20}
$$

where γ_{th_q} denotes the target rate of D_q.

Proposition 1: The closed-form OP of device D_m can be expressed as (7.21).

$$P_m = 1 - 2\Theta \sum_{i_1=0}^{m_{SR}-1} \cdots \sum_{i_{N_R}=0}^{m_{SR}-1} \sum_{n=0}^{\Lambda-1} \sum (a,b,c,d,e) \frac{\Xi(N_R)\Gamma(\Lambda)(-1)^{a+b}\omega_c^b(\Phi_3\vartheta_m^*)^d e^{-\Phi_2\vartheta_m^*}}{n!\Delta^{\Lambda-n}\Gamma(m_{RD}N_T)\left(\vartheta_m^*\vartheta_{r,k*}^2\right)^{-(m_{RD}N_T+c-e-1)}}$$

$$\times \left(\frac{\lambda_{RD_m}}{\eta_R}\right)^{m_{RD}N_T+c}\left(\frac{\vartheta_m^*}{\eta_S}\right)^n \left(\frac{\vartheta_m^*\Delta(\Phi_3\vartheta_m^*+1)}{\eta_S\Phi_1}\right)^{\frac{e-n+1}{2}} K_{e-n+1}\left(2\sqrt{\frac{\Delta\Phi_1\vartheta_m^*(\Phi_3\vartheta_m^*+1)}{\eta_S}}\right)$$

$$(7.21)$$

Proof: Substituting (7.7) into (7.20) and putting the result into (7.19), we can write P_m as (7.22).

$$P_m = 1 - \Pr\left(\rho_S > \frac{\vartheta_m^*\left(\rho_{D_m}L_{D_m}\vartheta_{d,m*}^2+1\right)}{\rho_{D_m}-\vartheta_m^*\vartheta_{r,k*}^2}, \rho_{D_m} > \vartheta_m^*\vartheta_{r,k*}^2\right)$$

$$= 1 - \int_{\vartheta_m^*\vartheta_{r,k*}^2}^{\infty} f_{\rho_{D_m}}(x)\left\{1 - F_{\rho_S}\left(\frac{\vartheta_m^*\left(xL_{D_m}\vartheta_{d,m*}^2+1\right)}{x-\vartheta_m^*\vartheta_{r,k*}^2}\right)\right\} dx$$

$$(7.22)$$

where $\vartheta_m = \dfrac{\gamma_{th_m}}{\bar{\eta}_m\left(\varpi_m - \gamma_{th_m}\sum\limits_{i=m+1}^{M}\varpi_i\right)}$, $\varpi_m > \gamma_{th_m}\sum\limits_{i=m+1}^{M}\varpi_i$, $\vartheta_m^* = \max(\vartheta_1,\vartheta_2,...,\vartheta_m)$.

Then, putting (7.13) and (7.18) into (7.22), we claim

$$P_m = 1 - \Theta \sum_{i_1=0}^{m_{SR}-1} \cdots \sum_{i_{N_R}=0}^{m_{SR}-1} \frac{\Gamma(\Lambda)\Xi(N_R)}{n!\Delta^{\Lambda-n}\eta_S^n} \sum_{a=0}^{M-m}\sum_{b=0}^{m+a-1}$$

$$\times \sum_{c=0}^{b(m_{RD}N_T-1)} \binom{M-m}{a}\binom{m+a-1}{b}\frac{(-1)^{a+b}\omega_c^b}{\Gamma(m_{RD}N_T)}$$

$$\times \int_{\vartheta_m^*\vartheta_{r,k*}^2}^{\infty} \left(\frac{\lambda_{RD_m}}{\eta_R}\right)^{m_{RD}N_T+c} x^{m_{RD}N_T+c-1}e^{-\frac{\lambda_{RD}(b+1)}{\eta_R}x}$$

$$(7.23)$$

$$\times \left(\frac{\vartheta_m^*\left(xL_{D_m}\vartheta_{d,m*}^2+1\right)}{x-\vartheta_m^*\vartheta_{r,k*}^2}\right)^n e^{-\frac{\vartheta_m^*\Delta\left(xL_{D_m}\vartheta_{d,m*}^2+1\right)}{\eta_S\left(x-\vartheta_m^*\vartheta_{r,k*}^2\right)}} dx$$

90

Put $t = x - \vartheta_m^* \vartheta_{r,k*}^2 \implies x = t + \vartheta_m^* \vartheta_{r,k*}^2$, (7.23) can be calculated as follows.

$$
P_m = 1 - \Theta \sum_{i_1=0}^{m_{SR}-1} \cdots \sum_{i_{N_R}=0}^{m_{SR}-1} \frac{\Gamma(\Lambda)\,\Xi(N_R)}{n!\,\Delta^{\Lambda-n}} \sum_{a=0}^{M-m} \sum_{b=0}^{m+a-1}
$$

$$
\times \sum_{c=0}^{b(m_{RD}N_T-1)} \binom{M-m}{a}\binom{m+a-1}{b} \frac{(-1)^{a+b}\,\omega_c^b}{\Gamma(m_{RD}N_T)}
$$

$$
\times \left(\frac{\lambda_{RD_m}}{\eta_R}\right)^{m_{RD}N_T+c} \left(\frac{\vartheta_m^*}{\eta_S}\right)^n e^{-\Phi_2 \vartheta_m^*} \tag{7.24}
$$

$$
\times \int_0^\infty (t + \vartheta_m^* \vartheta_{r,k*}^2)^{m_{RD}N_T+c-1} e^{-\Phi_1 t} e^{-\frac{\vartheta_m^* \Delta(\Phi_3 \vartheta_m^*+1)}{\eta_S t}}
$$

$$
\times \left(\frac{t L_{D_m}\vartheta_{d,m*}^2 + \vartheta_m^* L_{D_m}\vartheta_{d,m*}^2 \vartheta_{r,k*}^2 + 1}{t}\right)^n dt
$$

where $\Phi_1 = \frac{\lambda_{RD}(b+1)}{\eta_R}$, $\Phi_2 = \frac{\lambda_{RD}\vartheta_{r,k*}^2(b+1)}{\eta_R} + \frac{\Delta L_{D_m}\vartheta_{d,m*}^2}{\eta_S}$, $\Phi_3 = L_{D_m}\vartheta_{d,m*}^2 \vartheta_{r,k*}^2$. Next using [207, Eq 1.111], we can rewrite (7.24) as

$$
P_m = 1 - \Theta \sum_{i_1=0}^{m_{SR}-1} \cdots \sum_{i_{N_R}=0}^{m_{SR}-1} \sum_{n=0}^{\Lambda-1} \sum (a,b,c,d,e)
$$

$$
\times \frac{\Xi(N_R)\,\Gamma(\Lambda)\,(-1)^{a+b}\,\omega_c^b\, e^{-\Phi_2 \vartheta_m^*} (\Phi_3 \vartheta_m^*)^d}{n!\,\Delta^{\Lambda-n}\Gamma(m_{RD}N_T)\left(\vartheta_m^* \vartheta_{r,k*}^2\right)^{-(m_{RD}N_T+c-e-1)}} \left(\frac{\vartheta_m^*}{\eta_S}\right)^n \tag{7.25}
$$

$$
\times \left(\frac{\lambda_{RD_m}}{\eta_R}\right)^{m_{RD}N_T+c} \int_0^\infty t^{e-n} e^{-\Phi_1 t} e^{-\frac{\vartheta_m^* \Delta(\Phi_3 \vartheta_m^*+1)}{\eta_S t}} dt
$$

where

$$
\sum (a,b,c,d,e) = \sum_{a=0}^{M-m} \sum_{b=0}^{m+a-1} \sum_{c=0}^{b(m_{RD}N_T-1)} \sum_{d=0}^{n} \sum_{e=0}^{m_{RD}N_T+c+d-1}
$$

$$
\times \binom{M-m}{a}\binom{m+a-1}{b}\binom{n}{d}\binom{m_{RD}N_T+c+d-1}{e} \tag{7.26}
$$

Based on [207, Eq. 3.471.9], the integral in (7.25) can be calculated. And the proof is complete.

7.4.2 Diversity order

For more insights, the order of diversity is analyzed. For this, in the high SNR regime, we assume $\eta = \eta_S = \eta_R \to \infty$. Then, the diversity order of the terrestrial device can be given by

[196, 166]

$$D = -\lim_{\eta \to \infty} \frac{\log\left(P_m^\infty\left(\eta\right)\right)}{\log\left(\eta\right)} \tag{7.27}$$

where $P_m^\infty\left(\eta\right)$ denotes the asymptotic OP.

Proposition 2: The asymptotic OP of the device D_m in the high SNR regime is given by

$$\begin{aligned}
P_m^\infty &\approx \frac{\alpha^{N_R}}{(N_R)!\eta_S^{N_R}} \left(\frac{\bar{\vartheta}_m^*}{\vartheta_{r,k*}^2}\right)^{N_R} + \left(\frac{\lambda_{RD_m}}{\eta_R}\right)^{m_{RD}N_T m} \\
&\times \frac{\Theta}{m\left[\Gamma\left(m_{RD}N_T+1\right)\right]^m} \left(\frac{\bar{\vartheta}_m^*}{L_{D_m}\vartheta_{d,m*}^2}\right)^{m_{RD}N_T m}
\end{aligned} \tag{7.28}$$

Proof: See Appendix G (pp. 99).

Remark: Upon substituting (7.28) into (7.27), the achievable diversity order of m-th device is $\min\left(N_R, m_{RD}N_T m\right)$.

7.4.3 Ergodic Capacity (EC)

In this section, the ergodic rate of m-th device is discussed in detail, where the target rates of devices are determined by the channel conditions. Next, m-th device detects the q-th device's information successfully, since it holds $h_{R_k D_m} \geqslant h_{R_k D_p}$. In this situation, the achievable rate of m-th is expressed as $\tilde{R}_m = \frac{1}{2}\log_2(1+\gamma_m)$. Thus, the ergodic rates of m-th and M-th device are as follows

$$\tilde{R}_{m,ave} = \mathbb{E}\left\{\frac{1}{2}\log_2(1+\gamma_m)\right\} \tag{7.29}$$

and

$$\tilde{R}_{M,ave} = \mathbb{E}\left\{\frac{1}{2}\log_2(1+\gamma_M)\right\} \tag{7.30}$$

Proposition 3: The closed-form of ergodic rate for m-th and M-th device are given by (7.31) and (7.32), respectively.

$$\tilde{R}_{m,ave} \approx \frac{\Theta \pi \varpi_m}{2 \ln(2) I} \sum_{i_1=0}^{m_{SR}-1} \cdots \sum_{i_{N_R}=0}^{m_{SR}-1} \sum_{n=0}^{\Lambda-1} \sum (a,b,c,d,e)$$

$$\times \sum_{k=1}^{I} \sqrt{1-\varphi_k^2} \frac{\Xi(N_R) \Gamma(\Lambda) (-1)^{a+b} \omega_c^b (\lambda_{RD_m}/\eta_R)^{m_{RD}N_T+c} (\Phi_3)^d}{n! \Delta^{\Lambda-n} \Gamma(m_{RD}N_T) \left(\vartheta_{r,k*}^2\right)^{-(m_{RD}N_T+c-e-1)} \eta_S^n}$$

$$\times \frac{e^{-\Phi_2 \hat{\vartheta}_m\left(\frac{(\varphi_k+1)\varpi_m}{\tilde{\varpi}_m}\right)}}{(\tilde{\varpi}_m + (\varphi_k+1)\varpi_m)} \left(\frac{\Delta\left(\Phi_3 \hat{\vartheta}_m\left(\frac{(\varphi_k+1)\varpi_m}{\tilde{\varpi}_m}\right)+1\right)}{\eta_S \Phi_1}\right)^{\frac{e-n+1}{2}} \left(\hat{\vartheta}_m\left(\frac{(\varphi_k+1)\varpi_m}{\tilde{\varpi}_m}\right)\right)^{\frac{2(m_{RD}N_T+d+c)+n-e-1}{2}}$$

$$\times K_{e-n+1}\left(2\sqrt{\frac{\Delta \Phi_1 \hat{\vartheta}_m\left(\frac{(\varphi_k+1)\varpi_m}{\tilde{\varpi}_m}\right)\left(\Phi_3 \hat{\vartheta}_m\left(\frac{(\varphi_k+1)\varpi_m}{\tilde{\varpi}_m}\right)+1\right)}{\eta_S}}\right)$$

$$(7.31)$$

$$\tilde{R}_{M,ave} \approx \frac{\pi^2 \Theta}{4I \ln(2)} \sum_{i_1=0}^{m_{SR}-1} \cdots \sum_{i_{N_R}=0}^{m_{SR}-1} \sum_{n=0}^{\Lambda-1} \sum (a,b,c,d,e) \sum_{k=1}^{I} \sqrt{1-\varphi_k^2} \sec^2\left((\varphi_k+1)\frac{\pi}{4}\right)$$

$$\times \frac{\Xi(N_R) \Gamma(\Lambda) (-1)^{a+b} \omega_c^b (\Phi_3)^d}{n! \Delta^{\Lambda-n} \eta_S^n \Gamma(m_{RD}N_T) \left(\vartheta_{r,k*}^2\right)^{-(m_{RD}N_T+c-e-1)}} \frac{e^{-\Phi_2 \hat{\vartheta}_M\left(\tan\left(\frac{(\varphi_k+1)\pi}{4}\right)\right)}}{\left(1+\tan\left(\frac{(\varphi_k+1)\pi}{4}\right)\right)}$$

$$\times \left(\hat{\vartheta}_M\left(\tan\left(\frac{(\varphi_k+1)\pi}{4}\right)\right)\right)^{\frac{2(m_{RD}N_T+c+d)+n-e-1}{2}} \left(\frac{\Delta\left(\Phi_3 \hat{\vartheta}_M\left(\tan\left(\frac{(\varphi_k+1)\pi}{4}\right)\right)+1\right)}{\eta_S \Phi_1}\right)^{\frac{e-n+1}{2}}$$

$$\times \left(\frac{\lambda_{RD_m}}{\eta_R}\right)^{m_{RD}N_T+c} K_{e-n+1}\left(2\sqrt{\frac{\Delta \Phi_1 \hat{\vartheta}_M\left(\tan\left(\frac{(\varphi_k+1)\pi}{4}\right)\right)\left(\Phi_3 \hat{\vartheta}_M\left(\tan\left(\frac{(\varphi_k+1)\pi}{4}\right)\right)+1\right)}{\eta_S}}\right)$$

$$(7.32)$$

Proof: See Appendix H (pp. 100).

7.5 Numerical results

Table 7.3: Channel parameters [190, 199, 193]

Shadowing	Frequent heavy shadowing (FHS)	Average shadowing (AS)
b_{SR}	0.063	0.251
m_{SR}	1	5
Ω_{SR}	0.0007	0.279

Table 7.4: Simulation Parameter [209], [210], [211]

Parameter	Value
The number of device	$M = 3$
The number of Relay	$K = 2$
The number of received antenna at relays	$N_R = 2$
The number of transmit antenna at relays	$N_T = 2$
Satellite Orbit	GEO
Frequency band	38 GHz
Bandwidth	500 MHz
Noise temperature	300 K
Maximal beam gain	48 dBi
Antenna gain at R_{k*}	4 dBi
Angle between the satellite and relay	0.3^o
Angle ϕ_{3dB}	0.4^o
Path loss exponents	$\kappa = 118.77$, $\nu = 5.78$ and $\theta = 0.12$
Distance between R_{k*} and devices	$d_1 = 0.5$km, $d_2 = 0.4$km and $d_3 = 0.3$km
The power allocation	$\varpi_1 = 0.5$, $\varpi_2 = 0.4$ and $\varpi_1 = 0.1$
The target rate	$R_1 = 0.4$, $R_2 = 0.9$ and $R_3 = 1.2$
The fading severity	$m_{RD} = m_{RD_1} = m_{RD_2} = m_{RD_3} = 1$
The average power	$\Omega_{RD_1} = \Omega_{RD_2} = \Omega_{RD_3} = 1$
The expected rain attenuation	$\vartheta_{d_m} = 0.5$dB

In this section, to verify the mathematical analysis, it is necessary to simulate and illustrate the proposed assisted NOMA scheme. Here, the shadowing scenarios of the satellite links, including frequent heavy shadowing (FHS) and average shadowing (AS) being given in Table 7.3. Furthermore, the parameters can be provided in Table 7.4. Monte Carlo simulations are performed to validate the analytical results shown in the following figures.

Figure 7.2 shows the OP versus η in dB with different satellite links. First, the performance of the devices will be improved by increasing the transmit power. Next, the performance of device D_1 is the best due to the power allocation of D_1 is better than D_2 and D_3. Moreover, the improvement of satellite link also greatly improves device performance, i.e. AS is the best case. Furthermore, the system uses the NOMA scheme better than OMA. The fundamental cause is that OMA uses more time slots than NOMA to serve the same number of devices. Over the whole SNR range, Monte Carlo simulation curves and analytical results accord very well. At high SNR, it can be seen that the asymptotic OP curves closely reflect the actual findings.

Figure 7.3 shows the OP versus η in dB under the influence of the relay antenna. We can easily see that increasing the number of antennas at the relay will significantly improve the system's performance. It proves the superiority of installing multiple antennas in the system. Compared to the case of the relay with $N_R = N_T = 2$, the large OP gap can be seen once the relay is designed with $N_R = N_T = 3$. The explanation is that a design with
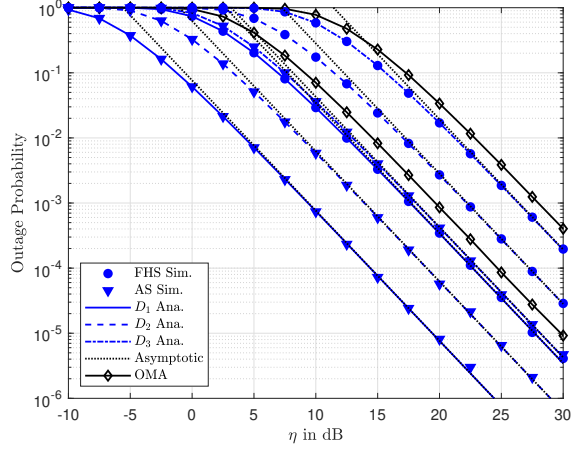
Figure 7.2: OP of D_m versus transmit η in dB varying the parameter of satellite links with $K = 1$.

Figure 7.3: OP of D_m versus transmit η in dB varying the transmit and received antenna of R_{k*} with $K = 1$ and the satellite link in FHS case.

more diversity from many antennas could enhance the signal received for the devices on the ground. Figure 7.4 shows the simulation OP versus η in dB with different numbers of relays. When the number of relays is increased, the performance is improved more. It demonstrates the effectiveness of using a relay selection scheme.

Fig. 7.5 shows the OP versus transmit η in dB varying the carrier frequency. It can be observed that the higher the carrier frequency, the worse the OP. The rationale behind this phenomenon is that with higher frequency, the path-loss drops dramatically thus an appropriate antenna beamforming gain is necessary to compensate for such losses. Regarding the selection of the 38GHz, we choose because it is in the range of GEO operation [204, 209].
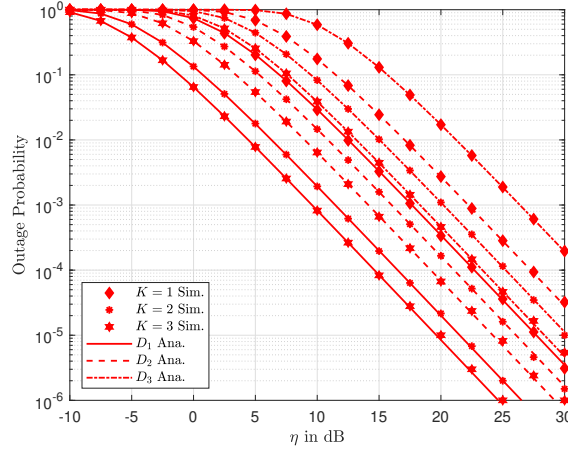
Figure 7.4: OP of D_m versus transmit η in dB varying the number of Relay with the satellite link in FHS case.
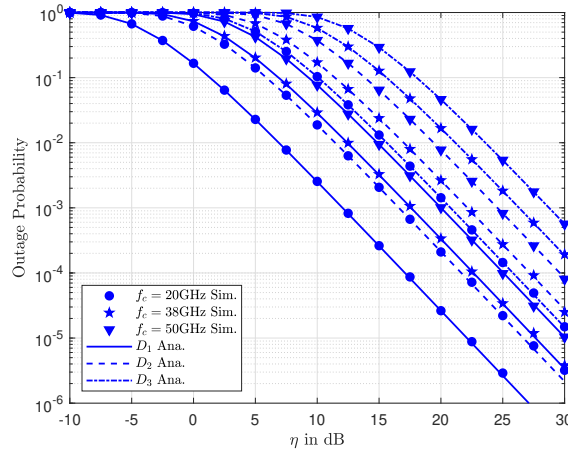
Figure 7.5: OP versus transmit η in dB varying the carrier frequency in FHS case.

Figure 7.6 indicates the EC versus η with different satellite links, as well as Figure 7.2. The EC rates at D_1 and D_2 are almost unchanged for the FHS and AS case. But the difference between the EC curves at D_3 in both modes is quite comparably large. Moreover, when increasing in high SNR, the gap of D_3 is different with D_2 and D_1.

Figure 7.7 and Figure 7.8 show the EC of D_m versus η in dB varying the number of relay antennas and the number of relays, respectively. For EC of D_1 and D_2, the gaps between cases change only in the low SNR region and will intersect at a point in the high region. Therefore, changing the number of antennas and the number of relays does not have much effect on EC. But for the EC of D_3, the gaps between instances will be large. It shows the effect of the number of antennas and the number of relays to the EC.

96
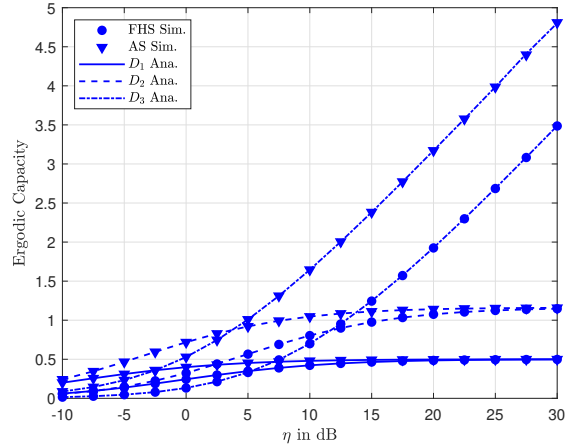
Figure 7.6: EC of D_m versus transmit η in dB varying the parameter of satellite links with $N_R = N_T = K = 1$.
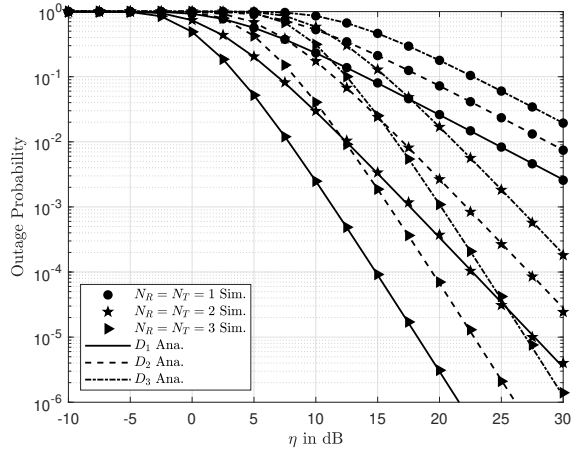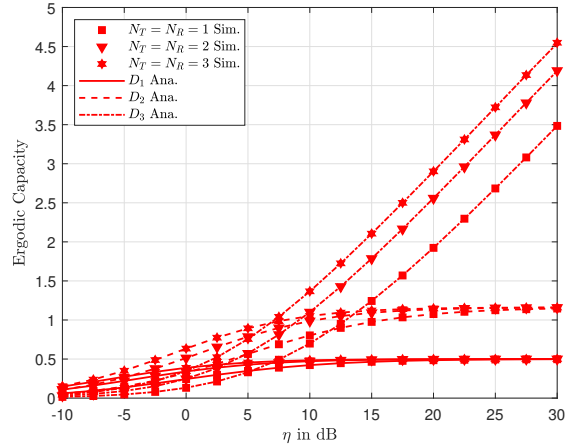

Figure 7.7: EC of D_m versus transmit η in dB varying the transmit and received antenna of R_{k*} with $K = 1$ and the satellite link in FHS case.

7.6 Conclusion

In this section, the performance of NOMA-based HSTRN using mmWave communications was investigated, where devices are supported by multiple relays. Multiple antennas receiving and transmitting at relay and NOMA were considered in the context of serving multiple devices. In addition, the rain attenuation value is used to choose the best relay. The closed form of OP, EC, and asymptotic expressions of OP were developed based on the model of the considered system. To support those performance studies and demonstrate how important factors such as fading and rain attenuation affect system performance, simulations have been made available. Our results showed that the OP of the system under consideration can be
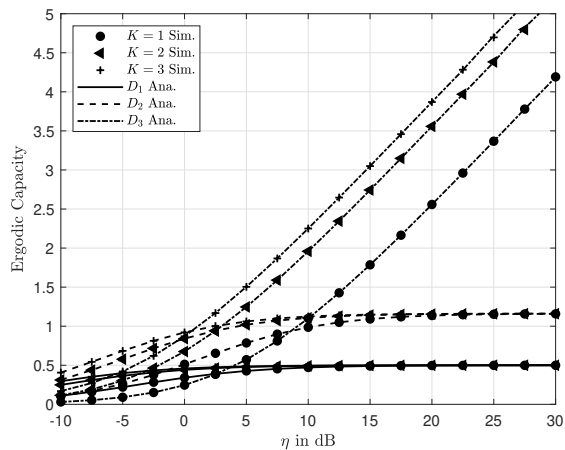
Figure 7.8: EC of D_m versus transmit η in dB varying the number of Relay with the satellite link in FHS case.

greatly improved compared to the OMA scheme, highlighting the advantages of implementing the NOMA scheme in the system. These results provide a theoretical framework for further investigation.

First, when $\eta_S \to \infty$ and apply the Maclaurin series expansion of the exponential function in (7.11). So, the PDF of ρ_S can be approximated as

$$f_{\rho_S}(x) = \frac{\alpha^{N_R} x^{N_R} - 1}{(N_R - 1)! \eta_S^{N_R}} \tag{7.33}$$

Next, the CDF ρ_S has asymptotic behavior as

$$F_{\rho_S}(x) = \frac{\alpha^{N_R} x^{N_R}}{(N_R)! \eta_S^{N_R}} \tag{7.34}$$

Furthermore, when $\eta_R \to \infty$ and taking the first term ($a = 0$ of series representation, the asymptotic behavior of CDF ρ_{D_m} can be obtained as

$$\begin{aligned} F_{\rho_{D_m}}(x) &= \frac{\Theta}{m\left[\Gamma(m_{RD} N_T + 1)\right]^m} \\ &\times \left(\frac{\lambda_{RD_m}}{\eta_R}\right)^{m_{RD} N_T m} x^{m_{RD} N_T m} \end{aligned} \tag{7.35}$$

Then, the asymptotic P_m^∞ can be expressed as

$$P_m^\infty \approx 1 - \Pr\left(\frac{\rho_{D_m} L_{D_m} \vartheta_{d,m*}^2 \rho_S \vartheta_{r,k*}^2}{\rho_{D_m} L_{D_m} \vartheta_{d,m*}^2 + \rho_S \vartheta_{r,k*}^2} > \bar{\vartheta}_m^*\right) \tag{7.36}$$

Using the inequality $\frac{uv}{u+v} \leqslant \min(u, v)$. Thus, the asymptotic P_m^∞ can be calculated as

$$\begin{aligned} P_m^\infty &\approx 1 - \Pr\left(\min\left(\rho_{D_m} L_{D_m} \vartheta_{d,m*}^2, \rho_S \vartheta_{r,k*}^2\right) > \bar{\vartheta}_m^*\right) \\ &\approx F_{D_m}^\infty\left(\frac{\bar{\vartheta}_m^*}{L_{D_m} \vartheta_{d,m*}^2}\right) + F_{\rho_S}^\infty\left(\frac{\bar{\vartheta}_m^*}{\vartheta_{r,k*}^2}\right) \\ &- F_{\rho_S}^\infty\left(\frac{\bar{\vartheta}_m^*}{\vartheta_{r,k*}^2}\right) F_{D_m}^\infty\left(\frac{\bar{\vartheta}_m^*}{L_{D_m} \vartheta_{d,m*}^2}\right) \end{aligned} \tag{7.37}$$

With help (7.34) and (7.35), we can obtain as

$$\begin{aligned} P_m^\infty &\approx \frac{\alpha^{N_R}}{(N_R)! \eta_S^{N_R}} \left(\frac{\bar{\vartheta}_m^*}{\vartheta_{r,k*}^2}\right)^{N_R} + \left(\frac{\lambda_{RD_m}}{\eta_R}\right)^{m_{RD} N_T m} \\ &\times \frac{\Theta}{m\left[\Gamma(m_{RD} N_T + 1)\right]^m} \left(\frac{\bar{\vartheta}_m^*}{L_{D_m} \vartheta_{d,m*}^2}\right)^{m_{RD} N_T m} \end{aligned} \tag{7.38}$$

Appendix H

The ergodic rate of m-th device can be calculated as

$$\tilde{R}_{m,ave} = \frac{1}{2\ln(2)} \int_0^{\frac{\varpi_m}{\tilde{\varpi}_m}} \frac{1 - F_{\gamma_m}(x)}{1+x} dx \tag{7.39}$$

where $\tilde{\varpi}_m = \sum_{i=m+1}^{M} \varpi_i$. Similarly, Proposition 1, the CDF of γ_m can be obtained as

$$F_{\gamma_m}(x) = 1 - 2\Theta \sum_{i_1=0}^{m_{SR}-1} \cdots \sum_{i_{N_R}=0}^{m_{SR}-1} \sum_{n=0}^{\Lambda-1} \sum (a, b, c, d, e)$$

$$\times \frac{\Xi(N_R)\Gamma(\Lambda)(-1)^{a+b}\omega_c^b \left(\Phi_3\hat{\vartheta}_m(x)\right)^d e^{-\Phi_2\hat{\vartheta}_m(x)}}{n!\Delta^{\Lambda-n}\Gamma(m_{RD}N_T)\left(\hat{\vartheta}_m(x)\vartheta_{r,k*}^2\right)^{-(m_{RD}N_T+c-e-1)}}$$

$$\times \left(\frac{\lambda_{RD_m}}{\eta_R}\right)^{m_{RD}N_T+c} \left(\frac{\hat{\vartheta}_m(x)\Delta\left(\Phi_3\hat{\vartheta}_m(x)+1\right)}{\eta_S\Phi_1}\right)^{\frac{e-n+1}{2}} \tag{7.40}$$

$$\times \left(\frac{\hat{\vartheta}_m(x)}{\eta_S}\right)^n K_{e-n+1}\left(2\sqrt{\frac{\Delta\Phi_1\hat{\vartheta}_m(x)\left(\Phi_3\hat{\vartheta}_m(x)+1\right)}{\eta_S}}\right)$$

where $\hat{\vartheta}_m(x) = \frac{x}{\tilde{\eta}_m(\varpi_m - x\tilde{\varpi}_m)}$. Putting (7.34) into (7.33), we can calculate $\tilde{R}_{m,ave}$ as

$$\tilde{R}_{m,ave} = \frac{\Theta}{\ln(2)} \sum_{i_1=0}^{m_{SR}-1} \cdots \sum_{i_{N_R}=0}^{m_{SR}-1} \sum_{n=0}^{\Lambda-1} \sum (a, b, c, d, e)$$

$$\times \frac{\Xi(N_R)\Gamma(\Lambda)(-1)^{a+b}\omega_c^b \left(\lambda_{RD_m}/\eta_R\right)^{m_{RD}N_T+c}}{n!\Delta^{\Lambda-n}\Gamma(m_{RD}N_T)\left(\vartheta_{r,k*}^2\right)^{-(m_{RD}N_T+c-e-1)}}$$

$$\times \int_0^{\frac{\varpi_m}{\tilde{\varpi}_m}} \frac{\left(\Phi_3\hat{\vartheta}_m(x)\right)^d e^{-\Phi_2\hat{\vartheta}_m(x)}}{(1+x)\left(\hat{\vartheta}_m(x)\right)^{-(m_{RD}N_T+c-e-1)}} \tag{7.41}$$

$$\times \left(\frac{\hat{\vartheta}_m(x)\Delta\left(\Phi_3\hat{\vartheta}_m(x)+1\right)}{\eta_S\Phi_1}\right)^{\frac{e-n+1}{2}} \left(\frac{\hat{\vartheta}_m(x)}{\eta_S}\right)^n$$

$$\times K_{e-n+1}\left(2\sqrt{\frac{\Delta\Phi_1\hat{\vartheta}_m(x)\left(\Phi_3\hat{\vartheta}_m(x)+1\right)}{\eta_S}}\right) dx$$

Using the Gauss-Chebyshev quadrature [212] into the equation (7.41) with $\varphi_k = \cos\left(\frac{2k-1}{2I}\pi\right)$, we obtain (7.31).

Next, the ergodic rate of M-th device can be calculated as

$$\tilde{R}_{M,ave} = \frac{1}{2\ln(2)} \int_0^\infty \frac{1 - F_{\gamma_M}(x)}{1+x} dx \tag{7.42}$$

Similarly, the PDF of γ_M can be expressed as

$$F_{\gamma_M}(x) = 1 - 2\Theta \sum_{i_1=0}^{m_{SR}-1} \cdots \sum_{i_{N_R}=0}^{m_{SR}-1} \sum_{n=0}^{\Lambda-1} \sum (a,b,c,d,e)$$

$$\times \frac{\Xi(N_R)\Gamma(\Lambda)(-1)^{a+b}\omega_c^b \left(\Phi_3\hat{\vartheta}_M(x)\right)^d e^{-\Phi_2\hat{\vartheta}_M(x)}}{n!\Delta^{\Lambda-n}\Gamma(m_{RD}N_T)\left(\hat{\vartheta}_M(x)\vartheta_{r,k*}^2\right)^{-(m_{RD}N_T+c-e-1)}}$$

$$\times \left(\frac{\lambda_{RD_m}}{\eta_R}\right)^{m_{RD}N_T+c} \left(\frac{\hat{\vartheta}_M(x)\Delta\left(\Phi_3\hat{\vartheta}_m(x)+1\right)}{\eta_S\Phi_1}\right)^{\frac{e-n+1}{2}}$$

$$\times \left(\frac{\hat{\vartheta}_M(x)}{\eta_S}\right)^n K_{e-n+1}\left(2\sqrt{\frac{\Delta\Phi_1\hat{\vartheta}_M(x)\left(\Phi_3\hat{\vartheta}_M(x)+1\right)}{\eta_S}}\right) \tag{7.43}$$

where $\hat{\vartheta}_M(x) = \frac{x}{\bar{\eta}_m\varpi_M}$. Putting (7.43) into (7.42), the ergodic rate of M-th device can be calculated as

$$\tilde{R}_{M,ave} = \frac{\Theta}{\ln(2)} \sum_{i_1=0}^{m_{SR}-1} \cdots \sum_{i_{N_R}=0}^{m_{SR}-1} \sum_{n=0}^{\Lambda-1} \sum (a,b,c,d,e)$$

$$\times \frac{\Xi(N_R)\Gamma(\Lambda)(-1)^{a+b}\omega_c^b \left(\lambda_{RD_m}/\eta_R\right)^{m_{RD}N_T+c}}{n!\Delta^{\Lambda-n}\Gamma(m_{RD}N_T)\left(\vartheta_{r,k*}^2\right)^{-(m_{RD}N_T+c-e-1)}}$$

$$\times \int_0^\infty \frac{\left(\Phi_3\hat{\vartheta}_M(x)\right)^d e^{-\Phi_2\hat{\vartheta}_M(x)}}{(1+x)\left(\hat{\vartheta}_M(x)\right)^{-(m_{RD}N_T+c-e-1)}}$$

$$\times \left(\frac{\hat{\vartheta}_M(x)\Delta\left(\Phi_3\hat{\vartheta}_M(x)+1\right)}{\eta_S\Phi_1}\right)^{\frac{e-n+1}{2}} \left(\frac{\hat{\vartheta}_M(x)}{\eta_S}\right)^n$$

$$\times K_{e-n+1}\left(2\sqrt{\frac{\Delta\Phi_1\hat{\vartheta}_M(x)\left(\Phi_3\hat{\vartheta}_M(x)+1\right)}{\eta_S}}\right) dx \tag{7.44}$$

Furthermore, we set $t = \frac{4\arctan(x)}{\pi} - 1 \Rightarrow x = \tan\left(\frac{(t+1)\pi}{4}\right)$, $dx = \frac{\pi}{4}\sec^2\left(\frac{(t+1)\pi}{4}\right)$ and using the Gaussian-Chebyshev quadrature. We can approximate the ergodic rate $\tilde{R}_{M,ave}$ as (7.32).

The proof is complete.

Chapter 8

Summary

The dissertation discussed EH relay models, NOMA networks, integrated terrestrial and satellite networks, and the deployment of new techniques which are applied to 5G networks and beyond, such as mmWave technology, NOMA power domain, SWIPT, AF, DF, BF, multiple antennae and energy-efficient clustering. The ultimate goal of this research was to provide models for improving network performance through network maintenance, throughput optimization, and improvement in overall power allocation and consumption efficiency. The dissertation described the design, analysis and simulation of the proposed system models to complete its three aims.

To fulfill the first aim, an energy harvesting model with k relay nodes was proposed. Exact throughput expressions and simulations for NOMA and OMA were derived. The simulation results showed that the time fraction and number of relays have a significant effect on throughput and provided important material for analysis of a multi-hop energy harvesting model applied in practice to improve coverage [NNT04]. The research also proposed SLCP in WSN for IoT applications, which indicated its ability to adapt to change in a dynamic network. The proposed protocol calculates the number of neighbors, the residual node energy, and the maximum number of cluster members. The simulation results indicated that the SLCP performed well, producing long network lifetime and high throughput compared to other clustering protocols [NNT10].

For the second aim, the research focused on analyzing the effect of fading and CCI on the NOMA communication technique, especially in HSRNs, which consist of two communication links from the satellite to the ground relay, which performs DF to forward the signal to users. System performance was analyzed and simulated for OP and EC under imperfect channel state information conditions and CCI at the relay. An interesting finding was that the performance of two destinations depends on the strength of the transmit power at the satellite. However, floor outage occurred because the system depends on other parameters such as satellite link modes, noise levels and the number of interference sources [NNT02],

[NNT03]. These important analyses will be an essential practical guide in designing and improving system performance which is impacted by generalized fading and CCI.

For the third aim, a NOMA-HSTRN system model was designed using mmWave communications. Multiple antennae were deployed at the relays and used the amplify and forward (AF) protocol to forward the satellite's superimposed information to multiple users, considering the rain attenuation as the fading factor of the mmWave band to choose the best relay. To characterize the transmission environment, shadowed-Rician fading and Nakagami-m fading models were widely adopted in the relevant hybrid channels. Closed-form expressions for the OP and EC were derived and enabled a detailed examination of the system performance metrics. Finally, results showed how the performance is improved due to a greater number of antennae and selecting the best relay in NOMA-HSTRNs. These observations contribute as essential guidelines for designing this type of NOMA-HSTRN system using mmWave communications [NNT01].

Bibliography

1. ANDREWS, Jeffrey G; BUZZI, Stefano; CHOI, Wan; HANLY, Stephen V; LOZANO, Angel; SOONG, Anthony CK; ZHANG, Jianzhong Charlie. What will 5G be? *IEEE Journal on selected areas in communications*. 2014, vol. 32, no. 6, pp. 1065–1082.

2. RAPPAPORT, Theodore S; SUN, Shu; MAYZUS, Rimma; ZHAO, Hang; AZAR, Yaniv; WANG, Kevin; WONG, George N; SCHULZ, Jocelyn K; SAMIMI, Mathew; GUTIER-REZ, Felix. Millimeter wave mobile communications for 5G cellular: It will work! *IEEE access*. 2013, vol. 1, pp. 335–349.

3. GIORDANI, Marco; ZORZI, Michele. Satellite communication at millimeter waves: A key enabler of the 6G era. In: *2020 International Conference on Computing, Networking and Communications (ICNC)*. IEEE, 2020, pp. 383–388.

4. KIZILIRMAK, Refik Caglar; BIZAKI, Hossein Khaleghi. Non-orthogonal multiple access (NOMA) for 5G networks. *Towards 5G Wireless Networks-A Physical Layer Perspective*. 2016, vol. 83, pp. 83–98.

5. ZHANG, Zhengquan; XIAO, Yue; MA, Zheng; XIAO, Ming; DING, Zhiguo; LEI, Xianfu; KARAGIANNIDIS, George K; FAN, Pingzhi. 6G wireless networks: Vision, requirements, architecture, and key technologies. *IEEE Vehicular Technology Magazine*. 2019, vol. 14, no. 3, pp. 28–41.

6. LATVA-AHO, Matti; LEPPÄNEN, Kari; CLAZZER, Federico; MUNARI, Andrea. Key drivers and research challenges for 6G ubiquitous wireless intelligence. 2020.

7. IMOIZE, Agbotiname Lucky; ADEDEJI, Oluwadara; TANDIYA, Nistha; SHETTY, Sachin. 6G enabled smart infrastructure for sustainable society: Opportunities, challenges, and research roadmap. *Sensors*. 2021, vol. 21, no. 5, p. 1709.

8. JIA, Min; GU, Xuemai; GUO, Qing; XIANG, Wei; ZHANG, Naitong. Broadband hybrid satellite-terrestrial communication systems based on cognitive radio toward 5G. *IEEE Wireless Communications*. 2016, vol. 23, no. 6, pp. 96–106.

9. HUANG, Tongyi; YANG, Wu; WU, Jun; MA, Jin; ZHANG, Xiaofei; ZHANG, Daoyin. A survey on green 6G network: Architecture and technologies. *IEEE access.* 2019, vol. 7, pp. 175758–175768.

10. SAKARELLOS, Vasileios K; KOUROGIORGAS, Charilaos; PANAGOPOULOS, Athanasios D. Cooperative hybrid land mobile satellite–terrestrial broadcasting systems: Outage probability evaluation and accurate simulation. *Wireless Personal Communications.* 2014, vol. 79, no. 2, pp. 1471–1481.

11. EVANS, Barry; WERNER, Markus; LUTZ, Erich; BOUSQUET, Michel; CORAZZA, Giovanni Emanuele; MARAL, Gerard; RUMEAU, Robert. Integration of satellite and terrestrial systems in future multimedia communications. *IEEE Wireless Communications.* 2005, vol. 12, no. 5, pp. 72–80.

12. JIAO, Jian; HU, Youjun; ZHANG, Qinyu; WU, Shaohua. Performance modeling of LTP-HARQ schemes over OSTBC-MIMO channels for hybrid satellite terrestrial networks. *IEEE Access.* 2018, vol. 6, pp. 5256–5268.

13. BAJAJ, Karan; SHARMA, Bhisham; SINGH, Raman. Integration of WSN with IoT applications: a vision, architecture, and future challenges. In: *Integration of WSN and IoT for Smart Cities.* Springer, 2020, pp. 79–102.

14. GHAYVAT, Hemant; MUKHOPADHYAY, Subhas; GUI, Xiang; SURYADEVARA, Nagender. WSN-and IOT-based smart homes and their extension to smart buildings. *Sensors.* 2015, vol. 15, no. 5, pp. 10350–10379.

15. ARTI, MK. Channel estimation and detection in hybrid satellite–terrestrial communication systems. *IEEE Transactions on Vehicular Technology.* 2015, vol. 65, no. 7, pp. 5764–5771.

16. BHATNAGAR, Manav R; ARTI, MK. Performance analysis of AF based hybrid satellite-terrestrial cooperative network over generalized fading channels. *IEEE Communications Letters.* 2013, vol. 17, no. 10, pp. 1912–1915.

17. GAWAS, Anju Uttam. An overview on evolution of mobile wireless communication networks: 1G-6G. *International Journal on Recent and Innovation Trends in Computing and Communication.* 2015, vol. 3, no. 5, pp. 3130–3133.

18. SHAFI, Mansoor; MOLISCH, Andreas F; SMITH, Peter J; HAUSTEIN, Thomas; ZHU, Peiying; DE SILVA, Prasan; TUFVESSON, Fredrik; BENJEBBOUR, Anass; WUNDER, Gerhard. 5G: A tutorial overview of standards, trials, challenges, deployment, and practice. *IEEE journal on selected areas in communications.* 2017, vol. 35, no. 6, pp. 1201–1221.

19. YASTREBOVA, Anastasia; KIRICHEK, Ruslan; KOUCHERYAVY, Yevgeni; BORODIN, Aleksey; KOUCHERYAVY, Andrey. Future networks 2030: Architecture & requirements. In: *2018 10th International Congress on Ultra Modern Telecommunications and Control Systems and Workshops (ICUMT)*. IEEE, 2018, pp. 1–8.

20. *Release 17 timeline agreed* [online]. [visited on 2022-10-17]. Available from: `https://www.3gpp.org/news-events/3gpp-news/rel-17-newtimeline`.

21. *3GPP specification series: 38series* [online]. [visited on 2022-10-17]. Available from: `https://www.3gpp.org/dynareport?code=38-series.htm`.

22. GIAMBENE, Giovanni; KOTA, Sastri; PILLAI, Prashant. Satellite-5G integration: A network perspective. *Ieee Network*. 2018, vol. 32, no. 5, pp. 25–31.

23. AHMAD, Wan Siti Halimatul Munirah Wan; RADZI, Nurul Asyikin Mohamed; SAMIDI, FS; ISMAIL, Aiman; ABDULLAH, Fairuz; JAMALUDIN, Md Zaini; ZAKARIA, MohdNasim. 5G technology: Towards dynamic spectrum sharing using cognitive radio networks. *IEEE Access*. 2020, vol. 8, pp. 14460–14488.

24. MITOLA, Joseph; MAGUIRE, Gerald Q. Cognitive radio: making software radios more personal. *IEEE personal communications*. 1999, vol. 6, no. 4, pp. 13–18.

25. HAYKIN, Simon. Cognitive radio: brain-empowered wireless communications. *IEEE journal on selected areas in communications*. 2005, vol. 23, no. 2, pp. 201–220.

26. MITOLA, J. Software radios-survey, critical evaluation and future directions. In: *[Proceedings] NTC-92: National Telesystems Conference*. IEEE, 1992, pp. 13–15.

27. COSTA, Max. Writing on dirty paper (corresp.) *IEEE transactions on information theory*. 1983, vol. 29, no. 3, pp. 439–441.

28. MITOLA, JI. Cognitive radio. An integrated agent architecture for software defined radio. 2002.

29. NASIR, Ali A; ZHOU, Xiangyun; DURRANI, Salman; KENNEDY, Rodney A. Relaying protocols for wireless energy harvesting and information processing. *IEEE Transactions on Wireless Communications*. 2013, vol. 12, no. 7, pp. 3622–3636.

30. ZAHEDI, Abdulhamid; ERGEN, Mustafa; SHAYEA, Ibraheem. Optimum time/power fraction of energy harvesting in TSR/PSR SWIPT-based cooperative communications with effective capacity maximization approach. *AEU-International Journal of Electronics and Communications*. 2019, vol. 111, p. 152889.

31. AN, Kang; LIANG, Tao; ZHENG, Gan; YAN, Xiaojuan; LI, Yusheng; CHATZINOTAS, Symeon. Performance limits of cognitive-uplink FSS and terrestrial FS for Ka-band. *IEEE Transactions on Aerospace and Electronic Systems*. 2018, vol. 55, no. 5, pp. 2604–2611.

32. LU, Weixin; AN, Kang; LIANG, Tao. Robust beamforming design for sum secrecy rate maximization in multibeam satellite systems. *IEEE Transactions on Aerospace and Electronic Systems.* 2019, vol. 55, no. 3, pp. 1568–1572.

33. EVANS, Barry G. The role of satellites in 5G. In: *2014 7th Advanced Satellite Multimedia Systems Conference and the 13th Signal Processing for Space Communications Workshop (ASMS/SPSC)*. IEEE, 2014, pp. 197–202.

34. GUIDOTTI, Alessandro; VANELLI-CORALLI, Alessandro; CONTI, Matteo; ANDRENACCI, Stefano; CHATZINOTAS, Symeon; MATURO, Nicola; EVANS, Barry; AWOSEYILA, Adegbenga; UGOLINI, Alessandro; FOGGI, Tommaso, et al. Architectures and key technical challenges for 5G systems incorporating satellites. *IEEE Transactions on Vehicular Technology.* 2019, vol. 68, no. 3, pp. 2624–2639.

35. GUPTA, Abhishek K; ALKHATEEB, Ahmed; ANDREWS, Jeffrey G; HEATH, Robert W. Gains of restricted secondary licensing in millimeter wave cellular systems. *IEEE Journal on Selected Areas in Communications.* 2016, vol. 34, no. 11, pp. 2935–2950.

36. MALEKI, Sina; CHATZINOTAS, Symeon; EVANS, Barry; LIOLIS, Konstantinos; GROTZ, Joel; VANELLI-CORALLI, Alessandro; CHUBERRE, Nicolas. Cognitive spectrum utilization in Ka band multibeam satellite communications. *IEEE Communications Magazine.* 2015, vol. 53, no. 3, pp. 24–29.

37. HAUSCHILDT, Harald; ELIA, Carlo; MOELLER, Hermann Ludwig; EL-DALI, Wael; NAVARRO, Tomas; GUTA, Maria; MEZZASOMA, Silvia; PERDIGUES, Josep. HydRON: High throughput optical network. In: *2019 IEEE International Conference on Space Optical Systems and Applications (ICSOS)*. IEEE, 2019, pp. 1–6.

38. BENJEBBOVU, Anass; LI, Anxin; SAITO, Yuya; KISHIYAMA, Yoshihisa; HARADA, Atsushi; NAKAMURA, Takehiro. System-level performance of downlink NOMA for future LTE enhancements. In: *2013 IEEE Globecom Workshops (GC Wkshps)*. IEEE, 2013, pp. 66–70.

39. SAITO, Yuya; BENJEBBOUR, Anass; KISHIYAMA, Yoshihisa; NAKAMURA, Takehiro. System-level performance evaluation of downlink non-orthogonal multiple access (NOMA). In: *2013 IEEE 24th Annual International Symposium on Personal, Indoor, and Mobile Radio Communications (PIMRC)*. IEEE, 2013, pp. 611–615.

40. KODHELI, Oltjon; LAGUNAS, Eva; MATURO, Nicola; SHARMA, Shree Krishna; SHANKAR, Bhavani; MONTOYA, Jesus Fabian Mendoza; DUNCAN, Juan Carlos Merlano; SPANO, Danilo; CHATZINOTAS, Symeon; KISSELEFF, Steven, et al. Satellite communications in the new space era: A survey and future challenges. *IEEE Communications Surveys & Tutorials.* 2020, vol. 23, no. 1, pp. 70–109.

41. WU, Qingqing; TAO, Meixia; NG, Derrick Wing Kwan; CHEN, Wen; SCHOBER, Robert. Energy-efficient resource allocation for wireless powered communication networks. *IEEE Transactions on Wireless Communications*. 2015, vol. 15, no. 3, pp. 2312–2327.

42. JU, Hyungsik; ZHANG, Rui. Throughput maximization in wireless powered communication networks. *IEEE Transactions on Wireless Communications*. 2013, vol. 13, no. 1, pp. 418–428.

43. DO, Nhu Tri; DA COSTA, Daniel Benevides; DUONG, Trung Q; AN, Beongku. A BNBF user selection scheme for NOMA-based cooperative relaying systems with SWIPT. *IEEE Communications Letters*. 2016, vol. 21, no. 3, pp. 664–667.

44. DO, Dinh-Thuan; VAEZI, Mojtaba; NGUYEN, Thanh-Luan. Wireless powered cooperative relaying using NOMA with imperfect CSI. In: *2018 IEEE Globecom Workshops (GC Wkshps)*. IEEE, 2018, pp. 1–6.

45. ZEWDE, Tewodros Aklilu; GURSOY, M Cenk. NOMA-based energy-efficient wireless powered communications. *IEEE Transactions on Green Communications and Networking*. 2018, vol. 2, no. 3, pp. 679–692.

46. GONG, Jie; CHEN, Xiang. Achievable rate region of non-orthogonal multiple access systems with wireless powered decoder. *IEEE Journal on Selected Areas in Communications*. 2017, vol. 35, no. 12, pp. 2846–2859.

47. LI, Yiqing; JIANG, Miao; ZHANG, Qi; LI, Quanzhong; QIN, Jiayin. Secure beamforming in downlink MISO nonorthogonal multiple access systems. *IEEE Transactions on Vehicular Technology*. 2017, vol. 66, no. 8, pp. 7563–7567.

48. NGUYEN, Thanh-Luan; DO, Dinh-Thuan. Exploiting impacts of intercell interference on SWIPT-assisted non-orthogonal multiple access. *Wireless Communications and Mobile Computing*. 2018, vol. 2018.

49. DO, Dinh-Thuan; LE, Chi-Bao. Application of NOMA in wireless system with wireless power transfer scheme: Outage and ergodic capacity performance analysis. *Sensors*. 2018, vol. 18, no. 10, p. 3501.

50. KHALIL, Nacer; ABID, Mohamed Riduan; BENHADDOU, Driss; GERNDT, Michael. Wireless sensors networks for Internet of Things. In: *2014 IEEE ninth international conference on Intelligent sensors, sensor networks and information processing (ISSNIP)*. IEEE, 2014, pp. 1–6.

51. BENSAID, Rahil; SAID, Maymouna Ben; BOUJEMAA, Hatem. Fuzzy C-means based clustering algorithm in WSNs for IoT applications. In: *2020 International Wireless Communications and Mobile Computing (IWCMC)*. IEEE, 2020, pp. 126–130.

52. ASIRI, Mohammed; SHELTAMI, Tarek; AL-AWAMI, Louai; YASAR, Ansar. A novel approach for efficient management of data lifespan of IoT devices. *IEEE Internet of Things Journal*. 2019, vol. 7, no. 5, pp. 4566–4574.

53. NGUYEN, Tien N; HO, Cuu V; LE, Thien TT. A topology control algorithm in wireless sensor networks for IoT-based applications. In: *2019 International Symposium on Electrical and Electronics Engineering (ISEE)*. IEEE, 2019, pp. 141–145.

54. ALHARBI, Mohammad Ali; KOLBERG, Mario; ZEESHAN, Muhammad. Towards improved clustering and routing protocol for wireless sensor networks. *EURASIP Journal on Wireless Communications and Networking*. 2021, vol. 2021, no. 1, pp. 1–31.

55. LI, Jingjing; LI, Xingwang; LIU, Yuanwei; ZHANG, Changsen; LI, Lihua; NALLANATHAN, Arumugam. Joint impact of hardware impairments and imperfect channel state information on multi-relay networks. *IEEE Access*. 2019, vol. 7, pp. 72358–72375.

56. YUE, Xinwei; QIN, Zhijin; LIU, Yuanwei; KANG, Shaoli; CHEN, Yue. A unified framework for non-orthogonal multiple access. *IEEE Transactions on Communications*. 2018, vol. 66, no. 11, pp. 5346–5359.

57. ARZYKULOV, Sultangali; TSIFTSIS, Theodoros A; NAURYZBAYEV, Galymzhan; ABDALLAH, Mohamed. Outage performance of cooperative underlay CR-NOMA with imperfect CSI. *IEEE Communications Letters*. 2018, vol. 23, no. 1, pp. 176–179.

58. KADER, Md Fazlul; SHAHAB, Muhammad Basit; SHIN, Soo Young. Exploiting non-orthogonal multiple access in cooperative relay sharing. *IEEE Communications Letters*. 2017, vol. 21, no. 5, pp. 1159–1162.

59. YANG, Zheng; DING, Zhiguo; FAN, Pingzhi; AL-DHAHIR, Naofal. A general power allocation scheme to guarantee quality of service in downlink and uplink NOMA systems. *IEEE transactions on wireless communications*. 2016, vol. 15, no. 11, pp. 7244–7257.

60. CAUS, Marius; VÁZQUEZ, Miguel Ángel; PÉREZ-NEIRA, Ana. NOMA and interference limited satellite scenarios. In: *2016 50th Asilomar Conference on Signals, Systems and Computers*. IEEE, 2016, pp. 497–501.

61. XIE, Silin; ZHANG, Bangning; GUO, Daoxing; ZHAO, Bing. Performance analysis and power allocation for NOMA-based hybrid satellite-terrestrial relay networks with imperfect channel state information. *IEEE Access*. 2019, vol. 7, pp. 136279–136289.

62. XIE, Silin; ZHANG, Bangning; GUO, Daoxing; YANG, Kongzhe. Outage analysis and optimization of NOMA-based integrated satellite-terrestrial system with an AF relay. In: *2019 IEEE/CIC International Conference on Communications in China (ICCC)*. IEEE, 2019, pp. 741–746.

63. ZHANG, Xiaokai; ZHANG, Bangning; AN, Kang; CHEN, Zhuyun; XIE, Silin; WANG, Heng; WANG, Long; GUO, Daoxing. Outage performance of NOMA-based cognitive hybrid satellite-terrestrial overlay networks by amplify-and-forward protocols. *IEEE Access.* 2019, vol. 7, pp. 85372–85381.

64. TANG, Xiaogang; AN, Kang; GUO, Kefeng; HUANG, Yuzhen, et al. Outage analysis of non-orthogonal multiple access-based integrated satellite-terrestrial relay networks with hardware impairments. *IEEE Access.* 2019, vol. 7, pp. 141258–141267.

65. YAN, Xiaojuan; XIAO, Hailin; AN, Kang; ZHENG, Gan; TAO, Weiping. Hybrid satellite terrestrial relay networks with cooperative non-orthogonal multiple access. *IEEE Communications Letters.* 2018, vol. 22, no. 5, pp. 978–981.

66. LI, Xingwang; LIU, Meng; DENG, Dan; LI, Jingjing; DENG, Chao; YU, Qingping. Power beacon assisted wireless power cooperative relaying using NOMA with hardware impairments and imperfect CSI. *AEU-International Journal of Electronics and Communications.* 2019, vol. 108, pp. 275–286.

67. YAN, Xiaojuan; XIAO, Hailin; WANG, Cheng-Xiang; AN, Kang. On the ergodic capacity of NOMA-based cognitive hybrid satellite terrestrial networks. In: *2017 IEEE/CIC International Conference on Communications in China (ICCC).* IEEE, 2017, pp. 1–5.

68. SHARMA, Shree Krishna; CHATZINOTAS, SYMEON; OTTERSTEN, BJORN. Cognitive radio techniques for satellite communication systems. In: *2013 IEEE 78th vehicular technology conference (VTC Fall).* IEEE, 2013, pp. 1–5.

69. VASSAKI, Stavroula; POULAKIS, Marios I; PANAGOPOULOS, Athanasios D; CONSTANTINOU, Philip. Power allocation in cognitive satellite terrestrial networks with QoS constraints. *IEEE Communications Letters.* 2013, vol. 17, no. 7, pp. 1344–1347.

70. LI, Zhetao; XIAO, Fu; WANG, Shiguo; PEI, Tingrui; LI, Jie. Achievable rate maximization for cognitive hybrid satellite-terrestrial networks with AF-relays. *IEEE Journal on Selected Areas in Communications.* 2018, vol. 36, no. 2, pp. 304–313.

71. LV, Lu; CHEN, Jian; NI, Qiang; DING, Zhiguo; JIANG, Hai. Cognitive non-orthogonal multiple access with cooperative relaying: A new wireless frontier for 5G spectrum sharing. *IEEE Communications Magazine.* 2018, vol. 56, no. 4, pp. 188–195.

72. LV, Lu; NI, Qiang; DING, Zhiguo; CHEN, Jian. Application of non-orthogonal multiple access in cooperative spectrum-sharing networks over Nakagami-m fading channels. *IEEE Transactions on Vehicular Technology.* 2016, vol. 66, no. 6, pp. 5506–5511.

73. LV, Lu; YANG, Long; JIANG, Hai; LUAN, Tom H; CHEN, Jian. When NOMA meets multiuser cognitive radio: Opportunistic cooperation and user scheduling. *IEEE Transactions on Vehicular Technology.* 2018, vol. 67, no. 7, pp. 6679–6684.

74. SINGH, Vibhum; UPADHYAY, Prabhat K; LIN, Min. On the performance of NOMA-assisted overlay multiuser cognitive satellite-terrestrial networks. *IEEE Wireless Communications Letters.* 2020, vol. 9, no. 5, pp. 638–642.

75. NHU NGUYEN, Hong. *New Approaches Using Cognitive Radio in Green Networking.* 2021, Thesis. VSB–Technical University of Ostrava, http://hdl.handle.net/10084/145898.

76. NGUYEN, Ngoc Long. *Non-Orthogonal Multiple Access schemes for Next Generation Cellular Networks: System Model and Performance Consideration.* 2021, Thesis. VSB–Technical University of Ostrava, http://hdl.handle.net/10084/145897.

77. RAPPAPORT, Theodore S; MURDOCK, James N; GUTIERREZ, Felix. State of the art in 60-GHz integrated circuits and systems for wireless communications. *Proceedings of the IEEE.* 2011, vol. 99, no. 8, pp. 1390–1436.

78. ROGERS, D. Propagation considerations for satellite broadcasting at frequencies above 10 GHz. *IEEE journal on selected areas in communications.* 1985, vol. 3, no. 1, pp. 100–110.

79. KOUROGIORGAS, Charilaos; PAPAFRAGKAKIS, Apostolos Z; PANAGOPOULOS, Athanasios D; SAKARELLOS, Vassileios K. Cooperative diversity performance of hybrid satellite and terrestrial millimeter wave backhaul 5G networks. In: *2017 International Workshop on Antenna Technology: Small Antennas, Innovative Structures, and Applications (iWAT).* IEEE, 2017, pp. 46–49.

80. DAVID, Klaus; BERNDT, Hendrik. 6G vision and requirements: Is there any need for beyond 5G? *IEEE vehicular technology magazine.* 2018, vol. 13, no. 3, pp. 72–80.

81. YANG, Ping; XIAO, Yue; XIAO, Ming; LI, Shaoqian. 6G wireless communications: Vision and potential techniques. *IEEE network.* 2019, vol. 33, no. 4, pp. 70–75.

82. LETAIEF, Khaled B; CHEN, Wei; SHI, Yuanming; ZHANG, Jun; ZHANG, Ying-Jun Angela. The roadmap to 6G: AI empowered wireless networks. *IEEE communications magazine.* 2019, vol. 57, no. 8, pp. 84–90.

83. KIBRIA, Mirza Golam; NGUYEN, Kien; VILLARDI, Gabriel Porto; ZHAO, Ou; ISHIZU, Kentaro; KOJIMA, Fumihide. Big data analytics, machine learning, and artificial intelligence in next-generation wireless networks. *IEEE access.* 2018, vol. 6, pp. 32328–32338.

84. KATO, Nei; FADLULLAH, Zubair Md; TANG, Fengxiao; MAO, Bomin; TANI, Shigenori; OKAMURA, Atsushi; LIU, Jiajia. Optimizing space-air-ground integrated networks by artificial intelligence. *IEEE Wireless Communications.* 2019, vol. 26, no. 4, pp. 140–147.

85. ULUKUS, Sennur; YENER, Aylin; ERKIP, Elza; SIMEONE, Osvaldo; ZORZI, Michele; GROVER, Pulkit; HUANG, Kaibin. Energy harvesting wireless communications: A review of recent advances. *IEEE Journal on Selected Areas in Communications.* 2015, vol. 33, no. 3, pp. 360–381.

86. LU, Xiao; WANG, Ping; NIYATO, Dusit; KIM, Dong In; HAN, Zhu. Wireless networks with RF energy harvesting: A contemporary survey. *IEEE Communications Surveys & Tutorials.* 2014, vol. 17, no. 2, pp. 757–789.

87. LAKSHMI, P Sethu; JIBUKUMAR, MG; NEENU, VS. Network lifetime enhancement of multi-hop wireless sensor network by RF energy harvesting. In: *2018 International Conference on Information Networking (ICOIN).* IEEE, 2018, pp. 738–743.

88. FAN, Rongfei; ATAPATTU, Saman; CHEN, Wen; ZHANG, Yihao; EVANS, Jamie. Throughput maximization for multi-hop decode-and-forward relay network with wireless energy harvesting. *IEEE Access.* 2018, vol. 6, pp. 24582–24595.

89. THOMAS, Richu Mary; SUBRAMANI, Malarvizhi. Multiuser-scheduling and resource allocation using max-min technique in wireless powered communication networks. *Indonesian Journal of Electrical Engineering and Computer Science.* 2022, vol. 27, no. 2, pp. 832–841.

90. MAO, Minghe; CAO, Ning; CHEN, Yunfei; ZHOU, Yulin. Multi-hop relaying using energy harvesting. *IEEE Wireless Communications Letters.* 2015, vol. 4, no. 5, pp. 565–568.

91. TIAN, Xiang; ZHANG, Baoxian; LI, Cheng; HAO, Kun. Throughput-Optimal Broadcast for Time-Varying Directed Acyclic Wireless Multi-Hop Networks With Energy Harvesting Constraints. *IEEE Transactions on Green Communications and Networking.* 2021, vol. 5, no. 4, pp. 2089–2103.

92. XU, Chi; ZHENG, Meng; LIANG, Wei; YU, Haibin; LIANG, Ying-Chang. End-to-end throughput maximization for underlay multi-hop cognitive radio networks with RF energy harvesting. *IEEE Transactions on Wireless Communications.* 2017, vol. 16, no. 6, pp. 3561–3572.

93. DO, Dinh-Thuan; LE, Chi-Bao. UAV-assisted underlay CR-NOMA network: performance analysis. *Bulletin of Electrical Engineering and Informatics.* 2022, vol. 11, no. 4, pp. 2079–2087.

94. MADAN, HT; BASARKOD, PI. An optimized power allocation algorithm for cognitive radio NOMA communication. *TELKOMNIKA (Telecommunication Computing Electronics and Control).* 2021, vol. 19, no. 4, pp. 1066–1077.

95. CHEN, Zhebiao; CHI, Kaikai; ZHENG, Kechen; LI, Yanjun; LIU, Xuxun. Common throughput maximization in wireless powered communication networks with non-orthogonal multiple access. *IEEE Transactions on Vehicular Technology*. 2020, vol. 69, no. 7, pp. 7692–7706.

96. LE, Anh-Tu; DO, Dinh-Thuan. Implement of multiple access technique by wireless power transfer and relaying network. *Bulletin of Electrical Engineering and Informatics*. 2021, vol. 10, no. 2, pp. 793–800.

97. LE, Anh-Tu; VAN NGUYEN, Minh-Sang; DO, Dinh-Thuan. Benefiting wireless power transfer scheme in power domain based multiple access: ergodic rate performance evaluation. *Bulletin of Electrical Engineering and Informatics*. 2021, vol. 10, no. 2, pp. 785–792.

98. BAO, Vo Nguyen Quoc; DUY, Tran Trung; VAN, Nguyen Toan. Exact outage analysis of energy-harvesting multihop cluster-based networks with multiple power beacons over Nakagami-m fading channels. In: *2018 2nd International Conference on Recent Advances in Signal Processing, Telecommunications & Computing (SigTelCom)*. IEEE, 2018, pp. 1–6.

99. ATAPATTU, Saman; JIANG, Hai; EVANS, Jamie; TELLAMBURA, Chintha. Time-switching energy harvesting in relay networks. In: *2015 IEEE International Conference on Communications (ICC)*. IEEE, 2015, pp. 5416–5421.

100. NAM, Pham Minh; NGUYEN, Thanh-Long; HUNG, Ha Duy; DUY, Tran Trung; BINH, Nguyen Thanh; NHAT, Nguyen Luong. Throughput analysis of power beacon-aided multi-hop MIMO relaying networks employing NOMA and TAS/SC. *TELKOMNIKA (Telecommunication Computing Electronics and Control)*. 2022, vol. 20, no. 4, pp. 731–739.

101. VAN NGUYEN, Minh-Sang; DANG, Phuc Huu; NGUYEN, Nhan Duc. Exploiting user grouping and energy harvesting in downlink cellular system. *Bulletin of Electrical Engineering and Informatics*. 2022, vol. 11, no. 2, pp. 870–877.

102. VAN NGUYEN, Minh-Sang; NGUYEN, Tu-Trinh; DO, Dinh-Thuan. User grouping-based multiple access scheme for IoT network. *TELKOMNIKA (Telecommunication Computing Electronics and Control)*. 2021, vol. 19, no. 2, pp. 499–506.

103. LE, Anh-Tu; DO, Dinh-Thuan; MUNOCHIVEYI, Munyaradzi. Outage performance of downlink NOMA-aided small cell network with wireless power transfer. *Bulletin of Electrical Engineering and Informatics*. 2021, vol. 10, no. 5, pp. 2686–2695.

104. CHEN, Erhu; XIA, Minghua; COSTA, Daniel B da; AISSA, Sonia. Multi-hop cooperative relaying with energy harvesting from cochannel interferences. *IEEE Communications Letters*. 2017, vol. 21, no. 5, pp. 1199–1202.

105. DING, Zhiguo; YANG, Zheng; FAN, Pingzhi; POOR, H Vincent. On the performance of non-orthogonal multiple access in 5G systems with randomly deployed users. *IEEE signal processing letters*. 2014, vol. 21, no. 12, pp. 1501–1505.

106. DING, Zhiguo; PENG, Mugen; POOR, H Vincent. Cooperative non-orthogonal multiple access in 5G systems. *IEEE Communications Letters*. 2015, vol. 19, no. 8, pp. 1462–1465.

107. DING, Zhiguo; DAI, Huaiyu; POOR, H Vincent. Relay selection for cooperative NOMA. *IEEE Wireless Communications Letters*. 2016, vol. 5, no. 4, pp. 416–419.

108. NGUYEN, Thanh-Luan; LE, Chi-Bao; DO, Dinh-Thuan. Performance analysis of multi-user NOMA over $\alpha - \kappa - \mu$ shadowed fading. *Electronics Letters*. 2020, vol. 56, no. 15, pp. 771–773.

109. DO, Dinh-Thuan; NGUYEN, Tu-Trinh Thi. Exploiting System Performance in AF non-orthogonal multiple access network under impacts of imperfect SIC and imperfect hardware. *Physical Communication*. 2020, vol. 38, p. 100912.

110. MATTHAIOU, Michail; PAPADOGIANNIS, Agisilaos; BJORNSON, Emil; DEBBAH, Mérouane. Two-way relaying under the presence of relay transceiver hardware impairments. *IEEE Communications Letters*. 2013, vol. 17, no. 6, pp. 1136–1139.

111. BJORNSON, Emil; MATTHAIOU, Michail; DEBBAH, Merouane. A new look at dual-hop relaying: Performance limits with hardware impairments. *IEEE Transactions on Communications*. 2013, vol. 61, no. 11, pp. 4512–4525.

112. DO, Dinh-Thuan; NGUYEN, Tu-Trinh Thi. Impacts of imperfect SIC and imperfect hardware in performance analysis on AF non-orthogonal multiple access network. *Telecommunication Systems*. 2019, vol. 72, no. 4, pp. 579–593.

113. WANG, Xinyu; JIA, Min; HO, Ivan Wang-Hei; GUO, Qing; LAU, Francis CM. Exploiting full-duplex two-way relay cooperative non-orthogonal multiple access. *IEEE Transactions on Communications*. 2018, vol. 67, no. 4, pp. 2716–2729.

114. DO, Dinh-Thuan; NGUYEN, Tu-Trinh Thi; LE, Chi-Bao; VOZNAK, Miroslav; KALEEM, Zeeshan; RABIE, Khaled M. UAV relaying enabled NOMA network with hybrid duplexing and multiple antennas. *IEEE Access*. 2020, vol. 8, pp. 186993–187007.

115. DO, Dinh-Thuan; NGUYEN, Tu-Trinh Thi; NGUYEN, Tu N; LI, Xingwang; VOZNAK, Miroslav. Uplink and downlink NOMA transmission using full-duplex UAV. *IEEE Access*. 2020, vol. 8, pp. 164347–164364.

116. JOSE, Justin; SHAIK, Parvez; BHATIA, Vimal. VFD-NOMA under imperfect SIC and residual inter-relay interference over generalized nakagami-m fading channels. *IEEE Communications Letters*. 2020, vol. 25, no. 2, pp. 646–650.

117. GRADŠTEJN, Izrail'S; RYŽIK, Iosif M. *Table of integrals, series, and products*. Acad. Press, 2000.

118. KHALIL, Nacer; ABID, Mohamed Riduan; BENHADDOU, Driss; GERNDT, Michael. Wireless sensors networks for Internet of Things. In: *2014 IEEE ninth international conference on Intelligent sensors, sensor networks and information processing (ISSNIP)*. IEEE, 2014, pp. 1–6.

119. BAJAJ, Karan; SHARMA, Bhisham; SINGH, Raman. Integration of WSN with IoT applications: a vision, architecture, and future challenges. In: *Integration of WSN and IoT for Smart Cities*. Springer, 2020, pp. 79–102.

120. SHARMA, Himanshu; HAQUE, Ahteshamul; BLAABJERG, Frede. Machine learning in wireless sensor networks for smart cities: a survey. *Electronics*. 2021, vol. 10, no. 9, p. 1012.

121. BENSAID, Rahil; SAID, Maymouna Ben; BOUJEMAA, Hatem. Fuzzy C-means based clustering algorithm in WSNs for IoT applications. In: *2020 International Wireless Communications and Mobile Computing (IWCMC)*. IEEE, 2020, pp. 126–130.

122. ASIRI, Mohammed; SHELTAMI, Tarek; AL-AWAMI, Louai; YASAR, Ansar. A novel approach for efficient management of data lifespan of IoT devices. *IEEE Internet of Things Journal*. 2019, vol. 7, no. 5, pp. 4566–4574.

123. HEIZELMAN, W; CHANDRAKASAN, A; BALAKRISHNAN, H. Energy-efficient routing protocols for wireless microsensor networks. In: *Proceeding of 33rd Hawaii International Conference System Sciences, Maui*. 2000, pp. 4–7.

124. ALHARBI, Mohammad Ali; KOLBERG, Mario; ZEESHAN, Muhammad. Towards improved clustering and routing protocol for wireless sensor networks. *EURASIP Journal on Wireless Communications and Networking*. 2021, vol. 2021, no. 1, pp. 1–31.

125. DAI, Linglong; WANG, Bichai; DING, Zhiguo; WANG, Zhaocheng; CHEN, Sheng; HANZO, Lajos. A survey of non-orthogonal multiple access for 5G. *IEEE communications surveys & tutorials*. 2018, vol. 20, no. 3, pp. 2294–2323.

126. BILIM, Mehmet; KAPUCU, Nuri. On the analysis of achievable rate for NOMA networks with cooperative users over κ-μ shadowed fading channels. *International Journal of Communication Systems*. 2019, vol. 32, no. 12, e4001.

127. YACOUB, Michel Daoud. The κ-μ distribution and the η-μ distribution. *IEEE Antennas and Propagation Magazine*. 2007, vol. 49, no. 1, pp. 68–81.

128. MILIŠIĆ, Mirza; HAMZA, Mirza; HADŽIALIĆ, Mesud. Outage Performance of L-branch Maximal-Ratio Combiner for Generalized κ-μ Fading. In: *IEEE Proceedings of International Conference on Vehicular Technology*. 2008, pp. 325–329.

129. CHEN, Shuaifei; ZHANG, Jiayi; ZENG, Wen; PEPPAS, Kostas P; AI, Bo. Performance Analysis of Wireless Powered UAV Relaying Systems Over κ-μ Fading Channels. In: *2018 IEEE Globecom Workshops (GC Wkshps)*. IEEE, 2018, pp. 1–6.

130. MORALES-JIMÉNEZ, David; PARIS, Jose F. Outage probability analysis for η-μ fading channels. *IEEE Communications Letters*. 2010, vol. 14, no. 6, pp. 521–523.

131. YACOUB, Michel Daoud. The α-μ Distribution: A Physical Fading Model for the Stacy Distribution. *IEEE Transactions on Vehicular Technology*. 2007, vol. 56, no. 1, pp. 27–34.

132. LE, Chi-Bao; DO, Dinh-Thuan. Study on transmission over Nakagami-m fading channel for multiple access scheme without orthogonal signal. *TELKOMNIKA (Telecommunication Computing Electronics and Control)*. 2020, vol. 18, no. 4, pp. 2205–2212.

133. DO, Dinh-Thuan; NGUYEN, Tu-Trinh Thi; LE, Chi-Bao; LEE, Jeong Woo. Two-way transmission for low-latency and high-reliability 5G cellular V2X communications. *Sensors*. 2020, vol. 20, no. 2, p. 386.

134. LE, Anh-Tu; DO, Dinh-Thuan; CHANG, Wen-Thong; VU, Chien-Thang. Cognitive IoT relaying NOMA networks with user clustering and imperfect SIC. *Peer-to-Peer Networking and Applications*. 2021, vol. 14, no. 5, pp. 3170–3180.

135. PEPPAS, Kostas P. Dual-Hop Relaying Communications with Cochannel Interference Over η-μ Fading Channels. *IEEE transactions on vehicular technology*. 2013, vol. 62, no. 8, pp. 4110–4116.

136. MARTOS-NAYA, Eduardo; ROMERO-JEREZ, Juan Manuel; LOPEZ-MARTINEZ, F Javier; PARIS-ANGEL, Jose Francisco, et al. A MATLAB program for the computation of the confluent hypergeometric function $\Phi 2$. 2016.

137. BALAM, Suresh Kumar; SIDDAIAH, P; NALLAGONDA, Srinivas. Optimization Analysis of Cooperative Spectrum Sensing System over Generalized κ-μ and $\eta - \mu$ Fading Channels. *Wireless Personal Communications*. 2021, vol. 116, no. 4, pp. 3081–3100.

138. DO, Dinh-Thuan; LE, Anh-Tu; LEE, Byung Moo. NOMA in cooperative underlay cognitive radio networks under imperfect SIC. *IEEE Access*. 2020, vol. 8, pp. 86180–86195.

139. ABRAMOWITZ, Milton; STEGUN, Irene A. Handbook of mathematical functions with formulas, graphs, and mathematical tables. In: *Appl*. 1972.

140. LE, Chi-Bao; DO, Dinh-Thuan; ZAHARIS, Zaharias D; MAVROMOUSTAKIS, Constandinos X; MASTORAKIS, George; MARKAKIS, Evangelos K. System performance analysis in cognitive radio-aided NOMA network: An application to vehicle-to-everything communications. *Wireless Personal Communications*. 2021, vol. 120, no. 3, pp. 1975–2000.

141. SHARMA, Shree Krishna; CHATZINOTAS, Symeon; ARAPOGLOU, Pantelis-Daniel. *Satellite communications in the 5G era*. Institution of Engineering and Technology, 2018.

142. LUTZ, E; JAHN, A; WERNER, M. Satellite Systems for Personal and Broadband Communications. *Satellite Systems for Personal and Broadband Communications*. 2000, pp. 1–433.

143. LI, Xingwang; LI, Jingjing; LIU, Yuanwei; DING, Zhiguo; NALLANATHAN, Arumugam. Residual transceiver hardware impairments on cooperative NOMA networks. *IEEE Transactions on Wireless Communications*. 2019, vol. 19, no. 1, pp. 680–695.

144. DO, Dinh-Thuan; VAN NGUYEN, Minh-Sang; VOZNAK, Miroslav; KWASINSKI, Andres; SOUZA, Jose Neuman de. Performance analysis of clustering car-following V2X system with wireless power transfer and massive connections. *IEEE Internet of Things Journal*. 2021.

145. DO, Dinh-Thuan; VAN NGUYEN, Minh-Sang. Device-to-device transmission modes in NOMA network with and without Wireless Power Transfer. *Computer Communications*. 2019, vol. 139, pp. 67–77.

146. DO, Dinh-Thuan; VAN NGUYEN, Minh-Sang; JAMEEL, Furqan; JÄNTTI, Riku; ANSARI, Imran Shafique. Performance evaluation of relay-aided CR-NOMA for beyond 5G communications. *IEEE Access*. 2020, vol. 8, pp. 134838–134855.

147. ZENG, Ming; YADAV, Animesh; DOBRE, Octavia A; TSIROPOULOS, Georgios I; POOR, H Vincent. On the sum rate of MIMO-NOMA and MIMO-OMA systems. *IEEE Wireless Communications Letters*. 2017, vol. 6, no. 4, pp. 534–537.

148. LIU, Yuanwei; DING, Zhiguo; ELKASHLAN, Maged; POOR, H Vincent. Cooperative non-orthogonal multiple access with simultaneous wireless information and power transfer. *IEEE Journal on Selected Areas in Communications*. 2016, vol. 34, no. 4, pp. 938–953.

149. LIN, Zhi; LIN, Min; WANG, Jun-Bo; DE COLA, Tomaso; WANG, Jiangzhou. Joint beamforming and power allocation for satellite-terrestrial integrated networks with non-orthogonal multiple access. *IEEE Journal of Selected Topics in Signal Processing*. 2019, vol. 13, no. 3, pp. 657–670.

150. ZHU, Xiangming; JIANG, Chunxiao; KUANG, Linling; GE, Ning; LU, Jianhua. Non-orthogonal multiple access based integrated terrestrial-satellite networks. *IEEE Journal on Selected Areas in Communications*. 2017, vol. 35, no. 10, pp. 2253–2267.

151. LIN, Min; YIN, Chunyan; LIN, Zhi; WANG, Jun-Bo; COLA, Tomaso de; OUYANG, Jian. Combined beamforming with NOMA for cognitive satellite terrestrial networks. In: *ICC 2019-2019 IEEE International Conference on Communications (ICC)*. IEEE, 2019, pp. 1–6.

152. GUO, Kefeng; JI, Zengxi; YANG, Bohang; WANG, Xueling. NOMA-based integrated satellite-terrestrial multi-relay networks with hardware impairments and partial relay selection scheme. In: *2019 IEEE 19th International Conference on Communication Technology (ICCT)*. IEEE, 2019, pp. 1099–1104.

153. AN, Kang; LIN, Min; LIANG, Tao; WANG, Jun-Bo; WANG, Jiangzhou; HUANG, Yongming; SWINDLEHURST, A Lee. Performance analysis of multi-antenna hybrid satellite-terrestrial relay networks in the presence of interference. *IEEE Transactions on Communications*. 2015, vol. 63, no. 11, pp. 4390–4404.

154. BANKEY, Vinay; UPADHYAY, Prabhat Kumar. Ergodic capacity of multiuser hybrid satellite-terrestrial fixed-gain AF relay networks with CCI and outdated CSI. *IEEE Transactions on Vehicular Technology*. 2018, vol. 67, no. 5, pp. 4666–4671.

155. HUSSEIN, Jamal Ahmed; IKKI, Salama S; BOUSSAKTA, Said; TSIMENIDIS, Charalampos C. Performance analysis of opportunistic scheduling in dual-hop multiuser underlay cognitive network in the presence of cochannel interference. *IEEE Transactions on Vehicular Technology*. 2015, vol. 65, no. 10, pp. 8163–8176.

156. COSTA, Daniel Benevides da; DING, Haiyang; YACOUB, Michel Daoud; GE, Jianhua. Two-way relaying in interference-limited AF cooperative networks over Nakagami-m fading. *IEEE Transactions on Vehicular Technology*. 2012, vol. 61, no. 8, pp. 3766–3771.

157. LIANG, Xiao; JIAO, Jian; WU, Shaohua; ZHANG, Qinyu. Outage analysis of multirelay multiuser hybrid satellite-terrestrial millimeter-wave networks. *IEEE Wireless Communications Letters*. 2018, vol. 7, no. 6, pp. 1046–1049.

158. UPADHYAY, Prabhat K; SHARMA, Pankaj K. Multiuser hybrid satellite-terrestrial relay networks with co-channel interference and feedback latency. In: *2016 European conference on networks and communications (EuCNC)*. IEEE, 2016, pp. 174–178.

159. BANKEY, Vinay; UPADHYAY, Prabhat K. Physical layer security of multiuser multirelay hybrid satellite-terrestrial relay networks. *IEEE Transactions on Vehicular Technology*. 2019, vol. 68, no. 3, pp. 2488–2501.

160. LI, Xingwang; WANG, Qunshu; PENG, Hongxing; ZHANG, Hui; DO, Dinh-Thuan; RABIE, Khaled M; KHAREL, Rupak; CAVALCANTE, Charles C. A unified framework for HS-UAV NOMA networks: Performance analysis and location optimization. *IEEE Access*. 2020, vol. 8, pp. 13329–13340.

161. ARTI, MK; BHATNAGAR, Manav R. Beamforming and combining in hybrid satellite-terrestrial cooperative systems. *IEEE Communications Letters*. 2014, vol. 18, no. 3, pp. 483–486.

162. ALFANO, Giuseppa; DE MAIO, Antonio. Sum of squared shadowed-rice random variables and its application to communication systems performance prediction. *IEEE Transactions on Wireless Communications*. 2007, vol. 6, no. 10, pp. 3540–3545.

163. COSTA, Daniel Benevides da; DING, Haiyang; GE, Jianhua. Interference-limited relaying transmissions in dual-hop cooperative networks over Nakagami-m fading. *IEEE Communications Letters*. 2011, vol. 15, no. 5, pp. 503–505.

164. DA COSTA, Daniel Benevides; YACOUB, Michel Daoud. Outage performance of two hop AF relaying systems with co-channel interferers over Nakagami-m fading. *IEEE Communications Letters*. 2011, vol. 15, no. 9, pp. 980–982.

165. LIU, Yuanwei; DING, Zhiguo; ELKASHLAN, Maged; YUAN, Jinhong. Nonorthogonal multiple access in large-scale underlay cognitive radio networks. *IEEE Transactions on Vehicular Technology*. 2016, vol. 65, no. 12, pp. 10152–10157.

166. YUE, Xinwei; LIU, Yuanwei; KANG, Shaoli; NALLANATHAN, Arumugam; CHEN, Yue. Modeling and analysis of two-way relay non-orthogonal multiple access systems. *IEEE Transactions on Communications*. 2018, vol. 66, no. 9, pp. 3784–3796.

167. AGRAWAL, RP. On certain transformation formulae and Meijer's G-function of two variables. *Indian J. Pure Appl. Math.* 1970, vol. 1, no. 4, pp. 537–551.

168. UPADHYAY, Prabhat K; SHARMA, Pankaj K. Max-max user-relay selection scheme in multiuser and multirelay hybrid satellite-terrestrial relay systems. *IEEE Communications Letters*. 2015, vol. 20, no. 2, pp. 268–271.

169. HAN, Lve; ZHU, Wei-Ping; LIN, Min. Outage analysis of NOMA-based multiple-antenna hybrid satellite-terrestrial relay networks. *IEEE Communications Letters*. 2020, vol. 25, no. 4, pp. 1109–1113.

170. MIRIDAKIS, Nikolaos I; VERGADOS, Dimitrios D; MICHALAS, Angelos. Dual-hop communication over a satellite relay and shadowed Rician channels. *IEEE Transactions on Vehicular Technology*. 2014, vol. 64, no. 9, pp. 4031–4040.

171. ADAMCHIK, VS; MARICHEV, OI. The algorithm for calculating integrals of hypergeometric type functions and its realization in REDUCE system. In: *Proceedings of the international symposium on Symbolic and algebraic computation*. 1990, pp. 212–224.

172. MATHAI, Arakaparampil M; SAXENA, Rajendra Kumar; SAXENA, Ram Kishore, et al. *The H-function with applications in statistics and other disciplines*. John Wiley & Sons, 1978.

173. TSE, D; VISWANATH, P. Fundamentals of Wireless Communication. Cambridge. *Google Scholar Digital Library Digital Library*. 2005.

174. JO, Kenneth Y. *Satellite communications network design and analysis*. Artech house, 2011.

175. HUANG, Qingquan; LIN, Min; ZHU, Wei-Ping; CHENG, Julian; ALOUINI, Mohamed-Slim. Uplink massive access in mixed RF/FSO satellite-aerial-terrestrial networks. *IEEE Transactions on Communications*. 2021, vol. 69, no. 4, pp. 2413–2426.

176. GUO, Kefeng; AN, Kang; ZHANG, Bangning; HUANG, Yuzhen; TANG, Xiaogang; ZHENG, Gan; TSIFTSIS, Theodoros A. Physical layer security for multiuser satellite communication systems with threshold-based scheduling scheme. *IEEE Transactions on Vehicular Technology*. 2020, vol. 69, no. 5, pp. 5129–5141.

177. LIN, Zhi; LIN, Min; CHAMPAGNE, Benoit; ZHU, Wei-Ping; AL-DHAHIR, Naofal. Secure and energy efficient transmission for RSMA-based cognitive satellite-terrestrial networks. *IEEE Wireless Communications Letters*. 2020, vol. 10, no. 2, pp. 251–255.

178. GU, Shushi; JIAO, Jian; HUANG, Zixuan; WU, Shaohua; ZHANG, Qinyu. ARMA-based adaptive coding transmission over millimeter-wave channel for integrated satellite-terrestrial networks. *IEEE Access*. 2018, vol. 6, pp. 21635–21645.

179. LIANG, Xiao; JIAO, Jian; FENG, Bowen; WU, Shaohua; CAO, Bin; ZHANG, Qinyu. Performance analysis of millimeter-wave hybrid satellite-terrestrial relay networks over rain fading channel. In: *2018 IEEE 88th Vehicular Technology Conference (VTC-Fall)*. IEEE, 2018, pp. 1–5.

180. CAI, Yunlong; QIN, Zhijin; CUI, Fangyu; LI, Geoffrey Ye; MCCANN, Julie A. Modulation and multiple access for 5G networks. *IEEE Communications Surveys & Tutorials*. 2017, vol. 20, no. 1, pp. 629–646.

181. HACI, Huseyin; ZHU, Huiling; WANG, Jiangzhou. Performance of non-orthogonal multiple access with a novel asynchronous interference cancellation technique. *IEEE Transactions on Communications*. 2017, vol. 65, no. 3, pp. 1319–1335.

182. LIU, Yuanwei; QIN, Zhijin; ELKASHLAN, Maged; DING, Zhiguo; NALLANATHAN, Arumugam; HANZO, Lajos. Non-orthogonal multiple access for 5G and beyond. *Proceedings of the IEEE.* 2017, vol. 105, no. 12, pp. 2347–2381.

183. CAO, Weifeng; ZOU, Yulong; YANG, Zhen; ZHU, Jia. Relay selection for improving physical-layer security in hybrid satellite-terrestrial relay networks. *IEEE Access.* 2018, vol. 6, pp. 65275–65285.

184. NGUYEN, Tan Nhat; TRAN, Dinh-Hieu; VAN CHIEN, Trinh; PHAN, Van-Duc; VOZNAK, Miroslav; CHATZINOTAS, Symeon. Security and Reliability Analysis of Satellite-Terrestrial Multirelay Networks With Imperfect CSI. *IEEE Systems Journal.* 2022.

185. AN, Kang; LIANG, Tao. Hybrid satellite-terrestrial relay networks with adaptive transmission. *IEEE Transactions on Vehicular Technology.* 2019, vol. 68, no. 12, pp. 12448–12452.

186. AN, Kang; LI, Yusheng; YAN, Xiaojuan; LIANG, Tao. On the performance of cache-enabled hybrid satellite-terrestrial relay networks. *IEEE Wireless Communications Letters.* 2019, vol. 8, no. 5, pp. 1506–1509.

187. SRENG, Sokchenda; ESCRIG, Benoit; BOUCHERET, Marie-Laure. Exact outage probability of a hybrid satellite terrestrial cooperative system with best relay selection. In: *2013 IEEE International Conference on Communications (ICC).* IEEE, 2013, pp. 4520–4524.

188. GUO, Kefeng; LIN, Min; ZHANG, Bangning; WANG, Jun-Bo; WU, Yongpeng; ZHU, Wei-Ping; CHENG, Julian. Performance analysis of hybrid satellite-terrestrial cooperative networks with relay selection. *IEEE Transactions on Vehicular Technology.* 2020, vol. 69, no. 8, pp. 9053–9067.

189. YANG, Liang; HASNA, Mazen O. Performance analysis of amplify-and-forward hybrid satellite-terrestrial networks with cochannel interference. *IEEE Transactions on Communications.* 2015, vol. 63, no. 12, pp. 5052–5061.

190. NGUYEN, Tan N; TU, Lam-Thanh; TRAN, Dinh-Hieu; PHAN, Van-Duc; VOZNAK, Miroslav; CHATZINOTAS, Symeon; DING, Zhiguo. Outage Performance of Satellite Terrestrial Full-Duplex Relaying Networks with Co-Channel Interference. *IEEE Wireless Communications Letters.* 2022.

191. LI, Xunan; CHEN, Yue; XUE, Ping; LV, Guocheng; SHU, Min. Outage performance for satellite-assisted cooperative NOMA systems with coordinated direct and relay transmission. *IEEE Communications Letters.* 2020, vol. 24, no. 10, pp. 2285–2289.

192. HAN, Lve; ZHU, Wei-Ping; LIN, Min. Outage of NOMA-based hybrid satellite-terrestrial multi-antenna DF relay networks. *IEEE Wireless Communications Letters.* 2021, vol. 10, no. 5, pp. 1083–1087.

193. SHUAI, Haifeng; GUO, Kefeng; AN, Kang; ZHU, Shibing. NOMA-based integrated satellite terrestrial networks with relay selection and imperfect SIC. *IEEE Access*. 2021, vol. 9, pp. 111346–111357.

194. HAN, Lve; ZHU, Wei-Ping; LIN, Min. Outage Analysis of Multi-relay NOMA-based Hybrid Satellite-Terrestrial Relay Networks. *IEEE Transactions on Vehicular Technology*. 2022.

195. TOKA, Mesut; VAEZI, Mojtaba; SHIN, Wonjae. Outage Analysis of Alamouti-NOMA Scheme for Hybrid Satellite-Terrestrial Relay Networks. *IEEE Internet of Things Journal*. 2022.

196. YUE, Xinwei; LIU, Yuanwei; YAO, Yuanyuan; LI, Tian; LI, Xuehua; LIU, Rongke; NALLANATHAN, Arumugam. Outage behaviors of NOMA-based satellite network over Shadowed-Rician fading channels. *IEEE Transactions on Vehicular Technology*. 2020, vol. 69, no. 6, pp. 6818–6821.

197. TEGOS, Sotiris A; DIAMANTOULAKIS, Panagiotis D; XIA, Junjuan; FAN, Lisheng; KARAGIANNIDIS, George K. Outage performance of uplink NOMA in land mobile satellite communications. *IEEE Wireless Communications Letters*. 2020, vol. 9, no. 10, pp. 1710–1714.

198. YAN, Xiaojuan; XIAO, Hailin; WANG, Cheng-Xiang; AN, Kang. Outage performance of NOMA-based hybrid satellite-terrestrial relay networks. *IEEE Wireless Communications Letters*. 2018, vol. 7, no. 4, pp. 538–541.

199. LE, Anh-Tu; HA, Nhat-Duy Xuan; DO, Dinh-Thuan; YADAV, Suneel; LEE, Byung Moo. Enabling NOMA in overlay spectrum sharing in hybrid satellite-terrestrial systems. *IEEE Access*. 2021, vol. 9, pp. 56616–56629.

200. SINGH, Vibhum; UPADHYAY, Prabhat K. Exploiting FD/HD cooperative-NOMA in underlay cognitive hybrid satellite-terrestrial networks. *IEEE Transactions on Cognitive Communications and Networking*. 2021, vol. 8, no. 1, pp. 246–262.

201. SINGH, Vibhum; UPADHYAY, Prabhat K. Exploiting cache-free/cache-aided TWR-NOMA in cognitive hybrid satellite-terrestrial networks. *IEEE Transactions on Vehicular Technology*. 2021, vol. 71, no. 2, pp. 1778–1793.

202. DA COSTA, Daniel Benevides; AISSA, Sonia. Cooperative dual-hop relaying systems with beamforming over Nakagami-m fading channels. *IEEE Transactions on Wireless Communications*. 2009, vol. 8, no. 8, pp. 3950–3954.

203. SHUAI, Haifeng; GUO, Kefeng; AN, Kang; HUANG, Yuzhen; ZHU, Shibing. Transmit Antenna Selection in NOMA-based Integrated Satellite-HAP-Terrestrial Networks with Imperfect CSI and SIC. *IEEE Wireless Communications Letters*. 2022.

204. MACCARTNEY, George R; ZHANG, Junhong; NIE, Shuai; RAPPAPORT, Theodore S. Path loss models for 5G millimeter wave propagation channels in urban microcells. In: *2013 IEEE global communications conference (GLOBECOM)*. IEEE, 2013, pp. 3948–3953.

205. LIN, Shuxian; ZHU, Lidong; GUO, Yantao; GOU, Xiaogang. Distribution characteristics and performance simulations of rain attenuation at Ka band for satellite communications. In: *Proceedings of 2012 5th Global Symposium on Millimeter-Waves*. IEEE, 2012, pp. 579–582.

206. DAI, Cui-Qin; HUANG, Nan-Nan; CHEN, Qianbin. Adaptive transmission scheme in Ka-band satellite communications. In: *2016 IEEE International Conference on Digital Signal Processing (DSP)*. IEEE, 2016, pp. 336–340.

207. GRADSHTEYN, Izrail Solomonovich; RYZHIK, Iosif Moiseevich. *Table of integrals, series, and products*. Academic press, 2014.

208. DAVID, Herbert A; NAGARAJA, Haikady N. *Order statistics*. John Wiley & Sons, 2004.

209. ZHANG, Qianfeng; AN, Kang; YAN, Xiaojuan; LIANG, Tao. Coexistence and performance limits for the cognitive broadband satellite system and mmWave cellular network. *IEEE Access*. 2020, vol. 8, pp. 51905–51917.

210. GUIDOLIN, Francesco; NEKOVEE, Maziar; BADIA, Leonardo; ZORZI, Michele. A study on the coexistence of fixed satellite service and cellular networks in a mmWave scenario. In: *2015 IEEE International Conference on Communications (ICC)*. IEEE, 2015, pp. 2444–2449.

211. AN, Kang; LIN, Min; GUYANG, Jian; LIANG, Tao; WANG, Jun-bo; ZHU, Wei-Ping. Outage performance for the cognitive broadband satellite system and terrestrial cellular network in millimeter wave scenario. In: *2017 IEEE International Conference on Communications (ICC)*. IEEE, 2017, pp. 1–6.

212. HILDEBRAND, Francis Begnaud. *Introduction to numerical analysis*. Courier Corporation, 1987.

List of own publication activities

Publications and further research directly related to the dissertation

Journal ratings are taken from ScimagoJR (scimagojr.com) for the area that best fits.

[NNT01] **NGUYEN, Nhat-Tien**; NGUYEN, Hong-Nhu; NGUYEN, Ngoc-Long; LE, Anh-Tu; NGUYEN, N. Tan; VOZNAK, Miroslav. *Performance Analysis of NOMA-based Hybrid Satellite-Terrestrial Relay System Using mmWave Technology*. IEEE Access. 2023, vol. 11, pp. 10696-10707. DOI: 10.1109/ACCESS.2023.3238335. (Engineering miscellaneous: 58/301, 15%).

[NNT02] **NGUYEN, Nhat-Tien**; NGUYEN, Hong-Nhu; LE, Anh-Tu; DO, Dinh-Thuan; VOZNAK, Miroslav. *Impact of CCI on Performance Analysis of Downlink Satellite-Terrestrial Systems: Outage Probability and Ergodic Capacity Perspective*. EURASIP Journal on Wireless Communications and Networking. 2022, Article number: 70 (2022). DOI: 10.1186/s13638-022-02140-4. (Computer Networks and Communications: 88/323, 27%).

[NNT03] **NGUYEN, Nhat-Tien**; NGUYEN, Hong-Nhu; VOZNAK, Miroslav; BAO, Le-Chi; NGUYEN, Nhan Duc. *Outage performance analysis of NOMA under $\eta - \mu$ fading channels in presence of imperfect SIC*. Bulletin of Electrical Engineering and Informatics. 2022, vol. 11, no. 4. DOI: 10.11591/eei.v11i4.3572. (Computer Science: 143/284, 50%).

[NNT04] TON, That Phung; **NGUYEN, Nhat-Tien**; HA, Duy-Hung; VOZNAK, Miroslav. *Throughput analysis of non-orthogonal multiple access and orthogonal multiple access assisted wireless energy harvesting K-hop relaying networks*. International Journal of Electrical and Computer Engineering (IJECE). 2023, Vol. 13, No. 1, pp. 522 530. DOI: 10.11591/ijece.v13i1.pp522-530. (Computer Science: 139/284, 49%).

[NNT05] NGUYEN, N. Tan; TRAN, Dinh-Hieu; TRINH, Van Chien; PHAN, Van-Duc; **NGUYEN, Nhat-Tien**; VOZNAK, Miroslav; CHATZINOTAS, Symeon; OTTERSTEN,

Björn; POOR, H. Vincent. *Physical Layer Security in AF-Based Cooperative SWIPT Sensor Networks.* IEEE Sensors Journal. 2022. DOI: 10.1109/JSEN.2022.3224128. (Instrumentation: 17/132, 13%).

[NNT06] **NGUYEN, Nhat-Tien**; NGUYEN, Hong-Nhu; HUYNH, Leminh Thien; VOZNAK, Miroslav. *Enabling unmanned aerial vehicle to serve ground users in downlink NOMA system.* Bulletin of Electrical Engineering and Informatics. 2022, vol. 11, no. 6, pp. 3338–3345. DOI: 10.11591/eei.v11i6.3945. (Computer Science: 143/284, 50%).

[NNT07] **NGUYEN, Nhat-Tien**; NGUYEN, Hong-Nhu; VOZNAK, Miroslav. *Secrecy Performance of Scenario with Multiple Antennas in Cooperative Satellite Networks.* Multimedia Communications, Services and Security (MCSS 2022), Kraków, NOV 2022, In Springer ed. Communications in Computer and Information Science, vol. 1689, pp. 1-10. DOI: 10.1007/978-3-031-20215-5_1.

[NNT08] **NGUYEN, Nhat-Tien**; NGUYEN, Hong-Nhu; NGUYEN, Ngoc-Long; LE, Anh-Tu; DO, Dinh-Thuan; VOZNAK, Miroslav. *Enhancing Spectrum Efficiency for Multiple Users in Hybrid Satellite-Terrestrial Networks.* IEEE Access. 2021, vol. 9, pp. 50291–50300. DOI: 10.1109/ACCESS.2021.3069247. (Engineering miscellaneous: 58/301, 15%).

[NNT09] **NGUYEN, Nhat-Tien**; LE, Thien TT; NGUYEN, Huy-Hung; VOZNAK, Miroslav. *Energy-efficient clustering multi-hop routing protocol in a UWSN.* Sensors. 2021, vol. 21, no. 2, pp. 1–16. DOI: 10.3390/s21020627. (Instrumentation: 24/132, 18%).

[NNT10] **NGUYEN, Nhat Tien**; LE, Thien TT; VOZNAK, Miroslav; et al. *A Self-learning Clustering Protocol in Wireless Sensor Networks for IoT Applications.* International Conference on Intelligent Networking and Collaborative Systems (INCOS 2021), Taichung, SEP 2021, In Springer ed. Lecture Notes in Networks and Systems, vol. 312, pp. 149–157. DOI: 10.1007/978-3-030-84910-8_16.

[NNT11] NGUYEN, Hong-Nhu; NGUYEN, Ngoc-Long; **NGUYEN, Nhat-Tien**; LE, Anh-Tu; HA, Nhat-Duy Xuan; DO, Dinh-Thuan; VOZNAK, Miroslav. *Reliable and secure transmission in multiple antennas hybrid satellite-terrestrial cognitive networks relying on NOMA.* IEEE Access. 2020, vol. 8, pp. 215044–215056. DOI: 10.1109/ACCESS.2020.3041680. (Engineering miscellaneous: 58/301, 15%).

[NNT12] DO, Dinh-Thuan; LE, Chi-Bao; NGUYEN, Hong-Nhu; KIEU, Tam Nguyen; LE, Si Phu; NGUYEN, Ngoc-Long; **NGUYEN, Nhat-Tien**; VOZNAK, Miroslav. *Wireless power transfer enabled NOMA relay systems: two SIC modes and performance evaluation.* Telkomnika. 2019, vol. 17, no. 6, pp. 2697–2703. DOI: 10.12928/TELKOMNIKA.v17i6.12218. (Electrical and Electronic Engineering: 393/635, 62%).

Publications and further research broadly related to the dissertation

[NNT13] TU, Lam-Thanh; PHAN, Van-Duc; NGUYEN, N. Tan; TRAN, T. Phuong; TRAN, Trung Duy; NGUYEN, Quang-Sang; **NGUYEN, Nhat-Tien**; VOZNAK, Miroslav. *Performance Analysis of Multihop Full-Duplex NOMA Systems with Imperfect Interference Cancellation and Near-Field Path-Loss.* Sensors 23.1 (2023): 524. DOI: 10.3390/s23010524.

[NNT14] NGUYEN, Hong-Nhu; NGUYEN, Ngoc-Long; **NGUYEN, Nhat-Tien**; NGUYEN, Ngoc Lan; VOZNAK, Miroslav. *Outage Probability of CR-NOMA Schemes with Multiple Antennas Selection and Power Transfer Approach.* International Conference on Network-Based Information Systems. 2021, pp. 131–142. DOI: 10.1007/978-3-030-84913-9_12.

[NNT15] LE, Si-Phu; VAN NGUYEN, Minh-Sang; DO, Dinh-Thuan; NGUYEN, Hong-Nhu; NGUYEN, Ngoc-Long; **NGUYEN, Nhat-Tien**; VOZNAK, Miroslav. *Enabling wireless power transfer and multiple antennas selection to IoT network relying on NOMA*. Elektronika ir Elektrotechnika. 2020, vol. 26, no. 5, pp. 59–65. DOI: 10.5755/j01.eie.26.5.27889.

[NNT16] NGUYEN, Ngoc-Long; NGUYEN, Hong-Nhu; **NGUYEN, Nhat-Tien**; et al. *On Secure Cognitive Radio Networks with NOMA: Design of Multiple-Antenna and Performance Analysis.* 2020 IEEE Microwave Theory and Techniques in Wireless Communications (MTTW). 2020, vol. 1, pp. 1–6. DOI: 10.1109/MTTW51045.2020.9245070.

[NNT17] NGUYEN, Hong-Nhu; LE, Si-Phu; LE, Chi-Bao; NGUYEN, Ngoc-Long; **NGUYEN, Nhat-Tien**; DO, Dinh-Thuan; VOZNAK, Miroslav. *Cognitive radio assisted non-orthogonal multiple access: Outage performance.* 2019 42nd International Conference on Telecommunications and Signal Processing (TSP). 2019, pp. 449–453. DOI: 10.1109/TSP.2019.8768873.

[NNT18] **NGUYEN, Nhat Tien**; LE, Thien TT; NGUYEN, Hong Nhu; VOZNAK, Miroslav; et al. *Cognitive Radio Architecture for WBAN in e-Health Applications: An Overview.* 2019 6th NAFOSTED Conference on Information and Computer Science (NICS). 2019, pp. 546–551. DOI: 10.1109/NICS48868.2019.9023802.

[NNT19] LE, Si-Phu; LE, Chi-Bao; NGUYEN, Hong-Nhu; NGUYEN, Ngoc-Long; **NGUYEN, Nhat-Tien**; DO, Dinh-Thuan; VOZNAK, Miroslav. *Exploitting Performance Of Miso Based Non-Orthogonal Multiple Access.* 2019 42nd International Conference on Telecommunications and Signal Processing (TSP). 2019, pp. 454–458. DOI: 10.1109/TSP.2019.8768834.

List of Citations

These non-self citations are known

- Wireless power transfer enabled NOMA relay systems: two SIC modes and performance evaluation

  1. Liyn, L. P., Ab Ghani, H., Roslim, F. N., Hamzah, N. A. A., Mohammed, S. M. A., Aziz, N. H. A., and Azizan, A. (2020). Ant-colony and nature-inspired heuristic models for NOMA systems: a review. Telkomnika, 18(4), 1754-1761.

  2. Liyn, L. P., Ab Ghani, H., Roslim, F. N., Hamzah, N. A. A., Mohammed, S. M. A., Aziz, N. H. A., ... and Azizan, A. (2020). Ant-colony and nature-inspired heuristic models for NOMA systems: a review. Telkomnika, 18(4), 1754-1761.

  3. Abusalama, J., Razali, S., Choo, Y. H., Momani, L., and Alkharabsheh, A. (2020). Dynamic real-time capacity constrained routing algorithm for evacuation planning problem. Indonesian Journal of Electrical Engineering and Computer Science, 20(3), 1388-1396.

  4. El Hanjri, A., Hayar, A., and Haqiq, A. (2020). Features detection based blind handover using kullback leibler distance for 5G HetNets systems. IAES International Journal of Artificial Intelligence, 9(2), 193.

  5. Serianni, A., De Rango, F., and Bertucci, M. (2021, November). A novel On Board Device for improving passengers safety. In 2021 29th Telecommunications Forum (TELFOR) (pp. 1-4). IEEE.

  6. EL HANJRI, A., HAYAR, A., and HAQIQ, A. (2021). Blind Handover Detection based on KLD: Channel Capacity and Outage Probability Estimations for Rice and Nakagami Models. IAENG International Journal of Computer Science, 48(4).

- Energy-efficient clustering multi-hop routing protocol in a UWSN

  1. Srivastava, A., and Mishra, P. K. (2021). A survey on WSN issues with its heuristics and meta-heuristics solutions. Wireless Personal Communications, 121(1), 745-814.

2. Karim, S., Shaikh, F. K., Aurangzeb, K., Chowdhry, B. S., and Alhussein, M. (2021). Anchor nodes assisted cluster-based routing protocol for reliable data transfer in underwater wireless sensor networks. IEEE Access, 9, 36730-36747.

3. Hayder, I. A., Khan, S. N., Althobiani, F., Irfan, M., Idrees, M., Ullah, S., ... and Martis, R. (2021). Towards controlled transmission: A novel power-based sparsity-aware and energy-efficient clustering for underwater sensor networks in marine transport safety. Electronics, 10(7), 854.

4. Jan, S., Yafi, E., Hafeez, A., Khatana, H. W., Hussain, S., Akhtar, R., and Wadud, Z. (2021). Investigating Master–Slave Architecture for Underwater Wireless Sensor Network. Sensors, 21(9), 3000.

5. Yang, Y., Wu, Y., Yuan, H., Khishe, M., and Mohammadi, M. (2022). Nodes clustering and multi-hop routing protocol optimization using hybrid chimp optimization and hunger games search algorithms for sustainable energy efficient underwater wireless sensor networks. Sustainable Computing: Informatics and Systems, 35, 100731.

6. Mahdi, O. A., Ghazi, A. B., and Al-Mayouf, Y. R. B. (2021). Void-hole aware and reliable data forwarding strategy for underwater wireless sensor networks. Journal of Intelligent Systems, 30(1), 564-577.

7. Mojarad, M., Sarhangnia, F., and Rezaeipanah, A. (2021). Energy-Aware Routing in UWSNs Using Cuckoo Algorithms For Improving Network Lifetime. Energy, 8(3), 01-05.

8. Brida, P., Krejcar, O., Selamat, A., and Kertesz, A. (2021). Smart sensor technologies for IoT. Sensors, 21(17), 5890.

9. Rani, Y. A., and Reddy, E. S. (2021). A novel energy-efficient clustering protocol in wireless sensor network: multi-objective analysis based on hybrid meta-heuristic algorithm. Journal of Reliable Intelligent Environments, 1-18.

10. Abbas, S. (2021). Blockchain based Privacy Preserving Authentication and Malicious Nodes Detection for Optimized Routing in IoT Networks (MS Thesis without Source Codes).

11. Bai, Q., and Jin, C. (2022). A K-Means and Ant Colony Optimization-Based Routing in Underwater Sensor Networks. Mobile Information Systems, 2022.

12. Farooq, U., Ullah, M., Khan, R. U., Alharbi, A., Uddin, M. I., Haq, M. I. U., and Alosaimi, W. (2021). IDBR: Iot Enabled Depth Base Routing Method for Underwater Wireless Sensor Network. Journal of Sensors, 2021.

13. Draz, U., Yasin, S., Ali, T., Ali, A., Faheem, Z. B., Zhang, N., ... and Suh, D. Y. (2021). ROBINA: Rotational Orbit-Based Inter-Node Adjustment for Acoustic Routing Path in the Internet of Underwater Things (IoUTs). Sensors, 21(17), 5968.

14. Chen, Y., Tang, Y., Fang, X., Wan, L., Tao, Y., and Xu, X. (2021). PB-ACR: Node Payload Balanced Ant Colony Optimal Cooperative Routing for Multi-Hop Underwater Acoustic Sensor Networks. IEEE Access, 9, 57165-57178.

15. Natarajan, R., Megharaj, G., Marchewka, A., Divakarachari, P. B., and Hans, M. R. (2022). Energy and Distance Based Multi-Objective Red Fox Optimization Algorithm in Wireless Sensor Network. Sensors, 22(10), 3761.

16. Khan, M. U., Otero, P., and Aamir, M. (2022, February). Underwater Acoustic Sensor Networks (UASN): Energy Efficiency Perspective of Cluster-Based Routing Protocols. In 2022 Global Conference on Wireless and Optical Technologies (GCWOT) (pp. 1-6). IEEE.

17. Priyanka, R., and K. Satyanarayan Reddy. "An End-to-End Security Aware WSN Approach with Localization & Authentication and Data Exchange Security." (2022).

18. Lilhore, Umesh Kumar, et al. "A depth-controlled and energy-efficient routing protocol for underwater wireless sensor networks." International Journal of Distributed Sensor Networks 18.9 (2022): 15501329221117118.

19. Basavaraju, Pramod Halebeedu, et al. "Statistical Channel Model and Systematic Random Linear Network Coding Based QoS Oriented and Energy Efficient UWSN Routing Protocol." Electronics 11.16 (2022): 2590.

20. Karim, Sarang, Faisal Karim Shaikh, and Bhawani Shankar Chowdhry. "Simulation-based quantitative analysis of efficient data transfer routing protocols for Internet of Underwater Things." Simulation Modelling Practice and Theory 121 (2022): 102645.

21. Shovon, Iftekharul Islam, and Seokjoo Shin. "Survey on Multi-Path Routing Protocols of Underwater Wireless Sensor Networks: Advancement and Applications." Electronics 11.21 (2022): 3467.

22. Bhaskarwar, Roshani V., and Dnyandeo J. Pete. "Energy efficient clustering with compressive sensing for underwater wireless sensor networks." Peer-to-Peer Networking and Applications 15.5 (2022): 2289-2306.

23. Begum, Afruza, and Md Anwar Hussain. "Projection-based throughput enhancement for 3D geographic routing technique in multi-hop wireless networks." International Journal of Communication Systems 35.14 (2022): e5269.

24. Bhaskarwar, Roshani V., and Dnyandeo J. Pete. "Clustering with Compressive Sensing Technique for Network Lifetime Enhancement in Underwater Wireless Sen-

sor Networks." Proceedings of International Conference on Communication and Computational Technologies. Springer, Singapore, 2023.

25. Liu, Na, et al. "Anomaly Detection of Underwater Sensor Data Based on Temporal and Spatial Correlation." International Conference on Artificial Intelligence and Security. Springer, Cham, 2022.

26. Jatoi, G. M., Das, B., Karim, S., Pabani, J. K., Krichen, M., Alroobaea, R., and Kumar, M. (2022). Floating Nodes Assisted Cluster-Based Routing for Efficient Data Collection in Underwater Acoustic Sensor Networks. Computer Communications, 195, 137-147.

27. Sathish, K., Venkata, R. C., Anbazhagan, R., and Pau, G. (2023, March). Review of Localization and Clustering in USV and AUV for Underwater Wireless Sensor Networks. In Telecom (Vol. 4, No. 1, pp. 43-64). Multidisciplinary Digital Publishing Institute.

28. Dhabliya, D., Soundararajan, R., Selvarasu, P., Balasubramaniam, M. S., Rajawat, A. S., Goyal, S. B., ... and Suciu, G. (2022). Energy-Efficient Network Protocols and Resilient Data Transmission Schemes for Wireless Sensor Networks—An Experimental Survey. Energies, 15(23), 8883.

29. PRIYANKA, R.; REDDY, K. Satyanarayan. An End-to-End Security Aware WSN Approach with Localization and Authentication and Data Exchange Security. 2022.

- Reliable and secure transmission in multiple antennas hybrid satellite-terrestrial cognitive networks relying on NOMA

1. Odeyemi, K., Owolawi, P., and Olakanmi, O. (2021). Reconfigurable intelligent surface in wireless-powered interference-limited communication networks. Symmetry, 13(6), 960.

2. Song, C., and Lee, K. J. (2022). Regularized artificial fast fading designs for secure transmission in multi-user MIMO wiretap channels. ICT Express.

3. Li, Q., and Zhao, S. (2021). Robust Secure Beamforming Design for Cooperative Cognitive Radio Nonorthogonal Multiple Access Networks. Security and Communication Networks, 2021.

4. Singh, V., and Upadhyay, P. K. (2021). Exploiting Cache-Free/Cache-Aided TWR-NOMA in Cognitive Hybrid Satellite-Terrestrial Networks. IEEE Transactions on Vehicular Technology.

5. Wu, H., Zheng, L., Li, Z., Ma, R., and Ou, J. (2021). Cooperative jamming in downlink satellite network with hardware impairments. Transactions on Emerging Telecommunications Technologies, 32(12), e4372.

6. Li, C., Sun, X., and Zhang, Z. (2021). Effective Methods and Performance Analysis of a Satellite Network Security Mechanism Based on Blockchain Technology. IEEE Access, 9, 113558-113565.

7. Abdelsalam, N., Al-Kuwari, S., and Erbad, A. (2023). Physical Layer Security in Satellite Communication: State-of-the-art and Open Problems. arXiv preprint arXiv:2301.03672.

• Cognitive radio assisted non-orthogonal multiple access: Outage performance

1. Zhu, M., Yang, Z., and Feng, Y. (2020, October). Physical layer security of NOMA with decode-and-forward relaying in underlay CR network. In 2020 International Conference on Wireless Communications and Signal Processing (WCSP) (pp. 783-788). IEEE.

2. Kontorovich, V. (2022). Comments on SIC Design for SISO NOMA Systems Over Doubly Selective Channels. IEEE Open Journal of Vehicular Technology, 3, 111-119.

3. Estrello, C. B. R., Ramos-Alarcón, F., and Kontorovich, V. (2022). NOMA Transmission Systems: Overview of SIC Design and New Findings.

4. Bansal, A., and Modem, S. (2021, July). Performance of Two Stage Cooperative NOMA Transmission for Full-Efficient Three User Network. In 2021 National Conference on Communications (NCC) (pp. 1-6). IEEE.

• Enhancing Spectrum Efficiency for Multiple Users in Hybrid Satellite-Terrestrial Networks

1. Odeyemi, K. O., Owolawi, P. A., and Olakanmi, O. O. (2022). On the Performance of Reconfigurable Intelligent Surface in Cooperative Decode-and-Forward Relaying for Hybrid RF/FSO Systems. Progress In Electromagnetics Research M, 110, 157-169.

2. Khalid, W., Yu, H., Cho, J., Kaleem, Z., and Ahmad, S. (2022). Rate-Energy Tradeoff Analysis in RIS-SWIPT Systems With Hardware Impairments and Phase-Based Amplitude Response. IEEE Access, 10, 31821-31835.

3. Heidarpour, Ali Reza, et al. "Network-Coded Cooperative Systems in Cognitive Radio Networks." IEEE Transactions on Wireless Communications (2022).

4. Zhao, Z., Xu, G., Wang, X., and Zhang, Q. (2022, August). Study on the Symbol Error Probability of the NOMA-Based Hybrid Satellite-Terrestrial Relay Networks. In 2022 IEEE MTT-S International Wireless Symposium (IWS) (Vol. 1, pp. 1-3). IEEE.

- Enabling wireless power transfer and multiple antennas selection to IoT network relying on NOMA

  1. Kabalci, Y., Ahmadi, M., and Ali, M. (2022). Optimal hybrid precoder design for millimeter-wave massive MIMO systems. Computers and Electrical Engineering, 99, 107746.

  2. Porkar Rezaeiye, P., Sharifi, A., Rahmani, A. M., and Dehghan, M. (2021). Access point selection in the network of Internet of things (IoT) considering the strategic behavior of the things and users. The Journal of Supercomputing, 77(12), 14207-14229.

  3. Chinipardaz, M., and Amraee, S. (2022). Study on IoT networks with the combined use of wireless power transmission and solar energy harvesting. Sādhanā, 47(2), 86.

- Study on outage performance gap of two destinations on CR-NOMA network

  1. Abdel-Razeq, S., Shakhatreh, H., Alenezi, A., Sawalmeh, A., Anan, M., and Almutiry, M. (2021). PSO-Based UAV Deployment and Dynamic Power Allocation for UAV-Enabled Uplink NOMA Network. Wireless Communications and Mobile Computing, 2021.

  2. Kumaravelu, Vinoth Babu, et al. "Outage Probability Analysis and Transmit Power Optimization for Blind-Reconfigurable Intelligent Surface-Assisted Non-Orthogonal Multiple Access Uplink." Sustainability 14.20 (2022): 13188.

  3. Jadhav, Hindavi Kishor, and Vinoth Babu Kumaravelu. "Blind RIS Aided Ordered NOMA: Design, Probability of Outage Analysis and Transmit Power Optimization." Symmetry 14.11 (2022): 2266.

- On Secure Cognitive Radio Networks with NOMA: Design of Multiple-Antenna and Performance Analysis

  1. Jiménez, Lenin Patricio Jiménez, et al. "Performance Analysis of Downlink MIMO-NOMA Systems Over Weibull Fading Channels." 2022 IEEE Globecom Workshops (GC Wkshps). IEEE, 2022.

List of Projects

Throughout my doctoral studies, the research leading to the results discussed in the dissertation received funding from:

- as team member

  1. Proj. reg. no. SP2018/59 - Networks and Communications Technologies for Smart Cities I., Student Grant Competition of VSB-TUO (2018).

  2. Proj. reg. no. SP2019/41 - Networks and Communications Technologies for Smart Cities II., Student Grant Competition of VSB-TUO (2019).

  3. Proj. reg. no. SP2020/65 - Networks and Communications Technologies for Smart Cities III., Student Grant Competition of VSB-TUO (2020).

  4. Proj. reg. no. SP2021/25 - Networks and Communications Technologies for Smart Cities IV., Student Grant Competition of VSB-TUO.(2021)

  5. Proj. reg. no. SP2022/5 - Networks and Communications Technologies for Smart Cities V., Student Grant Competition of VSB-TUO.(2022)